Feasibility study of a superconducting helicopter electrical propulsion motor

Master of Science Thesis

Colin Simons

Supervised by
Ir. Christian Sanabria-Walter (EADS)
Dr. Ir. Henk Polinder (TU Delft)

January 2013

EADS

TU Delft Delft University of Technology

Feasibility study of a superconducting helicopter electrical propulsion motor

by

Colin Simons

Thesis submitted to the faculty of Electical Engineering, Mathematics and Computer Science (EEMCS) group of Electical Power Processing (EPP) in partial fulfilment of the requirements of the degree of

Master of Science

Thesis committee:
Dr. ir. H. Polinder
Prof. Dr. Eng. J. A. Ferreira
Dr. O. Chevtchenko
Prof. Dr. J.J. Smit

January 2013

Faculty of Electrical Engineering, Mathematics and Computer Science (EEMCS)
Electrical Power Engineering (EPE) department
Electrical Power Processing (EPP) group

Visiting address
Mekelweg 4
2628 CD Delft

Postal address
P.O Box 5031
2600 GA Delft
The Netherlands

Author

Name:	Colin Anthony Bobby Amrit Edgar Simons
Student number:	1340166
E-mail:	C.A.B.A.E.simons@student.tudelft.nl

Abstract

As a response to the need for lower carbon transmissions for means of transportation, the aerospace industry is looking into more electric aircraft. One concept of such an aircraft is a hybrid helicopter that uses highly efficient diesel engines and electrical propulsion motors.

The feasibility of this concept is greatly determined by the feasibility of its main propulsion motor. The very challenging specifications of such a motor means that new technologies have to be used. One of these possible technologies is superconductivity.

In this thesis a first technical feasibility study on a direct drive superconducting electrical propulsion motor for a hybrid helicopter concept is performed.

Superconductors are special materials that have virtually no electrical resistance when cooled down below a certain critical temperature. This property makes it possible to build high field and low weight coils for electrical machines.

A helicopter's electrical propulsion motor requires a very high torque density. Conventional electrical machines like permanent magnet designs are too heavy for this application. Superconducting motors may achieve the required torque densities, because of their high performance at low weight.

In this thesis, first a literature study of superconductivity is presented. After that the machine is designed in three parts: The armature design, the superconducting field windings design and the cryostat design. After that all the results are combined and the complete machine parameters, like the power density and total weight, are defined. Finally a conclusion is given on the feasibility of the superconducting propulsion motor and recommendations are given for future work.

Table of Contents

1. Introduction

For the last decades the industry has been investing more and more in environmentally friendly forms of transportation. Also the aerospace industry is working on making airplanes and helicopters more energy efficient and less polluting. One of the most promising methods is by using a more electric propulsion system. This electrification in aerospace is a slow and challenging process, because of the safety and performance requirements, which are typical for this industry.

A lot of research has been done on using electrical propulsion in airplanes, but much less work is done on electrical helicopters. Due to the added weight of batteries, a full electrical helicopter is not yet feasible. A new hybrid helicopter concept that uses highly efficient diesel engines to power the electrical propulsion motors and systems is currently a more practical solution.

Of this hybrid concept, the design of the main electric propulsion motor is the most challenging part, since it has to deliver a lot of power and it has to be very lightweight. Different kind of electric machines are considered in literature, including permanent magnet machines, flux switching machines and superconducting machines in order to build a high power dense motor for the helicopter main propulsion.

The goal of this thesis is to perform a first technical feasibility study on an electrical main propulsion motor using superconducting technology for a hybrid helicopter concept.

In this study only the main rotor is considered and other rotors like the tail rotor are excluded. Since this is a first technical study the main focus lies in achieving the technical specifications like the power density and machine dimension restrictions. Aerospace specific conditions like safe factors, G forces during flight, mechanical vibrations etc are not considered for this first study.

Superconductivity means that a material completely loses its electrical resistance when cooled down to very low temperatures like 77 Kelvin. This property allows to build high power, high efficiency and low weight machines that use no iron. These properties of these superconductive machines make them an interesting technology for the aerospace industry.

Important to note is that superconducting machine technology is fairly new and only few demonstrators have been build. Therefore the superconducting machine aimed for in this thesis is expected to be practically feasible within 10-20 years.

The thesis layout is as following. The second chapter explains the background of the hybrid helicopter concept and also the specifications and goals of the propulsion motor are given. The third chapter describes the theoretical background of the superconducting technology that is considered for this thesis. Chapter four describes the different superconducting machine topologies that are considered in literature. In the following chapter the machine topology and machine structure are defined. Chapter 6 and 7 describe the armature and superconducting field winding design respectively. The next chapter deals with the cryostat design and cryostat losses. Chapter 9 combines the results of the previous chapters in order to give an answer on the feasibility of the design and how well it meets the specifications. Finally in chapter 10 the conclusion and recommendations are given.

2. Hybrid helicopter concept

The demand for more efficient and less polluting aircraft is a natural result of the changing global politics, industry and technology. From the developments in the aerospace industry a new hybrid helicopter concept is defined that responds to these changes in the industry.

The aim of this chapter is to describe the developments that resulted in the formulation of this hybrid helicopter concept. First the political and industrial motivations for more efficient aircraft are discussed. After that the existing electric aircraft projects that resulted from these motivations are described. Next the hybrid concept is explained, which again resulted from the advantages and disadvantages of the electric aircraft projects. Finally, as part of this concept, the specifications of the superconducting version of its propulsion motor are described, which also include the design targets for this thesis.

2.1.Social and political motivation

For the past 10 years, the aerospace industry has been working to improve the efficiency and pollution properties of its products. Also the European Union and United States policies aim to reduce emissions in the future.

The preservation of the environment for future generations is the main social motivation to develop more environmental friendly technologies. The increased popularity and social awareness has already significantly influenced different industries like power utilities and the automotive industry.

Although the social motivation is likely to be the most important one, also from the economical point of view there are important drivers. The economic dependence on the limited fossil fuel reserves and the continuous changing of the resources price encourage the development of technologies that depend less on oil or gas and its derivatives. The resulting technologies will then focus on more efficient, less polluting and more electrical systems.

These motivations are supported at a political level by governments in most developed countries around the world. For example in Europe, the European Union has summarized a set of very ambitious global environmental goals named the “20-20-20” goals [1]:

- 20% reduction of EU greenhouse gas emissions from levels of 1990
- 20% increase in energy efficiency
- 20% of European energy consumption from renewable resources by the year 2020

These objectives aim at combatting climate change, improving the EU energy security and competiveness [1].

The aerospace industry currently contributes about 2 percent of the global CO2 emission (12 percent of all transport sources). This contribution is expected to rise to 3 percent by 2050 [2]. In order to reduce these emissions, new technologies are necessary that require major investments which may be too much for individual companies alone.

2.2.Aerospace industry

As a reaction to the political and economic drives, major members of the aerospace industry and academic institutes have combined forces together with the European Commission to develop a public-private cooperation called the Clean Sky Joint Technology Initiative (JTI) that encourages research and innovation in order to comply with the European targets [2]. The JTI project requires an effective coordination of aeronautic research and development to set up an innovative and competitive air transport system at an European scale.

The main mission of this project is to develop breakthrough technologies in order to build improved environmental aircraft and air transport concepts, which aim for less noisy and more fuel-efficient aircraft. This is to be achieved by creating new solutions for the market and by testing them

on full-scale demonstrators [2]. In 2001 the Advisory Council for Aeronautical Research in Europe (ACARE) set up the following targets for the year 2020 as compared to the year 2000 [2]:

- Reduce fuel consumption and CO2 emissions by 50% per passenger kilometre
- Reduce NOx emissions by 80%
- Reduce perceived noise by 50%
- Make substantial progress in reducing the environmental impact of the manufacture, maintenance and disposal of aircraft and related products

The predicted contributions to the 50% CO2 emissions reduction target are:

- Efficient aircraft: 20-25%
- Efficient engines: 15-20%
- Improved air traffic management: 5-10%

The major improvements are to be gained with two approaches: the first one is by improving the aircraft efficiency by using new materials and improved aerodynamic designs. The other approach would be to increase the efficiency of the propulsion system, including the engines, which is directly related to the topic of this thesis. These goals are organised into 6 Integrated Technology Demonstrators (ITD's) that are defined to explore the new areas in order to characterize and coordinate the following research areas for this objective. The 6 ITD's are [3]:

- **SMART Fixed Wing Aircraft** will deliver active wing technologies and new aircraft configuration for breakthrough, news products.
- **Green Regional Aircraft** will deliver low-weight aircraft using smart structures, as well as low external noise configurations and the integration of technology developed in other ITD's, such as engines, energy management and new system architectures.
- **Green Rotorcraft** will deliver innovative rotor blades and engine installation for noise reduction, lower airframe drag, integration of diesel engine technology and advanced electrical systems for elimination of noxious hydraulic fluids and fuel consumption reduction. This thesis work partly contributes to the advances electrical systems of this demonstrator.
- **Sustainable and Green Engines** will design and build five engine demonstrators to integrate technologies for low noise and lightweight low pressure systems, high efficiency, low NOx and low weight cores and novel configurations such as open rotors and intercoolers.
- **Systems for Green Operations** will focus on all-electrical aircraft equipment and systems architectures, thermal management, capabilities for "green" trajectories and mission and improved ground operations to give any aircraft the capability to fully exploit the benefits of Single European Sky.
- **Eco-Design** will focus on green design and production, withdrawal, and recycling of aircraft, by optimal use of raw materials and energies thus improving the environmental impact of the whole products life cycle and accelerating compliance with the REACH directive.

Every integrated technology demonstrator focuses on a different set of technologies that should lead to new cutting edge products which are the first major steps to reach the environmental goals specified earlier.

There is much overlap between the different ITD's like for example most projects aims to use more electrical machines in their designs. This thesis focuses on superconducting electrical motors for propulsion systems for more electric aircraft and is therefore part of the Green Regional Aircraft, Green Rotorcraft, Sustainable and Green Engines, and Systems for Green Operations.

2.3.More Electric Aircraft

As can be seen from the previous section, improving aircraft can be done in many different ways of which using electrical propulsion is only one. There are several projects in the SMART Fixed Wing Aircraft and Green Regional Aircraft areas that aim for a purely electrically propelled aircraft that eventually could be extended to civilian transport.

Examples of experimental aircraft projects are the e-Genius [4], developed by the University of Stuttgart and sponsored by Airbus, and the Elektra One, which is a power glider produced by the German manufacturer PC-Aero (Figure 2-1) [5]**.** These aircraft use electrical motors for propulsion and use rechargeable batteries for energy supply.

These projects that aim to electrify the power generation, storage and propulsion are in line with the aim of this thesis. However, as is common in the avionics industry, most effort goes to improving fixed wing aircraft.

Figure 2-1 The e-Genius from the University of Stuttgart (left) and the Elektra One from PC-Aero (right) [5]

Figure 2-2 Sikorsky's Firefly [6]

2.3.1. More electric helicopters

Not much work has been done on electric rotary wing aircraft within the Clean Sky project, but outside this initiative, the Sikorsky's Firefly is an example of developments that aim for a more electric helicopter. Sikorsky Aircraft modified their popular S-300C helicopter with a complete electrical drivetrain, see Figure 2-2. The resulting concept demonstrator replaces the fuel engine with a 142 kW PM motor and include Li-ion batteries for energy supply.

Sikorsky claims 76.3% efficiency for the battery driven helicopter, which only includes the efficiency of the batteries and electrical motor. Compared to a fuel driven resulting in an almost 300% increase of efficiency from baseline configuration (disregarding the energy loss when charging the batteries from the grid). Very noticeable was the lower heat loss compared to a gas turbine version. Also the direct operating costs are reduced due to needing less moving parts.

However, the main disadvantage of using only battery driven motors is the very restricted flight range. The demonstrator has an expected flight time of only 15 minutes, compared to more than 3 hours for a comparable fuel helicopter [6]. This is a well-known issue also for the Electric Vehicle (EV) industry where fuel cars are replaced with electric variants. Possible solutions used in the EV industry like battery changing or wireless charging are not applicable for helicopters. So the capacity of batteries will have to increase a lot before this fully electric concept is feasible.

The principles of helicopter electrification are somewhat different than for fixed wing aircraft. As can be seen in the previous section, the electric airplanes can be fitted with efficient propeller propulsion systems using batteries for power. Improved aerodynamic designs allow the aircraft to fly more efficient, which makes the added weight of the electric motor and batteries acceptable.

In the case of more electric helicopters it is more difficult. Since the main rotor does not only provide propulsion but it also provides the lift to keep the helicopter in the air. This puts a major power and torque requirement on the main rotor. Any increase in weight will also require more lift. Therefore using more electric components in the helicopter drivetrain is a formidable challenge.

The current helicopter drivetrain consists of a high power dense, high-speed turbine that uses a high gear-ratio gearbox to directly drive the rotors (see Figure 2-3)**.** The main advantage of this drivetrain is the high power to weight ratio. The disadvantages are the low efficiency of the turbine and the low reliability of the gearbox. The different components and the possible electrical improvements are now briefly discussed.

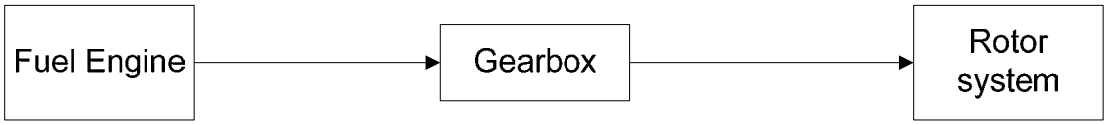

Figure 2-3 Conventional helicopter drivetrain

The gas turbines or turboshafts are widely used because of their high power density or high power to weight ratio. This is the reason they are the most used propulsion systems for aircraft where weight is a critical factor. Nevertheless, an inherent property of these engines is the low efficiency of a maximum of 45%, although this efficiency is seldom reached in practice [7].

Because of this, diesel engines are considered to be a greener alternative with a practical efficiency of more than 50% and a theoretical maximum efficiency of about 75% [8]. Combining this with electrical generators and motors of more than 90% efficiency, this drivetrain can be more efficient and flexible than the existing turboshaft system.

2.4.Hybrid helicopter concept

The main disadvantages of the conventional helicopter drivetrain have been briefly discussed: the low efficiency of the gas turbine, the high maintenance of the gearbox and the lower flexibility of the direct mechanical connection of the turbine and the rotor system. The main reason that this system is used is because of the low weight. Yet it is possible to increase the efficiency and flexibility of the drivetrain by using high efficient diesel engines and electrical motors.

Fully electrical helicopters, like the Firefly, have a very high efficiency, but need batteries to store the energy. Although a lot of progress is being made on the development of batteries, due to their high weight and volume, this drivetrain is not yet feasible for a commercial helicopter that can compete with conventional aircraft.

With the hybrid concept, the best of both worlds is attempted to achieve. By combining the high energy density of fossil fuel and the high efficiency and reliability of electrical machines, a hybrid helicopter can be made. This design would not have zero emissions, but by using diesel engines the emissions can be greatly reduced.

The hybrid helicopter would mainly generate energy by using a diesel engine that drives an electrical generator that feeds the power network. This network consists of an on board DC voltage "grid", from which a direct drive electrical motor can draw energy to power the rotor system.

Such an electrical helicopter is very unconventional and the feasibility is not straightforward. To realize this system no off-the-shelf components are available, but new components have to be designed that can meet the strict requirement on performance, weight and reliability.

The hybrid drivetrain can be split into three main parts: Energy generation, conversion and transmission. On all domains a lot of innovation is needed before the hybrid helicopter can become a reality. In Figure 2-4 a schematic overview of the hybrid helicopter can be seen.

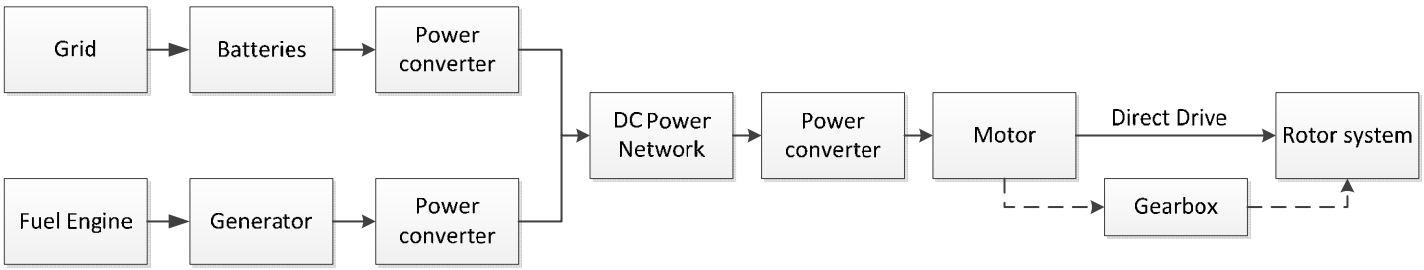

Figure 2-4 Figure drivetrain a hybrid helicopter

An illustration of the hybrid drive train is illustrated in Figure 2-5**.** The focus of this thesis is on the main rotor drive system and more specific the electrical motor itself. The challenges of this drivetrain can be split in the energy generation, energy conversion and electric transmission and they are now briefly discussed below.

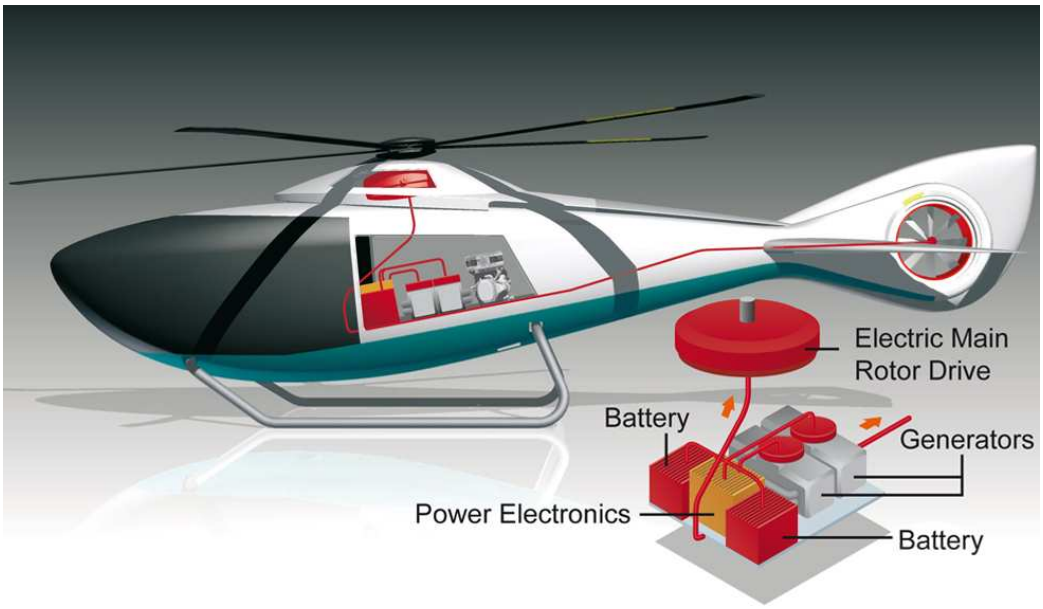

Figure 2-5 Hybrid concept [9]

2.4.1. Energy generation

The energy to power the electric system can come either from batteries or directly from a generator powered by a diesel engine. Currently, the Opposed Piston Opposed Combustion (OPOC) engine is considered the best choice, because of its very high efficiency and high power density [10]. Since there is no direct coupling to the rotors, the engine can work at the optimal rotation speed. In this way the lack of a high power engine (like a gas turbine) is partly counteracted with the highly efficient OPOC machine [9].

The main challenge with using diesel engines is to achieve a comparable performance in power to weight ratio and power to volume ratio. The current gas turbines used in helicopters are optimized for compact and light design that reach power to weight ratios of about 5-8 kW/kg [7]. Since comparable diesel engines achieve power-to-weight ratios of about 2-3 kW/kg, it is clear that diesel engines still need a lot of improvement.

The batteries can be operated as a buffer to supply the peak power during landing and takeoff. Also the batteries can be pre-charged off the grid so that it can easily take off without using a fuel engine. This principle is attractive for civilian helicopters like trauma helicopters that land at hospitals [11].

2.4.2. Power conversion

The power conversion is very important for the efficiency of an electric helicopter, since the generator, batteries and motor have to be connected to the DC power network. Electrical power converters have to be used to operate and control all components in their most efficient states.

2.4.3. Electric transmission

Eventually the electrical energy powers the electric motors that drive the rotor systems. The motors have to be able to provide a high power and high reliability performance. Essential is a high power-to-weight and power-to-volume ratio. In principle a gearbox can be used to increase the torque density, but the aim is to completely remove any gearbox from the drivetrain.

To fulfil these requirements first permanent magnet motors are considered [6]. However, for more demanding helicopters the PM motors are no longer the best choice. Although their efficiency can be very high, the maximum power-to-weight ratio is only about 1-2 kW/kg. Especially when the motor has to directly drive the rotor system, the PM motors become too big and heavy to supply the torque and power.

Different electrical motor topologies are considered like a transverse flux machine and a flux switching machine. In this thesis the feasibility of a motor using superconduction technology is researched.

2.4.4. Other advantages of a hybrid helicopter

Other than the advantages mentioned before, there are more advantages of a hybrid solution other than a higher efficient drivetrain [3]:

- Optimum rotational speed of the main rotor. Since the main rotor is no longer mechanically coupled with generator the main rotor can operate at it most efficient operating point in any situation. Not only will this result in an optimum power requirement, but also to an adaptable noise profile.

- Increased configuration flexibility due to non-mechanical connections between components. The modularity of a hybrid architecture allows for a better component distribution throughout the aircraft as most components are linked through the electrical network.

- Adjustable position of main rotor electrical motor**,** unlike in conventional helicopters where the main rotor is tilted in a fixed position. In the case of the hybrid helicopter the electrical motor is directly mounted to the rotor so both the motor and the rotor can be tilted during operation. In this way the aerodynamic properties of the flight during landing, takeoff and cruise can be more efficient.

- Mechanical decoupled tail rotor electrical motor. Since there is no longer a direct mechanical coupling between the engine and the main and tail rotor, the rotors can operate at their most efficient speed. The tail rotor can even be switched off during cruise and it would only be operational during the phases where it's vital like during take-off, landing and hovering [11]. Depending on the specific design, the tail rotor consumes about 5-30% of the main rotor power [12]. Switching off the rotor can therefore decrease the emissions of flight.

2.5.Propulsion motor specifications

In this section the specifications of the superconducting propulsion motor, of which the feasibility is studied in this thesis, are presented. As described in the previous sections, the propulsion motor for a helicopter has very strict requirements on the design like the high machine power density and machine dimensions and therefore no "off the shelf' design is available.

The problem statement for an electrical motor that is part of a new type of drivetrain for a helicopter is not straightforward. In aerospace engineering change comes slow since reliability is extremely important and only long experience with certain technologies can guarantee reliability.

Since there is a lot of experience with conventional drive systems the initial aim for the electrical system is to have similar weight, volume and performance criteria. These constrains would not necessarily be the most optimal for electrical machines, but they aim to make the concept more feasible in the very conservative aerospace industry.

Although the reliability of the machine is very important and it determines by a great part the feasibility of this machine, the reliability of the motor is not central in this feasibility study since in this early stage of development it is not possible to conduct a good reliability analysis. Yet in the designing phase the reliability is kept in mind.

Important specifications of the machine are the requirements in terms of power, torque and rotational speed. These depend on the aircraft design and the mission profile like the payload and flight range. Fairly average values for power and torque are given in [3], based on a civilian helicopter with a payload of between 7 and 8 persons (including flight crew), 1,5 tons empty weight and 3 tons maximum take-off weight, see also Table 2-1.

Property	Value
Nominal power (kW)	590
Nominal rotation speed (rpm)	341
Nominal torque (kNm)	16,5
Diameter (mm)	1400
Axial length (mm)	250
Expected weight (kg)	150

Table 2-1Technical specifications [3]

During flight the operational speed and power requirements change and for instance for a few seconds 120% of the nominal power can be required [3]. For this feasibility study only the nominal operating values are considered. The operational requirements could be reached by for instance by temporarily overloading the machine, but this is beyond the scope of this thesis.

From these requirements the final values are derived in Table 2-2.

Main rotor electrical machine final requirements	
Volume (m^3)	0,3848
Power-to-Weight Ratio (kW/kg)	4 - 5
Torque-to-Weight Ratio (Nm/kg)	110 - 130
Torque Volumetric Density (kNm/m^3)	43 - 51
Gear box	No (Direct drive)

Table 2-2 Derived technical specifications [3]

2.5.1. Requirements of superconducting components

The requirements mentioned in the previous section are the same for all conceptual motors. The superconducting variant considered here creates extra requirements. A coil made out of superconductors can have more than ten times the performance with a lower weight compared to conventional copper coils.

The drawback of superconductors it that they have to be constantly cooled down to cryogenic temperatures of at least 77 K in order to work. In order to do this reliable, a cryosystem has to be introduced that shield the cold part from the warm environment. This cryostystem is not conventional in aerospace (with the exception of space applications) and it might be very bulky and heavy. Therefore another design requirement for the superconducting propulsion motor is that the most simple, lightest and most reliable cooling system has to be used.

2.6.Conclusion on the hybrid helicopter concept

In this chapter it is explained that the need for more environmentally friendly aircraft has resulted in a hybrid helicopter concept. This concept will still use fossil fuels, but with the use of electric systems, the total efficiency will increase. The feasibility of such a helicopter is mostly determined by the feasibility of its main electrical propulsion motor. The technical requirements of the motor are defined and a new machine has to be designed for this application.

One of the possible electric machine designs considered is the superconducting machine. Therefore in this thesis the feasibility of such a superconducting machine design is researched. The strict requirements of this machine are given, which are used for the design throughout the following chapters.

3. Superconductivity

Some materials are able to conduct a current with virtually no electrical resistance when cooled down to very low temperatures. These superconductors could be used for many electrical applications with significant benefits.

Although the aim of the author is to design the superconducting motor without concerning too much about the underlying theory of superconductivity, a basic understanding of the theory and current state of technology is essential.

This chapter covers briefly the theory of superconductivity, focussing on the properties and effects that are vital to the designing process. Since there are many ways to build a superconducting motor, in this chapter also several designing choices are made, beginning with a choice between different types of superconductors based on their performance. Also a few methods of building coils with this superconductor for machines are studied.

After describing the superconductors, the possibilities of the cooling system are researched. Finally, the complexity of the reliability of the cooling system is briefly mentioned before a conclusion on the design choices is given.

3.1.Brief history of superconductivity

Superconductivity is first discovered by Heike Kamerlingh Onnes in 1911 in Leiden where he experimented with mercury at liquid helium temperatures [13]. In his experiments he measured a sudden complete loss of electrical resistance in mercury at 4.2 K. In the following years a lot of research has been done to find other superconductors. The first were pure metals like mercury and lead which had practically no current carrying capability in high fields, making superconducting coils impossible.

In the late 1950s the discovery of a new class of superconductors such as niobium-titanium (NbTi) and niobium-tin (NbSn) resulted in high field superconductor magnets in commercial devices like MRI machines and also major projects like ITER and LHC. Also these materials have to be cooled down with liquid helium to about 4 K for operation, making the reliability and cost of cooling a challenge. The result is that these superconductors have not found many other applications [14].

One of the major discoveries in the history of superconductivity came in 1986 when lanthanum barium copper oxide (LaBaCuO) was found to be superconducting by Bednorz and Mueller [15]. This material had a previously believed impossible high critical temperature of 35K and the discovery of yttrium barium copper oxide (YBaCuO) with a critical temperature of 93 K in 1987 created a major boost in searching for even higher temperature superconductors.

In the following years few new superconductors have been found like MgB2 and FeAs. The search for even higher temperature superconducting materials still goes on and the fabled room temperature superconductor remains still the ultimate goal. An overview of the discovery of the superconductors is presented Figure 3-1**.**

3.2.Superconductor Theory

Understanding of the physics of superconductivity has grown over the last 100 years and new theories were developed after the discovery of different superconductors. Yet an all covering theory of the physics is still to be found so new superconductors are discovered by trial and error. The currently accepted theories like the BCS theory and Beans model give an in depth quantum physical explanation of the phenomena. In this thesis only the relevant engineering theory needed for electrical machine design is considered.

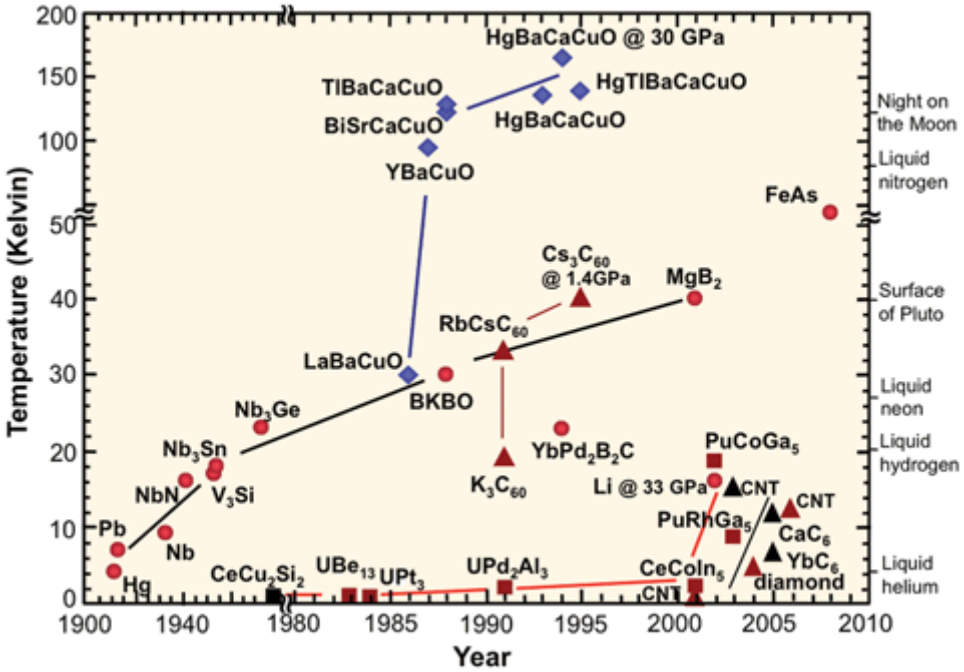

Figure 3-1 Discovery of different superconductors during the last century [16].

3.2.1. Critical surface

Next to a critical temperature also the critical field (H_C) and the critical current density (J_C) describe a critical surface below which superconductivity can exist, see Figure 3-2. When the operating point goes above the surface the material goes into its normal state. Every superconductor has a different surface which can be influenced until a certain level using advanced processing techniques like doping [17].

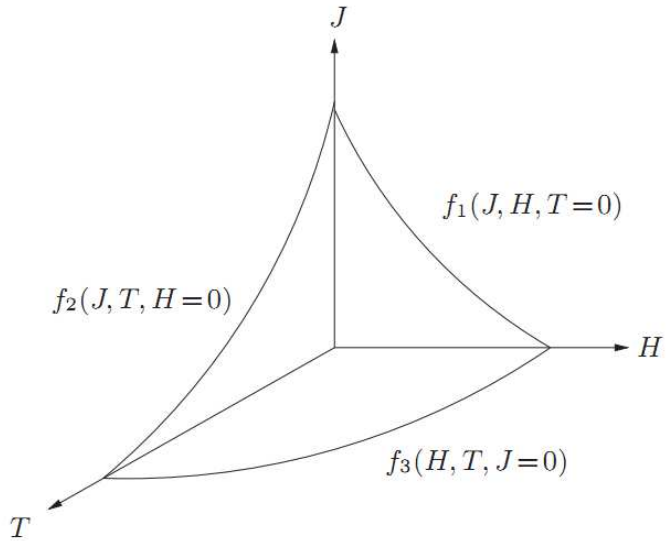

Figure 3-2 Critical surface [17]

The critical current an important measure of the performance of a superconducting wire. Since the transition is usually not sharp but gradual the critical current is defined as the current where the voltage drop across the wire exceeds the specified field like 1 uV/cm. This current voltage relation can be approximated with the power law:

$$E = E_0 \left(\frac{I}{I_c}\right)^n \qquad \textbf{(3-1)}$$

Here Ic is the critical current and the n value is a material property that defines how steep the transition between the superconducting and the normal state occurs. The I-V curve describes this graphically in Figure 3-3.

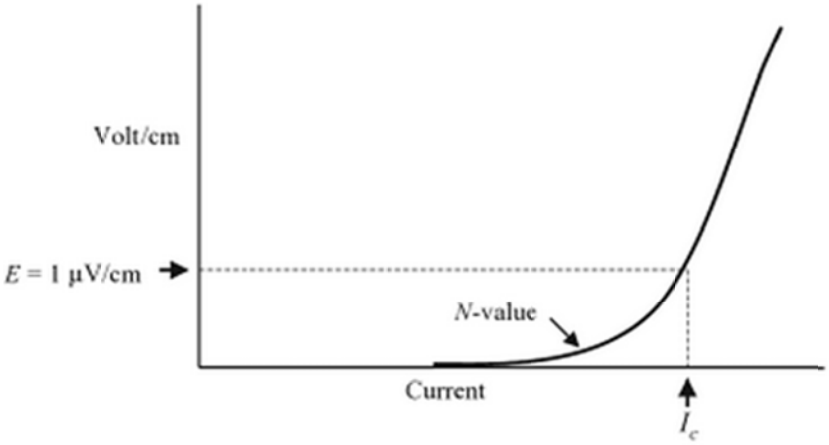

Figure 3-3 I-V curve for a superconductor [14]

The I-V curve is used to determine the I_C experimentally of a wire in self field (the field that the single straight wire produces by itself) or in other configurations like a wire wound coil. As can be seen from the I-V curve when a material is in the superconducting state and the current is near its critical value a voltage and thus electrical losses occur.

This seems contradictory to the definition of superconductivity, but this happens because most superconductors are operated in the mixed state. The mixed state is described in the next paragraph.

3.2.2. Superconductor classification

Superconductors can be classified based on two properties: the transition type and the critical temperature. The classification on transition is based on the phase transition of the material from superconducting to normal. There are two groups defined: type I and type II (see Figure 3-4). For type I material when increasing the temperature, current or field from superconducting state the material will instantly lose superconductivity after surpassing the critical value.

For the type II two critical fields can be described: H_{C1} and H_{C2}.When the field (applied or self-induced) is below H_{C1}, the material is in the Meissner state and no flux penetrates the material [17]. When the field is between the H_{C1} and H_{C2}, the material is in the mixed state and when the field passed the H_{C2} the material is in the normal state. During the mixed state, the material gradually loses its superconducting properties and due to the flux penetration, a voltage can be measured.

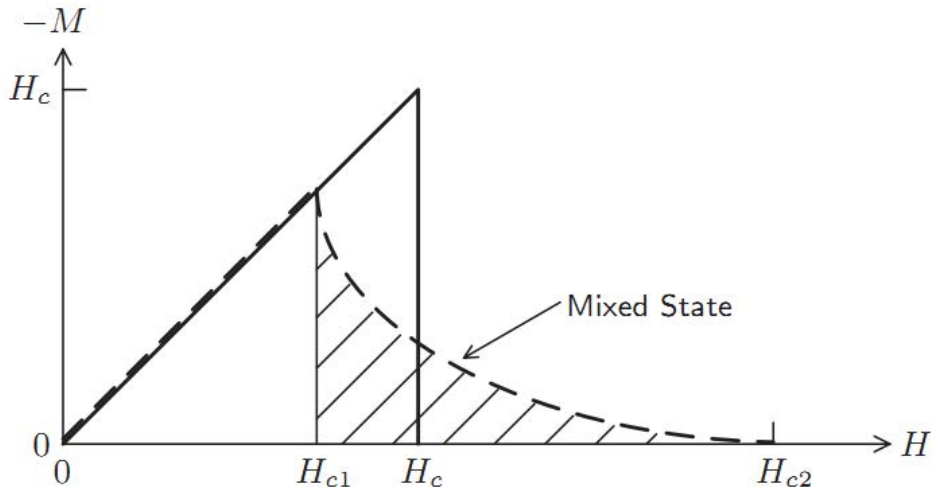

Figure 3-4 Phase transition type I and type II superconductor [17]

The classification by the critical temperature is a more widely used classification. The Low Temperature Superconductors (LTS) have a critical temperature of about 30K and lower and are usually type I superconductors [17]. The LTS materials are made from pure metals and have a low critical temperature, field and current density. Examples are NbTi and Nb_3Sn.

The High Temperature Superconductor (HTS) is usually type II and is made from metal alloys, ceramic compounds or oxides [17] (see in Figure 3-5). Examples of these materials are YBCO, BiSCCO and MgB2. The HTS give rise to more possible applications for superconductors. Because of the higher critical temperature, the cooling system can become cheaper, but also the critical field and critical current density can be higher at these temperatures. Since these properties also depend on the material internal orientations, doping concentration etc., the superconductor can be specifically optimized for certain applications.

3.2.3. Meissner effect, flux pinning and hysteresis

The Meissner effect defines the superconductor's complete repulsion of magnetic fields inside the bulk of the material [17]. This complete diamagnetism can be explained by the superconductor not allowing a magnetic field to change inside the bulk of the material. If the field tries to change (like moving a magnet near the material) it induces a voltage in the superconductor (Law of Faraday) like in most conductors. But since the superconductor has no resistance and thus no losses, the induced voltage will lead to a high current without any losses producing a magnetic field that cancels the external field change completely. Because of this effect the superconductor maintains the same internal magnetic field as when the material was brought into the superconductor state.

Due to the Meissner effect a superconductor repels flux lines, however when they become too strong they can penetrate the material and the superconducting mode for a Type I superconductor is lost. For a type II superconductor when the flux lines start penetrating the material, it enters the mixed state of superconduction. The flux lines keep on penetrating into the material with increasing flux strength until they have fully penetrated the material and the superconductivity is lost [18].

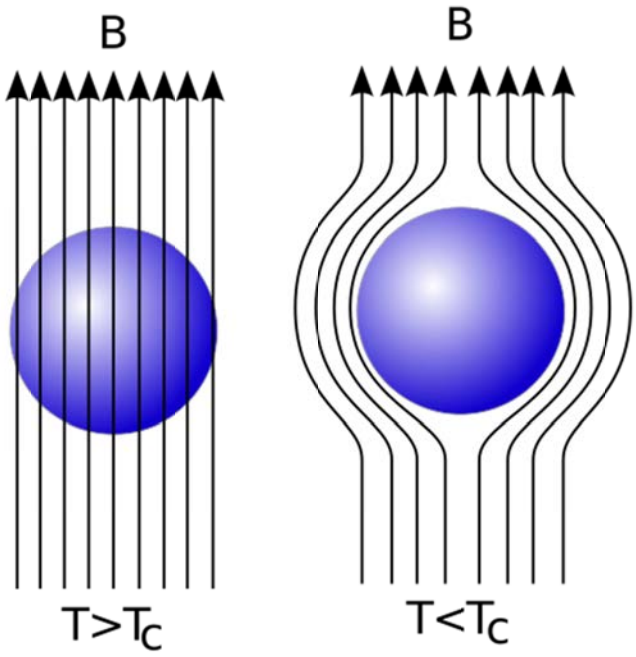

Figure 3-5 Flux repulsion: left the material is not in the superconducting state and right the material is superconducting and no flux lines penetrate the material. [19]

When the flux lines try to penetrate the bulk of a type II superconductor extra work is needed, because the flux inside the superconductor is "pinned" due to e.g. inhomogeneities or impurities in the material [20]. This flux pinning effect is very similar to hysteresis in ferromagnetic materials with three important consequences.

Firstly, when an external magnetic field is applied and later removed, some of the flux remains "pinned" which offers the possibility to trap a magnetic field inside a superconductor to use the material as a kind of a strong permanent magnet.

Secondly, the extra work needed to overcome the flux pinning effect introduces losses comparable with the ferromagnetic hysteresis losses. This means that when a changing magnetic field inside the superconductor is stronger than a certain critical value, **heat losses** occur [21].

Thirdly, because heat losses occur inside superconductors when exposed to changing fields, most applications use superconductors only to produce DC fields or to transport DC currents. This has consequences for the possible applications.

3.2.4. Superconducting materials

There are many different superconductors known today, yet few have critical values that are practical. Also a lot of research and development is needed on these materials before they can be used for high performance applications. Only five materials are considered mature enough in the present or the near future. These materials are: NbTi, Nb3Sn, MgB2, BiSCCO and YBCO. An overview of the basic properties of the practical superconductors can be seen in Table 3-1.

Material	T_c (K)	Anisotropy	J_c (A cm^{-2})	H_c (T)	H_{irr} (T)	Normal state R (μΩcm)
NbTi	9	Negligible	~10^6	11-12	10-11	60
Nb_3Sn	18	Negligible	~10^6	25-29	21-24	5
MgB2	39	1.5-5	~10^6	15-20	6-12	0.4
Bi-2223	110	20-200	~10^7	>100	0.2 (77K)	40-60
YBCO	93	5-7	~10^6	>100	5-7 (77K)	150-800

Table 3-1 Overview of the basic properties of the practical superconductors [22]

3.2.5. Low temperature Superconductors

NbTi and Nb_3Sn are low temperature superconductors with a critical temperature of 9 and 18 K respectively. As a material they are relatively easy and cheap to produce in long wires and a lot of experience has been gained in the industry by their application as superconductive coils for projects like the ITER or LHC [22]. Very powerful magnets are made with these materials, but the common disadvantage for the low temperature superconductors is that they have to be cooled with the expensive liquid helium. Because of the low working temperature these materials are considered less optimal for aerospace applications (see paragraph 3.5 Cryocooling).

3.2.6. MgB_2

A rather recent discovered superconductor is Magnesium diboride. With a critical temperature of 39K it is barley considered a high temperature superconductor. Being a simple bionic compound this material is very easy and cheap to produce and it can be shaped in virtually any shape.

This material can be cooled down with gaseous helium, which makes it more practical than LTS, but the critical temperature is much lower than that of the high temperature superconductors. Yet the possibility of producing thin stranded wire makes it more resilient to AC losses. This allows MgB_2 to be used in applications where other superconductors suffer from major AC losses. However, since helium is necessary for cooling, most of the advantages of using MgB2 for aerospace are negated, making this material also less suitable.

3.2.7. High Temperature Superconductors

The High Temperature Superconductors (HTS) of most interest are the cuprate materials. At this moment there are two major cuprate families considered for commercial application: Yttrium Barium Copper Oxide, or YBCO and Bismuth Strontium Calcium Copper Oxide, or BiSCCO. These materials are complex ceramics that are characterized by their oxide layered atomic structure as can be seen in Figure 3-6.

These high temperature superconductors have high critical temperatures of more than 77K and can be cooled with liquid nitrogen. Because of their high critical values these materials are chosen for most high performance electrical machines and magnets in literature. Also for the design of the electrical motor in this thesis they are considered the better choice.

Compared to the low temperature superconductors, the cuprates are much more difficult to produce, but because of the high critical values, especially the temperature, a lot of research is being carried out in order to make the material commercially available.

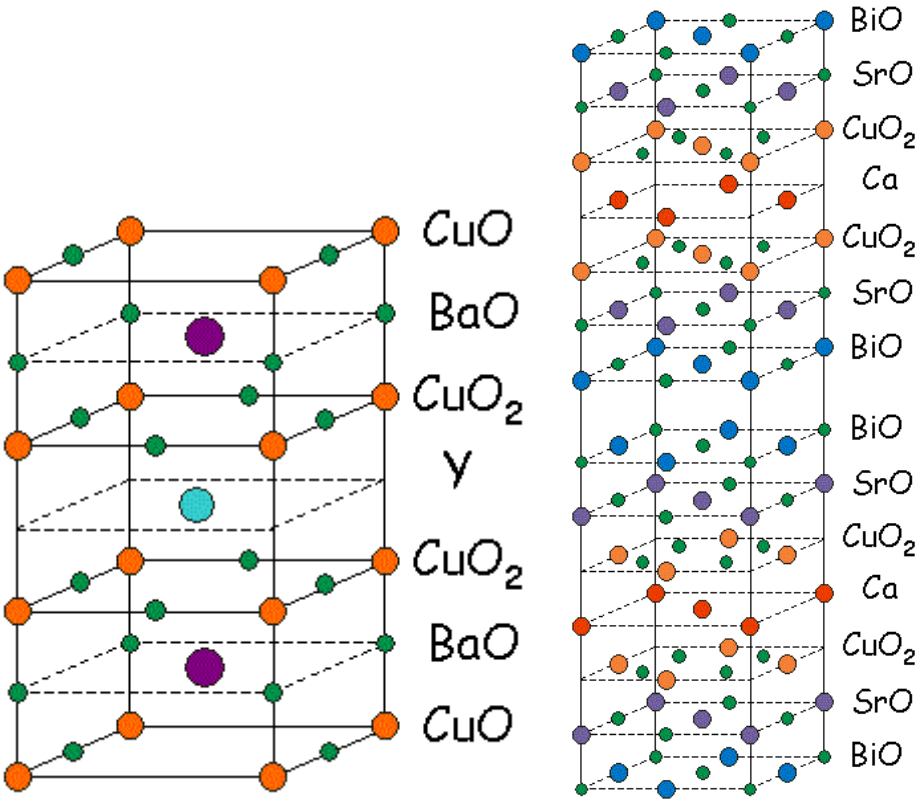

Figure 3-6 Atomic structure of YBCO (left) and BISCCO (right) [23]

Both HTS materials are used in literature for building coils, however most projects involve BiSCCO taped coils because of its currently better availability and price compared to YBCO. But when comparing the material properties YBCO is superior in terms of mechanical robustness and magnetic field critical values.

The most important difference between BiSCCO and YBCO is the anisotropy of the critical current depending on the direction of the magnetic field. In the industry the normal and the perpendicular field with respect to the face of the tape are defined as illustrated in Figure 3-7. These two field directions result in the maximum and minimum critical current of the HTS tape, but the transition is as shown in Figure 3-8 where 0 degrees corresponds with the normal direction and 90 degrees with the perpendicular direction. From the figure it seen that the critical current for the normal direction is about 2-3 times higher compared to the current of the parallel component in the case of YBCO tape.

This anisotropy effect is much higher in BiSCCO. The difference is critical current between the two components for these tapes is about 10-200 times. This means that e.g. with a normal critical field of 2 Tesla, the perpendicular critical field is 0.2 Tesla or lower [24]. This direction dependency has to be taken into account when designing a HTS coil. For example to build high field magnets with BISCCO, most groups like at the university of Southampton use iron flux diverters to lower the normal field [25]. This approach does not result in an optimal high field and low weight design.

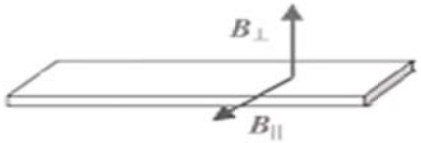

Figure 3-7 Definition normal and perpendicular field direction [14]

As a conclusion, the high temperature superconductors are the best choice to design the highest performance coils without cooling down to extreme low temperatures. The two HTS materials are very similar, but because of the better mechanical performance and anisotropy YBCO is chosen to be the material for the design of this thesis. From here on only YBCO technology is considered.

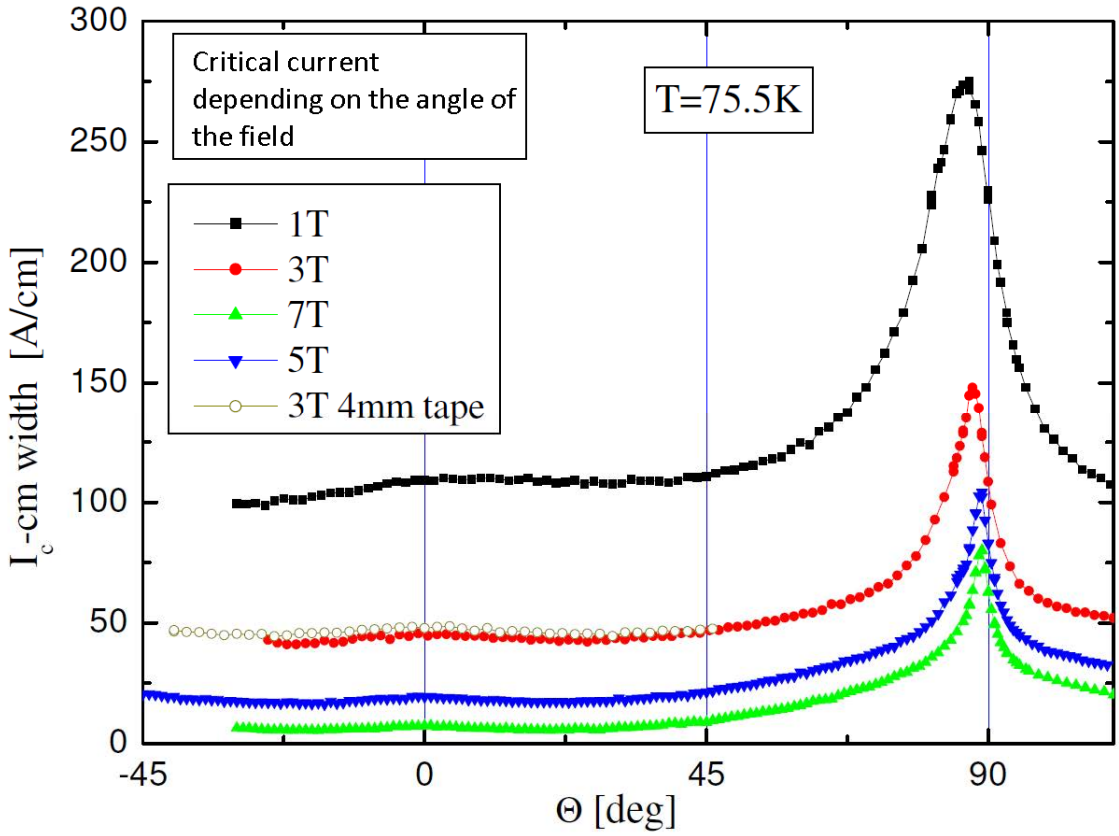

Figure 3-8 Dependence of the critical current as function of the direction of the magnetic field for a YBCO tape sample (courtesy of Superpower inc.)

3.3.YBCO tapes

The performance of the cuprate superconductors like YBCO is greatly determined by the alignment of the CuO2 planes in the unit cell of the material lattice (Figure 3-6). Achieving a high level of alignment in the planes of the grains of the superconductor material is essential to have high performance [26]. In order to realise this the superconducting wire has to be made as tapes in a carefully controlled production process.

One way to obtain the bi-axial alignment of the planes is to grow the YBCO on a bi-axially textured substrate using thin film technology [27]. Most coated conductors are produced with either the rolling assisted biaxially textured substrates (RABITS) technology or the ion beam assisted deposition (IBAD) or variants of these technologies [28].

The RABITS technology is mainly developed by American Superconductor (AMSC) and is a high speed, continuous reel-to-reek deposition process. This production process comparable to the production of motion picture film and is therefore low cost oriented. The IBAD or similar technology is used at companies like Superpower to produce YBCO coated conductors. Using an ion beam to assist the physical vapour deposition (PVD), multi-layer structures are produced [14].

A very important property of the YBCO is that as a ceramic it is very brittle by nature. Mechanical stresses like bending or even the self-induced magnetic forces can damage the material. Therefore to

provide the necessary mechanical strength, the superconductor material is sandwiched between different layers of materials that provide mechanical strength and thermal conductance [29]. A typical coated conductor consist of only about 1 volume percent of superconductor material, see Figure 3-9 for the layered structure of the tape made by Superpower [30].

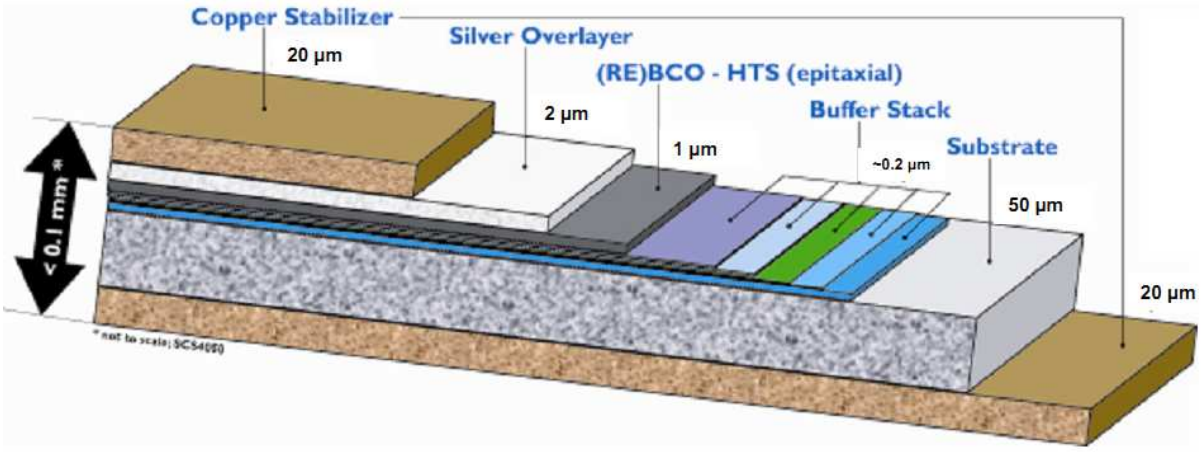

Figure 3-9 Layered coated conductor from Superpower [30]

3.4.Superconducting coils

Producing coils made of superconductors is not always straightforward. Some superconductors like the LTS and MgB2 are produced as wires very similar to conventional copper wires that can be wound into coils.

Compared with conventional wires, YBCO tapes have strict bending restrictions that make conventional coil winding not possible. A popular method to construct HTS coils is using stacked double pancake racetrack coils. These coils are made out of a disk (or pancake) consisting of a single tape winding which is then stacked. In Figure 3-10 an example of such a coil is illustrated.

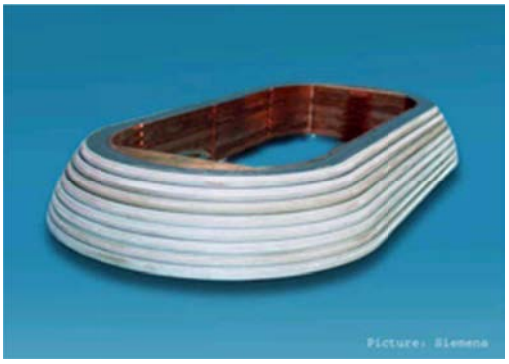

Figure 3-10 HTS stacked pancake coil [31]

Aside from wires or tapes also superconductor bulk material is of interest. These bulks are made with a different production process that is much easier and cheaper. By using the Meissner effect field differences can be made in an existing DC field and by using flux pinning an external applied field can be trapped inside the material creating a kind of superconducting “permanent magnet”.

HTS YBCO Bulk material is fabricated using the quench and melt growth process (QMG) in rather large sizes as single of multiple crystals [28]. This method is very different from RABITS or IBAD producing quasi-crystals called grains instead of wires. These grains are produced in different shapes like round or squared pucks with sizes varying from 20 mm in diameter up to 75 mm. Some different bulk products from THEVA can be seen in Figure 3-11.

The main challenges in the bulk material processing are the increase of flux pinning and material strength. The increase of material strength is not only important when high forces act on the material, but more because of the high magnetic forces inside the material.

The bulk production technology is less matured than for the coated conductor technology meaning that a lot of the production and research is still done at universities and research centres like IPHT or some companies like Nippon Steel and THEVA.

Figure 3-11 Samples of bulk material manufactured by THEVA [32]

3.5.Cryocooling

As is explained in the previous section, every superconductor has to be cooled down to extremely low temperatures of between 4 and 77 Kelvin. To achieve these temperatures a cryocooling system has to be used. The main parts of such a system are the cryogenic coolant, the cryocooler and the cooling loop that connects the cold part with the cryocooler.

3.5.1. Cryogenic coolants

The purpose of the coolant is to bring the superconductor on its operating temperature, to remove any additional heat and to act as an extra thermal mass. There are five different materials that are not solid at these low temperatures: Helium, hydrogen, neon, nitrogen and oxygen. Their properties together with water for comparison are listed in Table 3-2 [17].

Of the fluids, hydrogen and oxygen are not preferred due to the danger of fire. Especially oxygen, since in combination with materials like aluminium and Teflon, it can become combustible [14]. Hydrogen can be used in certain applications where the safety can be guaranteed. The remaining cryogens are not combustible and do not react with other materials.

Most low temperature superconductors operate around liquid helium temperatures (4 K) so only (liquid) helium can be used. Considering MgB_2, also neon is available, but for higher performance only helium is suitable. In the case of the high temperature superconductors liquid nitrogen can be used for lower field applications [14]. For higher field applications neon, helium or even hydrogen can be used.

Property	**He**	**H_2**	**Ne**	**N_2**	**O_2**	**H_2O**
Boiling temperature (K)	4.22	20.39	27.09	77.39	90.18	373.15
Triple point (K)	-	13.96	24.56	63.16	54.36	273.15
Specific heat of liquid (kJ/kg K) @ 1 atm	5.193	9.668	1.877	2.042	1.669	4.186
Heat of vaporization, liquid (kJ/kg)	20.9	443	85.9	199.3	213	2257

Table 3-2 Properties of relevant cryocoolants and water [17]

3.5.2. Cryocooler

The cryocooler is the device that subtracts heat from a cold source and can cool it down to cryogenic temperatures. There are five common cryocooler types which operate on different principles, but they are all based on compression and expansion of a gas to produce temperature changes [33]. Although not for every application a particular operating principle may provide the best performance, here the properties of the cryocoolers in general are discussed. For aerospace the most important properties are the efficiency, volume, mass and reliability of the cooler.

The first important aspect of a crycooler is the low efficiency. The Carnot efficiency explains the maximum theoretical efficiency a cryocooler can have according to the second law of thermodynamics:

$$\eta_{th} \leq \frac{T_C}{T_H - T_C} \qquad \textbf{(3-2)}$$

T_C and T_H stands for the temperature of the cold and the hot part of the system respectively. According to the formula, the maximum efficiency of a cryocooler at room temperature and cooling a cold mass at 65 K, would have a maximum efficiency of only 25% and when cooling down a mass to 20 K the maximum efficiency drops to 7%. The efficiency of the cryocoolers themselves can be expressed in the percentage of the Carnot efficiency and reaches from about 1-20% not taking into account special systems like those for space applications.

Brake & Wieferinck [34] have performed a good survey on the state of technology of cryocoolers. The maximum efficiency of the cryocoolers as a function of the operating temperature is given in Table 3-3. As can be seen from the table, the total cryocooler efficiency is very low even for temperatures as high as 80K.

The mass of a cryocooler is determined by its operating principle, temperature and cooling power. Generally when more heat has to be removed (Q_C) and when the operating temperature is lower, the heavier the device becomes. The mass for different cooling capacities at 40K and 80K is given in Figure 3-12 and Figure 3-13 respectively**.** Based on examples in literature, the heat that has to be removed from the cryostat is expected to be in the range of 100 – 200 W. From the figures, the mass of the cryocooler alone would expectedly be 100 kg or more. The volume of the cryocooler is directly proportional to its weight and is given in Figure 3-14. Assuming a cryocooler of 100 kg the volume of the cryocooler alone would be about 125 litres or 0.125 m^3.

$T_H\ (K)$	$\eta\ (\%\ of\ carnot)$	$\eta_{total}\ (\%)$
4	1-2	0.01-0.03
10	2-5	0.07-0.17
20	5-10	0.33-0.67
40	10-20	1.33-2.67
80	10-20	2.67-5.33

Table 3-3 Efficiency of cryocoolers at different operating temperatures [34]

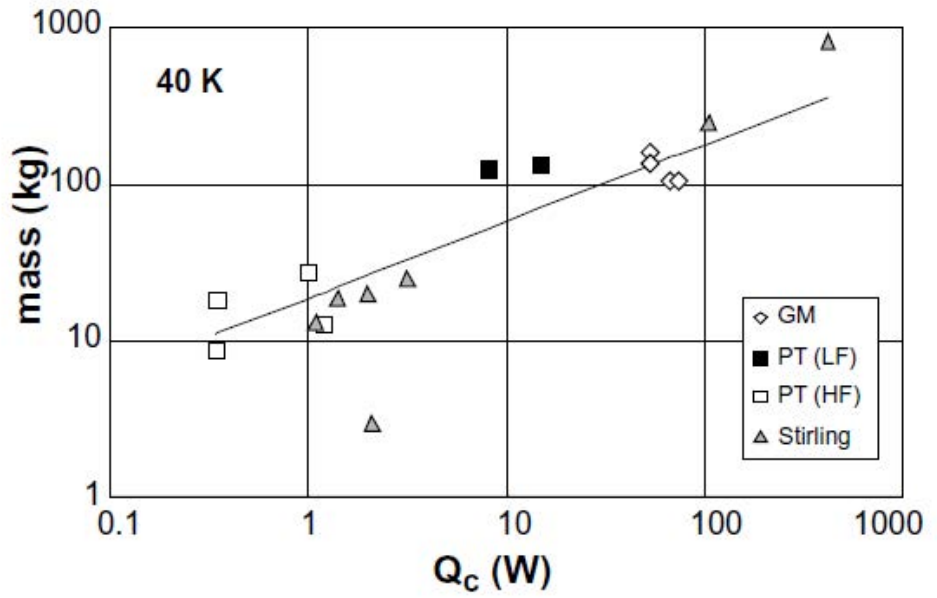

Figure 3-12 Mass versus cooling capacity of cryocoolers operating at 40K [34]

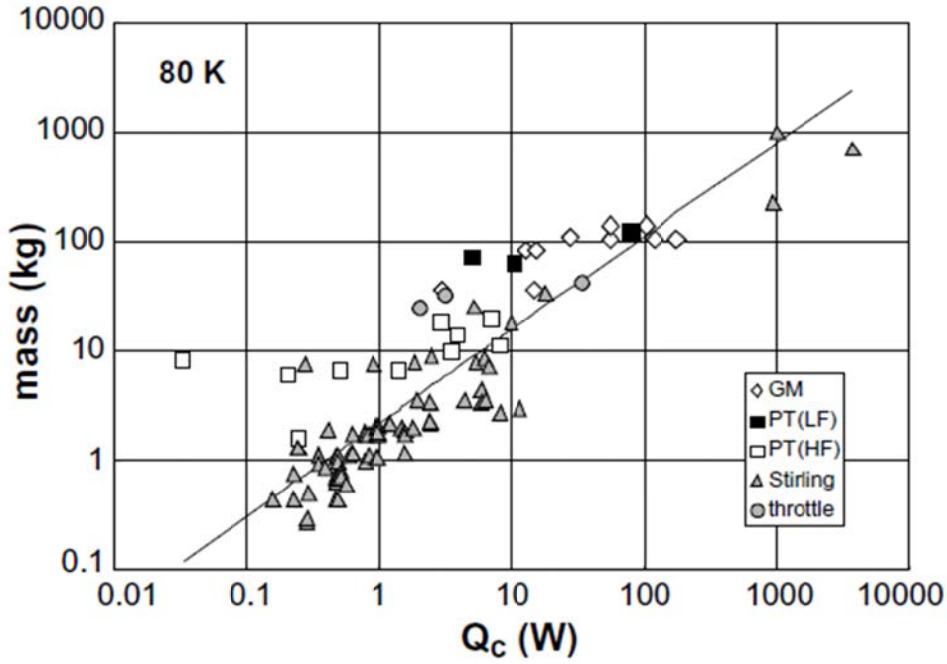

Figure 3-13 Mass versus cooling capacity of cryocoolers operating at 80K [34]

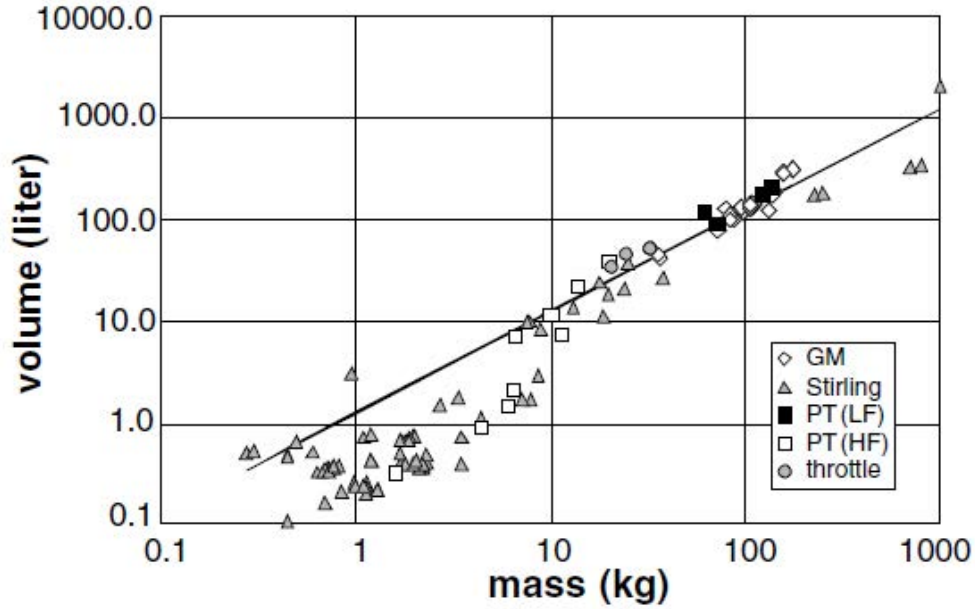

Figure 3-14 Volume versus mass of cryocoolers [34]

According to Brake & Wieferinck [34] their survey on cryocoolers matches well with nearly all the available cryocoolers excluding the newer pulse tube types. Pulse tube cryocoolers start to become useful for temperatures above 60K and they excel in their power density. These coolers are therefore only useful when operating at liquid nitrogen temperatures. Also important to note is that most commercially available cryocoolers are designed for long and economical operation where efficiency is very important and weight and volume are unimportant, while for aerospace the design goals are quite the contrary.

Because of these reasons Lockheed Martin developed a new pulse tube cryocooler that is fully optimized for low weight, low volume and high capacity that is aimed for space applications like cooling optical components for satellites (see Figure 3-15) [35]. This device weighs only 7 kg and can provide 20 W of cooling at 70K at a 300K ambient temperature, see Figure 3-16. From the figure it can be seen that the cooler can achieve a good cooling power at very low efficiencies, which is acceptable.

Considering the Lockheed Martin cryocooler for the helicopter propulsion motor, the cryocooler weight to remove 100 W at 65 K would be about 50 kg which is 50% lighter than when using commercial cryocoolers. This makes the use of a cryocooler more feasible when operating at higher temperatures like the liquid nitrogen range.

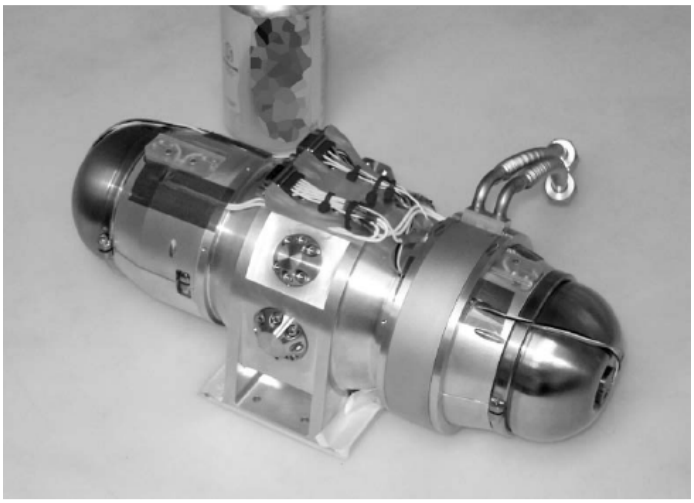

Figure 3-15 Aerospace cryocooler from Lockheed Martin [35]

3.5.3. Cryosystem

The whole cryosystem consists of the cryostat containing the cold mass, the cryocooler and the cryocoolant that transports the heat from the cold mass to the cryocooler. This closed loop system is considered for most superconductor applications like power cables, windturbines and utility generators. These are all stationary systems that require continuous and (cost) efficient operation. Important for aerospace is the total weight of the closed loop system which is mainly determined by the cryocooler.

For aerospace also an open system is considered. The open system breaks open the coolant loop by storing the coolant in tanks after production by a stationary cryocooler. The coolant is then used from the tank and after use it is disposed in the air.

Since the coolant has to be produced and is disposed in air after use, the open loop system limits the available coolant to cheaper and more abundant materials like nitrogen or hydrogen.

The open loop system restrains the cooling materials and therefore the operating temperature. It loses the possibility of continuous operation, but it can gain the important lower weight and volume. Yet the actual properties of the cooling system are determined by the total system design and optimization.

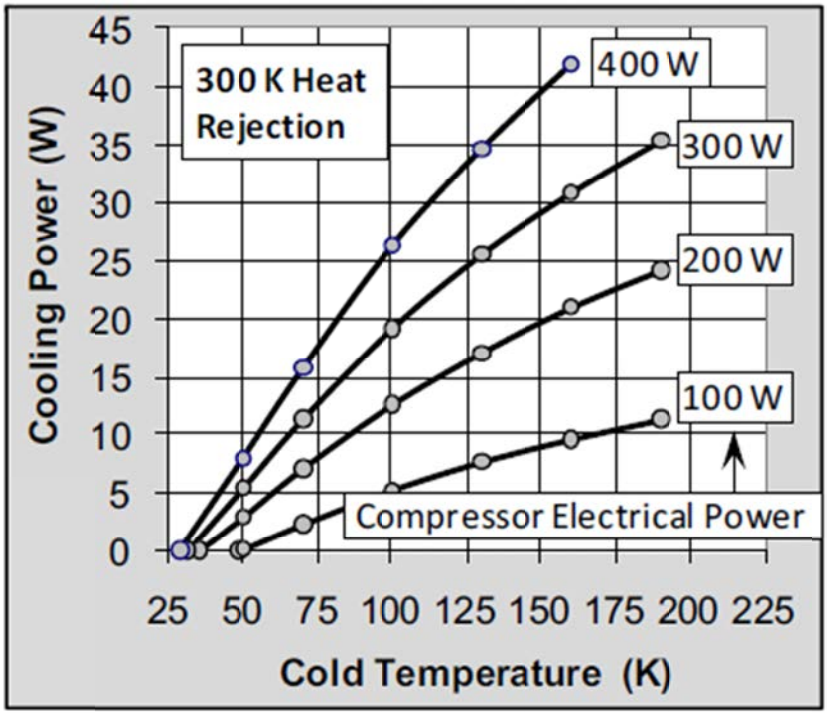

Figure 3-16 Cooling power at different cold temperatures for different input powers [35]

3.5.4. Thermal stability

Important for any cooling system is the guarantee that a certain temperature is maintained during the whole operating time. On a superconductor wire local hot spots can occur due to non-uniform critical currents or due to cooling issues. These hotspots can locally drive the superconductor out of its superconducting state. The resulting local high resistance and high current will lead to extreme heating is called a quench, which can seriously damage the superconductor [36].

Clearly, these quenches need to be avoided at all costs. First the cooling system should reliably keep the cold mass on the specified temperature. But still because of e.g. a cooling failure, a local degradation of wire and insulation, pollution of the coolant, power spikes on the power supply etc, a quench can occur. Therefore a quench has to be detected on time and adequately be removed before the material is damaged.

Experience on quench detection and removal methods is abundant for the low temperature superconductors due to its use in MRI systems and for projects like the LHC and ITER. For the high temperature superconductors this experience is almost non-existent and yet because of their non-uniform properties these quenches might become a very important issue [36].

Although thermal stability is an essential part of the feasibility of any superconducting application, it can only be included into the final stages of the design and thus it falls outside the scope of this thesis.

3.6.Conclusion on superconductivity

In this chapter, the most important parts of the superconducting theory, including the critical parameters and flux repelling effects, are discussed. Also different superconductors are analysed for their performance with the result that YBCO technology is chosen for its electrical performance and high operating temperature. It is concluded that the technology can be used as tapes or Bulks to make coils. It is noted that superconductors suffer from AC heat losses and that therefore DC applications are advised.

Finally, the cooling system is studied which resulted in the choice of using liquid nitrogen at 65 Kelvin. Also the issue of the cryocooler weight is covered and the possibility of an open loop system is described. The actual choice on how the cryostat will be cooled will be made after the machine and cryostat are designed.

4. HTS machines

In the previous chapter the theory of superconductivity and how it can be used to build coils was explained. In this chapter the implementation of superconducting coils for electrical machines is discussed.

Because of the specifications of this thesis design it is not obvious what type of design is best, since there are many different ways to build superconducting machines. In literature many papers can be found for this application, but only few consider this technology for aerospace applications. This makes it impossible to select a specific machine type without first studying the different topologies.

The aim of this chapter is therefore to perform a literature study to select one or two possible superconducting machine topologies as candidates for the thesis motor design. To accomplish this, first the performance of conventional machines is discussed for comparison. After that the advantages and disadvantages of superconducting machines are explained and lastly the different promising topologies of superconducting machines are evaluated. The selected topologies are then further analysed in chapter 5.

4.1.Conventional electrical machines for aerospace

In aerospace, several conventional electric machines are currently used or considered for different applications. Examples are the electrical generators that are directly coupled to the turbo fan engines to provide electrical power to the airplane, the electrical motors that are considered for compressors to maintain the cabin pressure and the experimental propulsion motors for the more electric aircraft mentioned in chapter 2.

It is useful to mention the performance of current conventional machines so that they can be compared with the superconducting types. To make a good comparison between the different topologies, the torque densities should be compared. However, here only the power densities are compared, since mostly only the power densities are available in literature.

Conventional electrical machines commonly have poor power densities due to the use of high dense materials like iron and copper. In order to meet the requirements of the aerospace industry, the common design solution is to use high operating speeds of 2000 - 4000 RPM. At these high speeds, power densities in the range of 0.5-2.5 kW/kg are possible. These motors can be used for the direct drive propulsion of small airplanes [5] or, when using a gearbox or belt pulley, to propel a small helicopter [6].

The target power density for the direct drive helicopter propulsion motor is 4-5 kW/kg, which is about double of what most high speed conventional motors can achieve. Taking into account that the propulsion motor of this thesis has to achieve this power density at a much lower speed of 341 RPM, it is clear that conventional machines cannot reach the specifications.

4.2.Advantages and disadvantages of superconducting machines

Superconducting machines are currently researched in literature for many different applications where usually a high efficiency or a high power density is required. Yet using superconductivity has not only advantages but also machine specific disadvantages.

The main advantages of using superconducting wire come from their extremely high current density of between 10 to 1000 times that of copper [30]. This allows very high field coils which lead to higher airgap fields or a higher armature loading, which in turn result in a very high power dense machine.

Because of the high current densities, it is possible reach the high airgap fields without any active iron [37]. Without the heavy iron, these ironless or aircore machines have a very high specific power density. Removing the iron also removes the iron specific issues like iron core saturation and hysteresis losses.

Using superconductors often results in increased machine efficiency [37]. This is because the superconductors usually replace copper wires. The reduced losses due to the removal of the copper joule losses are typically greater than the extra cooling power required to maintain the cryogenic temperatures.

Apart from using superconducting wires, also the bulk materials can be used. By using their flux trapping and flux shaping properties, different machine designs are possible which can be lighter or more power dense than comparable conventional machines.

Using superconductors also comes with several disadvantages. Firstly the complete cooling system can be bulky, heavy and may require a lot of maintenance. This could counteract the advantages of using a superconducting machine at all. Therefore it is important to limit the cooling requirements as much as possible.

Secondly, to keep the superconducting components cooled down efficiently, they have to be placed in a well-designed cryostat. An essential part of the cryostat is the vacuum wall that reduces the thermal conduction to the cold part and it has to surround the whole bulk of superconducting components. Usually only the field coils are superconducting, which means that the vacuum wall also participates to the airgap length. This increases the airgap from several millimetres in conventional machines, to several centimetres for superconducting machines. This has negative effects on the machine power density, but in turn it also increases the machine reluctance which has a positive effect on the machine dynamic performance.

Another possible complexity of the cryostat is the issue of transporting the cryogenic coolant to the superconductors. Most designs in literature have the cryostat placed in the rotor. This means that a special rotating coupling is required to transport the coolant back and forth between the stationary and rotating parts. The cryogenic coupling doesn't have direct influence on the machine performance, but the component can be quite bulky which can result in design problems.

A less superconducting specific disadvantage is the requirement to transport current to the rotor. This is the case for most superconducting topologies, like the synchronous machine design, but also for many conventional machines. The current is usually transported with the use of brushed slip rings, or if possible with a brushless exciter. In aerospace the trend is to remove all brushes, because of their inherent high maintenance requirements. For this reason most aerospace designs are permanent magnet machines and thus using a superconducting machine would go against the industry trend.

In literature, superconducting machines are equipped with brushes to supply current to the superconducting field windings on the rotor if the current rating is low or with brushless exciters if the current becomes too high for brushes. Although the brushed slip rings have a higher maintenance requirement they are lightweight and small in volume compared to the brushless exciter, which uses a high frequency air coil together with power electronics to transport the power without mechanical contacts. Since both solutions have their disadvantages, it is not evident which solution is best although a machine design that needs no current at all in the rotor is preferred.

Finally a very important issue with superconducting machines is the limited experience and matureness of the current technology. This means that there is currently not much knowledge and experience with the reliability of these machines. Yet compared with conventional machines, superconducting machines add additional components that can fail like those of the cooling system. On top of that the superconductors introduce the quench failure mode, which implies that when the cooling systems (temporarily) fail, the superconductors have to be completely switched off to prevent damage. Especially for aerospace a backup solution for this is required like a safely torque squirrel cage [38]. In Table 4-1 the advantages and disadvantages are listed.

Finding a good solution for the disadvantages while keeping the advantages like the power density is great challenge for the designing phase. The choice of the machine topology has an important influence on the effects of the advantages and disadvantages, since some may suffer more from certain drawbacks than others. In the next chapter different topologies are discussed.

Advantages	**Disadvantages**
Ironless machine (less weight)	Need cryostat and cryogenic cooling system
No iron saturation (linear characteristic)	May need cryogenic rotating coupling
High torque (specific) density	Limited availability of HTS material
High reluctance and low inductance resulting in mechanical stiff behaviour	Large airgap due to cryostat
Higher efficiency (including cooling system)	Reliability not well researched
	Introduces new failure modes (quenching)

Table 4-1 Advantages and disadvantages of using superconductivity for electrical machines

4.3.Fully or partly superconducting machines

An electrical machine is made by replacing its copper/aluminium coils with superconducting variants. In literature most designs only replace the field windings that produce the stationary airgap field. The armature coils are still conventional. This partly superconducting machine type has a possible higher torque density compared to conventional machines.

Only few designs consider to also replace the armature coils with superconducting windings. Using superconductors to build these AC current carrying coils increases the armature loading, which results in an even higher possible torque density. This fully superconducting machine benefits most of superconductivity and has the highest torque capability. However, as explained in chapter 3.2.3, applying AC currents (and thus changing fields) on superconductors results in AC losses in the material. These losses resulted in the failure of one of the first fully superconducting concepts [39].

Currently few concepts are proposed using MgB_2 superconductor with helix windings for windturbine applications [40]. These designs require long axial lengths and low operating temperatures and are therefore not suitable for this thesis design.

Because of these disadvantages only the partly superconducting machine topology is considered for this thesis. This means that the armature coils will be made of copper or other resistive material and the field windings are made of superconductors.

4.4.HTS machine topologies

Most designs are proposed for applications like windturbines, ship propulsion and utility services. Especially windturbines are believed to be the thriving application for superconducting machines. Most designs in literature are focussing on these applications and they adopt the synchronous machine topology.

These applications have design conditions that are usually not comparable with those for aerospace applications. Only a few groups are researching superconducting machines for aerospace applications and also their designs are aim for different goals than the design in this thesis. Therefore the choice of machine topology is not straightforward.

Most designs are existing topologies of which the field windings are replaced with superconductors. Yet there are many different methods to design these field coils. Effectively any of the many different conventional electrical machines can be improved with superconductors up to a certain extend. Every topology has its own strengths and weaknesses which are dependent on the application. In this paragraph a small literature survey is done on the most promising topologies.

The following electrical machine types are currently described in literature:

- Hysteresis machine
- Synchronous machine
- Induction machine
- Trapped flux machine
- Bulk flux concentrated machine
- Homopolar DC machine
- Homopolar alternator inductor (HIA)

Of these topologies the hysteresis, induction and homopolar DC are only theoretical or not actively researched to be considered. The trapped flux topology is currently too underperforming and the HIA, although considered for aerospace, only performs well at very high speeds of more than 10.000 RPM. The remaining topologies are considered for this thesis design and they are now described. A choice in topology is made in the next chapter.

4.4.1. Synchronous machine

The most popular machine topology is the synchronous machine where a conventional copper stator is used and the excitation coils in the rotor are replaced with superconducting coils. In literature, this machine type is considered for nearly every possible application from direct drive windturbines to electric vehicle propulsion.

Of the countless designs in literature, the most interesting are the concepts that made it to the concept demonstrator phase. They show what is practical possible with current technology. Therefore, the most important demonstrators are now briefly described.

The first interesting concept demonstrators are the 400 kW and the 4 MVA generators made by Siemens aiming for utility applications [41]. The generators are 1500 RPM machines using BiSCCO field coils and copper stator coils with no iron. The Siemens machines showed very high power densities and very good dynamic properties due to the small synchronous reactance. Also, the 400kW machine is operated for more than 3 years without major issues, proving that stable operation is possible.

Another very important machine is the American Superconductor ship propulsion motor which is successfully build and is being tested at the US Navy [28]. This motor operates at 120 RPM and has a power rating of 36.5 MW. Using BiSCCO coils and an iron core design, the machine weights 75 tons and with a volumetric power density of 88 kNm/m^3 it proves that a the synchronous topology

can practically deliver a very high power dense machine. It can be concluded that this design is an important step into building superconducting machines for mobile applications.

Another concept design is the Hydrogenie project that aims to install a superconducting synchronous hydroelectric generator in a hydro power plant in Germany [42]. The Hydrogenie generator is also built with BiSCCO coils for the field coils and it uses a conventional copper stator. In order to reduce the flux leakage a full iron design was used.

The generator was planned to be installed and tested in the summer of 2011, however there are no reports of the project progress since the successful testing in February 2011. The major delay of the project is possibly the result of certain setbacks during testing including cooling problems and delamination of the HTS tapes due to the high torque of the machine and effectively stating the continuous existing difficulty of this technology [18].

The great amount of research that is performed on this topology, the high number of concept demonstrators and the very promising results in terms of performance show great progress and possibilities, but there is still a lot of progress necessary before the technology is fully mature. The synchronous machine topology is therefore considered as a very good candidate for the hybrid helicopter propulsion motor.

4.4.2. Bulk concentrating flux machine

The bulk flux concentrated machine topology is one of the few topologies of which their operating principle differs much from most conventional machines. This topology creates the excitation field with one or more HTS coils that produce a DC magnetic field in the airgap. This field by itself cannot produce any torque, but by inserting HTS bulks inside the coils, the DC field is concentrated and suppressed at certain points. The magnetic field inside the HTS bulks will be reduced, because of the Meissner effect and the flux is concentrated to the spaces between the bulks. In this way magnetic poles are created that can produce torque.

The bulk concentrated flux topology is considered for windturbines and for aerospace applications. Ohsaki et all [43] proposed a superconducting windturbine using HTS bulks for flux concentration, see Figure 4-1. The superconducting rotor consists of several HTS coils that are wound around the whole rotor with superconducting bulks between the coils. The resulting current and fields are illustrated in Figure 4-2. The author chose an operating temperature of 20 K and the resulting field distributions at different radial distances from the coils is shown in Figure 4-3.

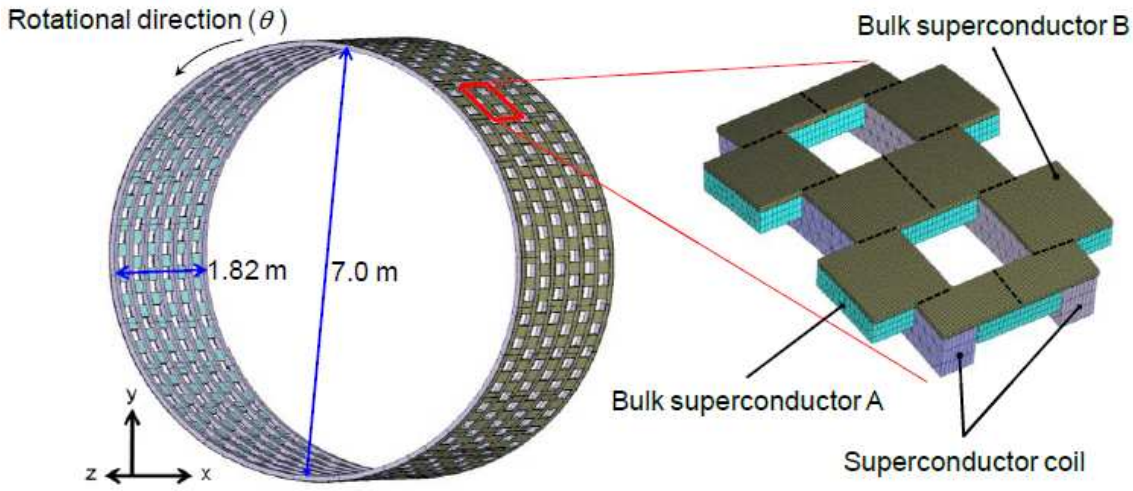

Figure 4-1 Windturbine design using a bulk concentrating flux design [43]

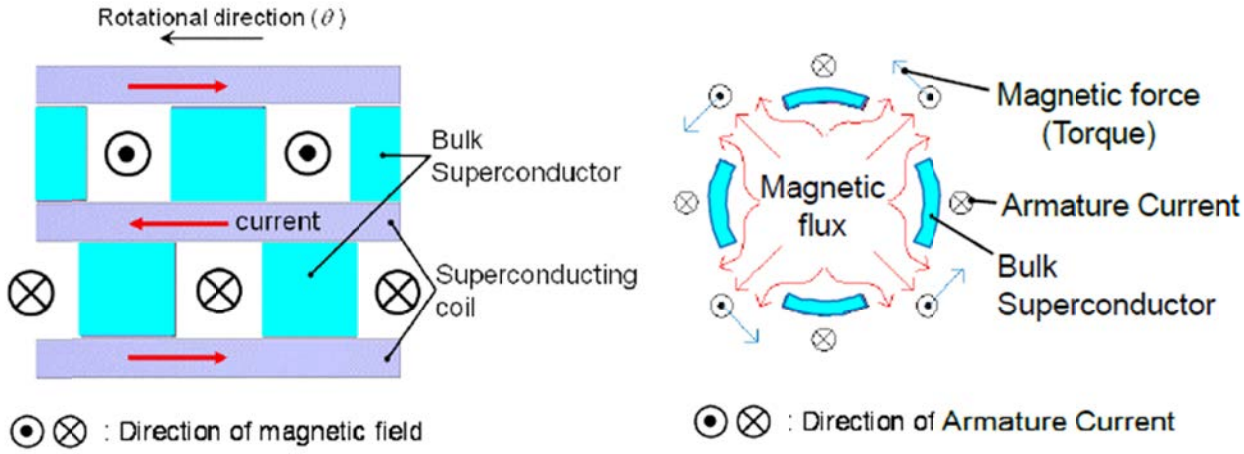

Figure 4-2 Fields and currents in the axial plane (left) and in the radial plane (right) [43]

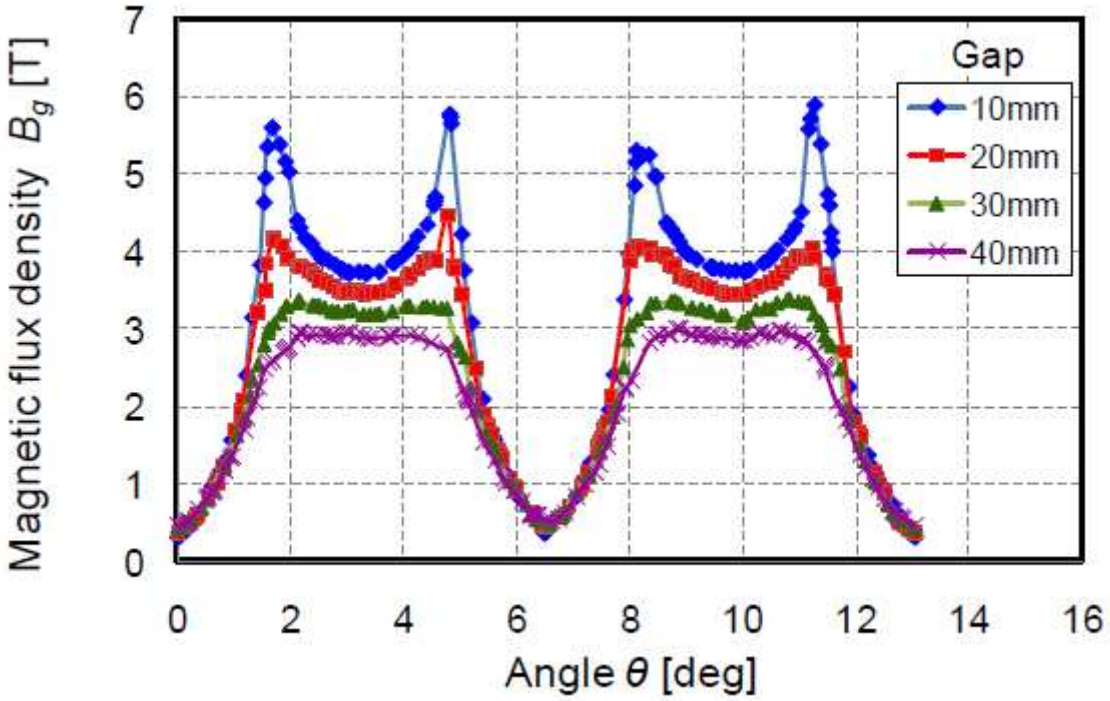

Figure 4-3 Airgap field in rotational direction at different radial distances from the coils [43]

The results show that rather high flux densities are achievable, but that the field rapidly decreases at greater distances from the coils (Figure 4-3). Using this field distribution and a conventional armature, the authors concluded that with this design a 10MW windturbine can be build. This study proves that high power dense HTS machines can be build using the bulk flux concentrating topology, but the effects on the rapid decrease of the flux at greater distances and the performance at higher temperatures is not clarified.

The bulk concentrating flux topology is also considered particularly for aerospace applications by P. Masson and C. Luongo [44] [45]. They performed a feasibility study to replace the gas turbine engines with a superconducting motor for aircraft (mainly airplanes). Their design aims to keep the current fan propulsion principle, but to replace the turbo engine with a high speed superconducting motor as illustrated in Figure 4-4. This is only possible if the motor can achieve a power density comparable to the turbo engine. The authors claim this is possible and they estimate a power density of more than 5 kW/kg for their motor [45].

The operation of the proposed motor is similar to the windturbine design by Ohsaki et all, but in this case the concentration effect of the bulks is increased by also trapping a field in the bulks [45]. This is done by keeping the bulks in the resistive state (about 90 K) with heaters, while the coils are in the superconducting state. Then the coils are activated and the bulks are cooled down, resulting in a trapped field in the bulks. Afterwards the current in the coils is reversed so that the bulks not only create the flux concentrations with the Meissner effect, but also the trapped field contributes.

The eventual motor concept that has to be placed in the turbofan has a high operation speed of 2700 RPM while cooling down to 30 Kelvin. The power density of more than 5 kW/kg is achieved mainly due to the high rotation speed, but the torque density is only 19 Nm/kg.

The studies of Ohsaki and Masson show that high power dense machines can be made with the bulk flux concentrated topology, but from both designs it is not clear how they perform at higher temperatures or when optimizing for different rotating speeds. Nevertheless, it is considered a good candidate for the propulsion system of this thesis, since the topology is particularly considered for aircraft propulsion systems and because of the high power density and low weight.

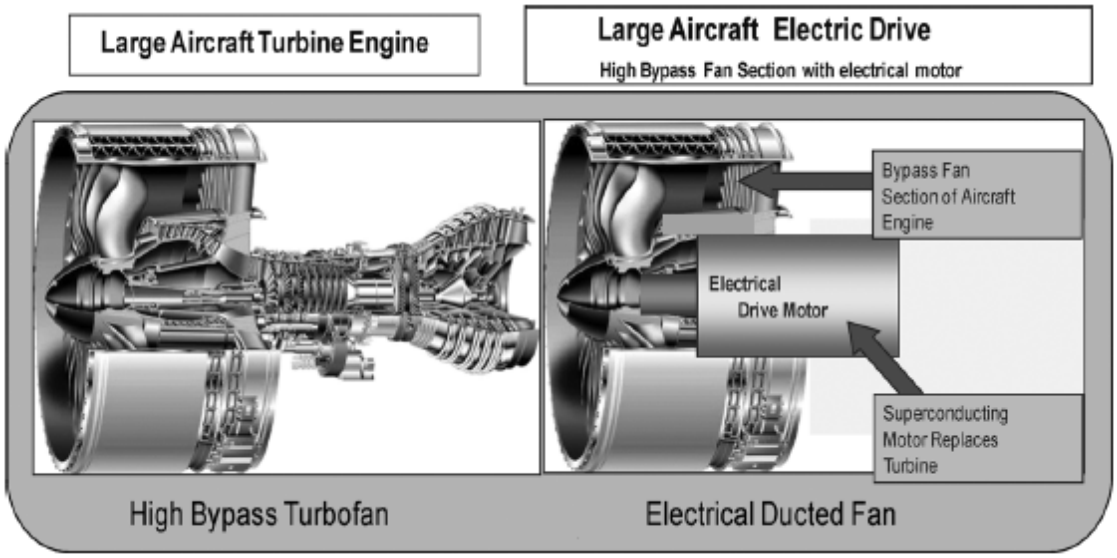

Figure 4-4 Replacement of a gas turbine (left) by a superconducting motor (right) [45]

4.5.Conclusion on HTS machines

In this chapter the implementation of superconducting technology for electrical machines is discussed. By performing a small literature study, the most suitable machine topologies are selected for the thesis design.

First the motor target specifications are compared to conventional machine technology. From this it was concluded that using conventional machines are not able to meet the specifications. Also the advantages and disadvantages of superconducting machines are described.

After that the most suitable machine topologies are analysed. The fully superconducting machine topology was first considered, because it theoretically offers the best performance of any other topology. Yet due to the expected high AC losses this topology is not selected for this thesis.

Of the partly superconducting machine topology, only the synchronous machine and the bulk flux concentrating machine are both very high performing and they are also considered in literature for aerospace applications. However, since a good comparison between the two topologies cannot be found in literature, the actual choice will be made in the next chapter after a more in depth analysis.

5. Machine Setup

In the previous chapters, the superconducting technology and two candidate machine topologies were selected by conducting a literature research. In this chapter the actual design of the whole machine is started. First, a plan of the design steps is given that is followed through the next chapters. Also several design choices are made that affect the machine as a whole. After these choices are made, the machine specifications like the airgap radius and stack length are given as a starting point for the designing process in the next chapters.

5.1.Design plan

The design of the total machine is subdivided in the following sections:

- **Total machine setup**. Here the main decisions are made that greatly affect the other design parts (discussed in this chapter).
- **Armature design**. Here calculations are made in order to make several choices on the design of the non-superconducting armature (discussed in chapter 6).
- **Superconducting field windings and cryostat design.** This part takes the design of the superconductors and cryostat into account, including most of the calculations needed for the next section (discussed in chapter 7 and 8).
- **Full machine analysis and optimization**. Here the results from the previous 3 sections are combined and the total machine performance is analysed and optimized. Calculations like the torque density and machine weight are performed (discussed in chapter 9).

In this chapter only the total machine setup section will be covered in this chapter. The other 3 parts are individually discussed in the following chapters. The total machine analysis consists of making three major informed choices:

- A choice between the bulk flux concentrating and wound coils has to be made
- The machine can be built as an axial machine or radial machine
- The machine can have a rotating armature or rotating field coils

The analysis needed to make these choices involve both literature studies and calculations. For the calculations often together with analytical models, also the Finite Element Method (FEM) is used. FEM simulations provide accurate calculations on magnetic fields for complex configurations and are therefore a very useful tool to design any electrical machine. However, the complexity of the method requires that it has to be briefly explained before it is used.

5.2.The Finite Element Method

The Finite Element Method (FEM) is a very useful tool to calculate complex magneto static problems. The advantage of using finite elements is that the field distribution of complex models can be calculated, which makes it very useful for design and optimization. However, because of the complexity of the method, errors can easily be made. Therefore analytical models are used to verify the results. For the FEM modelling and calculations, Comsol 4.3 is used together with Matlab 2011b for model building and post processing.

FEM numerically calculates an approximation of the solution of a partial differential equation. Since FEM is only used as a tool in this thesis no description of the method itself is given. Though, it is important to mention the fundamental equations used for the simulations. For the magneto static problems in this thesis the following Maxwell equations are used:

$$-\nabla^2 A = \mu J_{ext} \qquad \textbf{(5-1)}$$

$$B = \nabla \times A \qquad \textbf{(5-2)}$$

With **A** the magnetic field potential, which is calculated with FEM and from this most other variables are derived. With these equations, together with the boundary condition set by the design and handled by Comsol, the simulations are performed.

5.3.Choice of topology

In this section a choice between the two candidate topologies, the synchronous machine and the bulk flux concentrating machine (explained in chapter 4), is made. Since in literature no direct comparison could be found in order to make a well informed choice, a direct comparison is made here using FEM simulations.

The aim is to compare the HTS coils of the two topologies of comparable weight and size. The performance is measured with the airgap magnetic field at a certain distance from the coil. The topology that offers the highest airgap field will be used in the design.

The study is done for comparison and only simple geometrical optimizations are made. The actual values may not be comparable to a fully optimized coil.

For the simulation the following assumptions are made:

- 3D FEM models
- Radial flux design
- Volume per pole: 15 cm axial length, 20 cm coil pitch and 5 cm slot depth
- Similar weight, obtained by using no iron at all
- The magnetic field is measured 2.5 cm above the face of the coil
- The comparing parameter is the maximum field difference between two adjacent coils. This difference is also the amplitude of the changing field or **the AC field**. This value is most important since it represents the contribution to the machine torque.
- Assume YBCO taped coils and YBCO bulks
- The operating temperature is liquid nitrogen at 65 K
- At 65 K a critical current density of 70 A/mm2 and a critical field of 2 T is considered a good starting point
- The coils are simulated as a solid material with the current density applied
- The HTS bulk material is simulated as simple as possible by using a material with a relative permittivity of 0.01 to include the diamagnetic effects [43].

5.3.1. Bulk concentrating flux setup

As proposed by Osaki and Masson, the bulk concentrating flux design consists of minimal two sets of HTS windings with HTS bulks in between. In this case only two windings are used, because of the small available axial length for the machine (25 cm for the total machine). In Comsol, the model of a section was made as seen in Figure 5-1**.** The section consists of two HTS windings with in the middle a piece of HTS bulk. On the left and the right side a periodic boundary condition is applied in order to simulate an infinite repetition.

There are two parameters still undefined: the axial lengths of the coils and bulks and the axial gap size between the bulks and coils. The axial length distribution has a direct impact on the measured magnetic field, since more coil windings result in a higher DC field. However, this means that there is less space for bulk material, resulting in a lower shaping effect of the DC flux.

The gap between the bulks and coils also influences the field distribution. The flux is also concentrated in this gap and these fields directly affect the HTS coils. Because of this in these gaps the critical field and current are determined. The gap length can be optimized, since a larger gap would result in a lower field in the gap and thus in a higher current density for the superconductors, but that means that there is less space left for the bulk material, resulting in a lower AC field.

With FEM simulations, an optimum of both the gap length and the length of the bulks and coils was calculated by sweeping both parameters, see Figure 5-2 for the results.

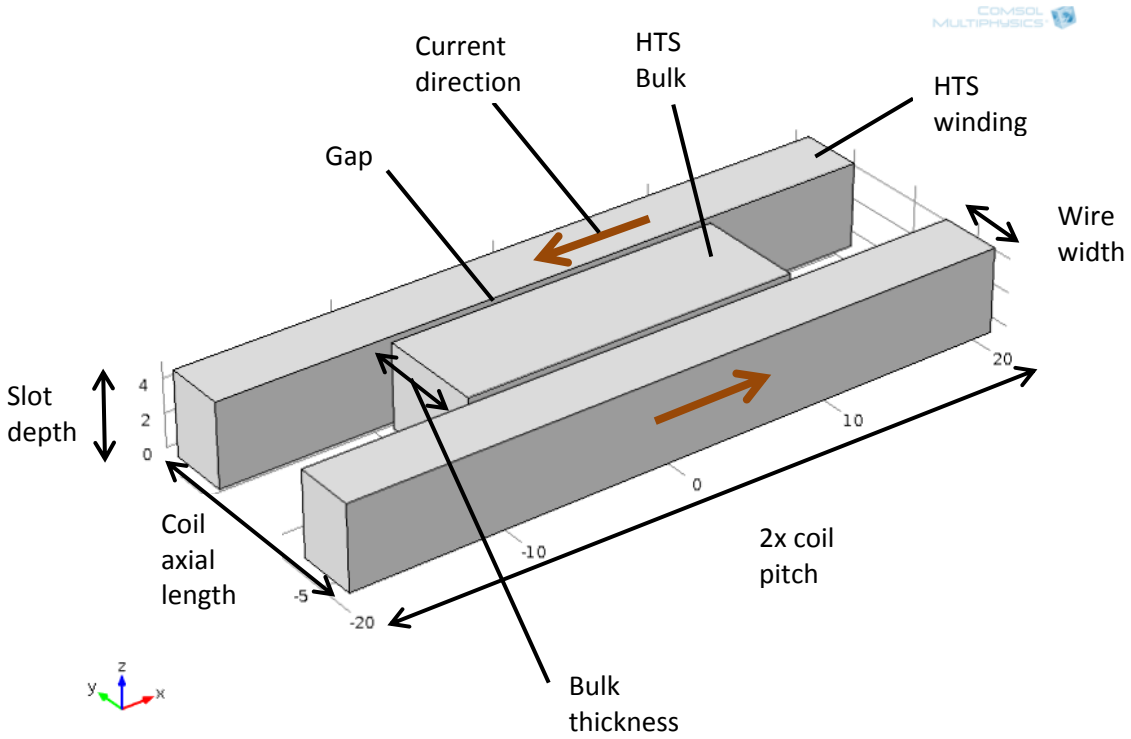

Figure 5-1 FEM model of the bulk flux concentrating setup

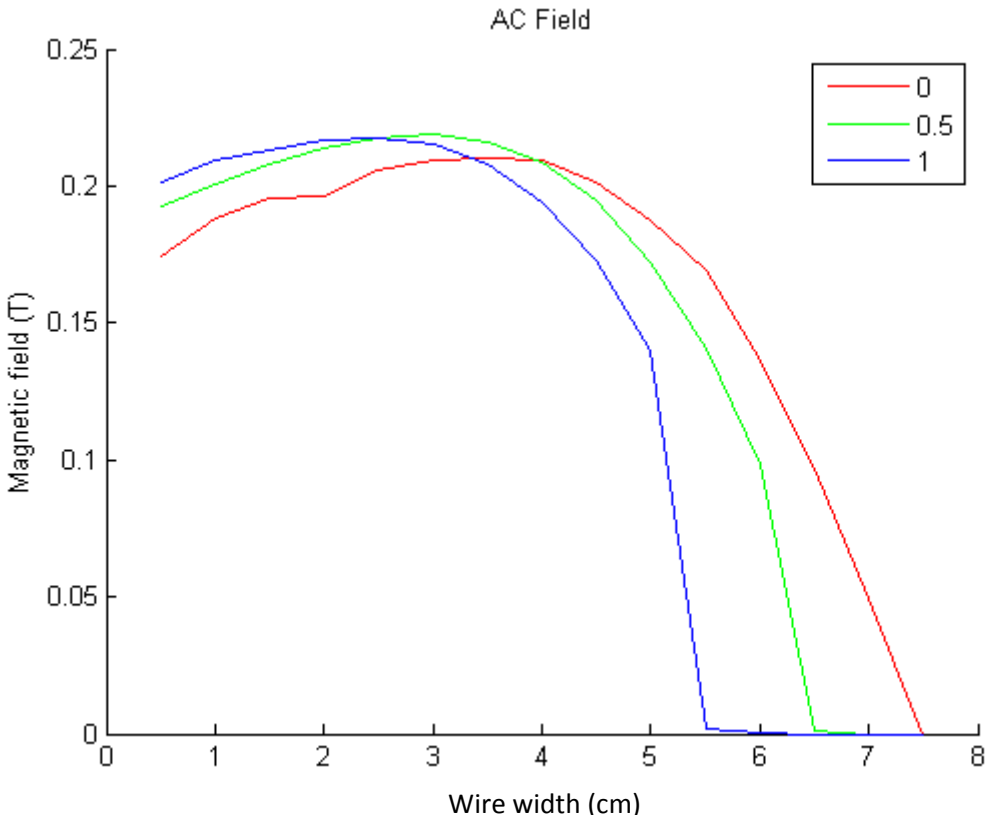

Figure 5-2 Resulting AC field from sweeping the wire axial length for different gap lengths

From the results the following can be concluded:

- The optimal gap length is 0.5 cm
- The optimal axial thickness of the bulk is 8 cm
- The optimal axial wire width is 3 cm

With the final parameters of the coil setup defined, the comparison with the wound coils setup can be made.

5.3.2. Synchronous machine setup

The field coils for the synchronous machine are wound coils which can only be built as racetrack coils. The model of such a coil is found in Figure 5-3. The only parameter that is still undefined is the inner bore of the coil.

Since it is an aircore coil, the performance is highly dependent on the MMF, thus the largest amount of turns is preferred, which results in an as small as possible inner bore (since the outer dimensions are fixed). Yet because of mechanical constrains, a realistic value for the inner bore of 1/3 of the available axial length (=5 cm) is chosen.

Now that this parameter is defined, the comparison with the other setup can be made.

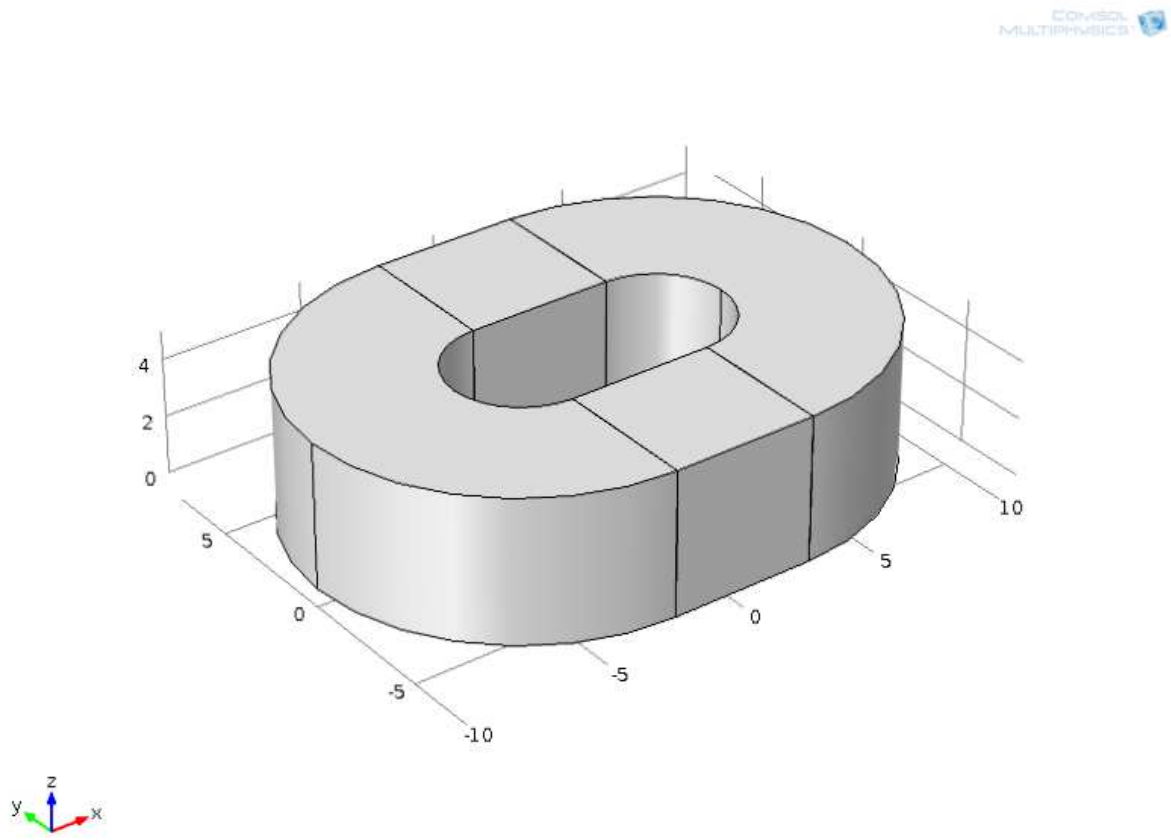

Figure 5-3 FEM model of the wound coils setup

5.3.3. Simulation results

From the FEM simulations, the acquired magnetic fields for the two setups along the coils are displayed in
Figure **5-4** and
Figure **5-5**.

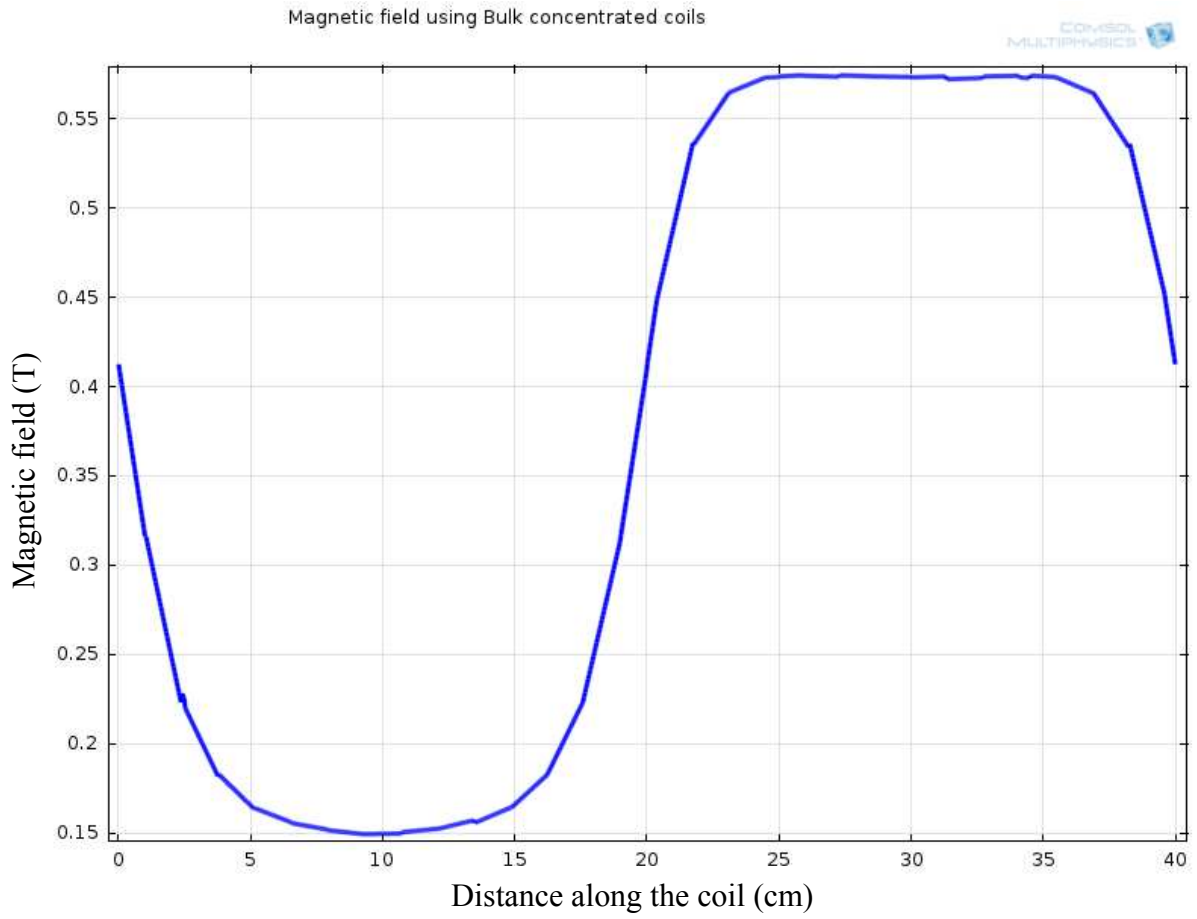

Figure 5-4 FEM result of the bulk concentrating flux coils topology

The torque producing component (or the amplitude of the AC fields) is displayed in Figure 5-6. From the figure it is clear that the wound coil prevails over the concentrated flux setup.

What is observed is that the peak field of both designs is similar, because this field determines the critical current in the coils. However, the amplitude of the torque producing field is in the case of the coils design equal to the peak field. For the bulk concentrated design the amplitude is maximal half of the peak field, since the lowest field possible with a (theoretical) perfect bulk is zero Tesla.

From the results, it is concluded that the wound coil setup, belonging to the synchronous machine topology, offers the highest airgap field and thus the highest torque density. Therefore the **synchronous machine topology is chosen** for the thesis design.

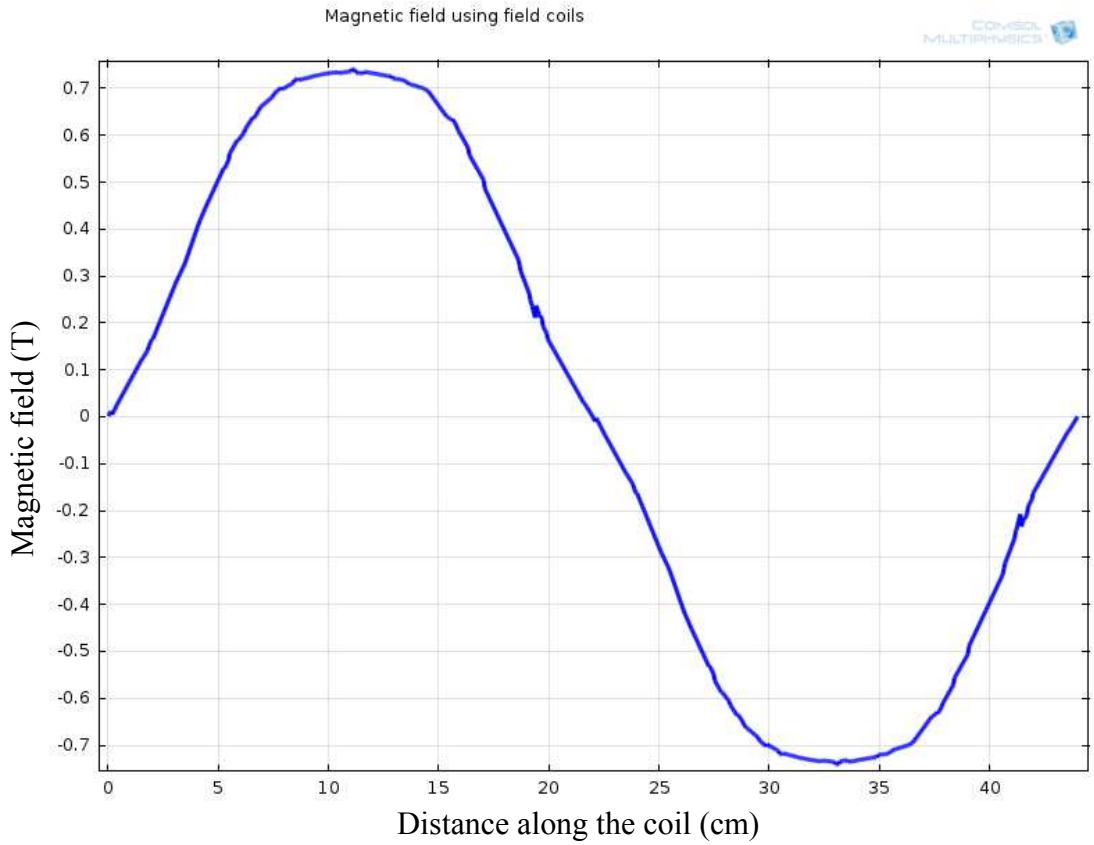

Figure 5-5 FEM result of the wound coils topology

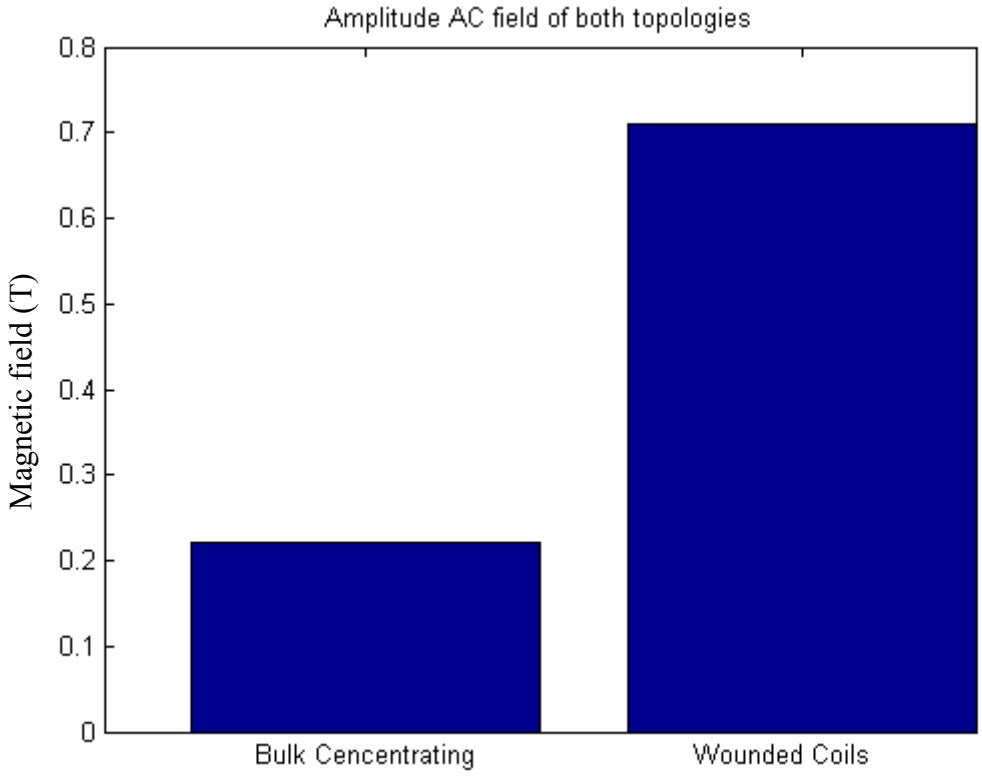

Figure 5-6 Resulting amplitude of the AC field of both topologies aquired with FEM

5.4.Axial or Radial Machine

Any electrical machine can be built as an axial or radial flux machine. Here a small comparison is made in order to choose one of the configurations for the thesis design. Although there are many papers that compare permanent magnet axial and radial machine topologies, very few include superconducting variants.

For conventional machines the radial designs are most often used. Axial topologies can offer greater torque densities when the ratio between the machine axial length and airgap radial length is small. Parviainen [46] suggests that a ratio of 0.5 or less would favour the axial design over the radial design. The ratio for the propulsion motor design is about 0.3, which would indicate that the axial design should be used.

Parviainen considered only permanent magnet designs which use a very small airgap. The large airgap of superconducting designs (see chapter 4.2) may take too much axial space. Also, an axial machine does not experience symmetrical forces like in the radial machine and it is therefore often build with two stators and one rotor.

This means that when assuming axial flux rotating field windings, an active axial length of 15 cm and 2.5 cm airgap length, only 10 cm axial length is left for the slots of both the superconducting coils and the armature coils. This problem worsens when the field windings are stationary, meaning that an additional airgap is introduced, which takes up another 2.5 cm of the available axial length.

In the radial design the radial length is limited to 70 cm. The effects of the large (radial) airgap and cryostat will only reduce the airgap radius and the resulting active surface. Because of the limited axial length available for this thesis design it is therefore chosen to use the radial design.

5.5.Rotating or stationary armature/field windings

Conventional synchronous machines usually have their field windings mounted on the rotor and the armature placed on the stator. The reason for this standard configuration is that the current for the coils on the rotor have to be transported with e.g. a slip ring. These slip rings are prone wear and they have to be replaced regularly. The wear worsens with increasing operating speed and increasing current.

When the field windings are on the rotor, their DC current can be limited by connecting the coils in series. This will result in a higher voltage across the slip rings and a slower response of the coils, which is acceptable. In applications where the availability of the machine has to be very high, a brushless exciter is considered. The brushless exciter is essentially an aircore transformer that transports the current from the stator to the rotor without physical contact. It uses power electronics to first substantially increase the frequency of the current before it is send to the rotor, where it is rectified again. This exciter can be big and heavy, but it requires much less maintenance than slip rings.

If the armature is placed on the rotor, a multi-phase AC current has to be transported to the rotor. Not only is a different slip ring per phase needed, also most current limiting methods like reconnecting the coils cannot be done without (substantially) influencing the performance of the armature. A brushless exciter could be considered, but unlike in the case of the field windings, an AC current at the correct frequency has to be produced on the rotor. In order to have fewer losses and a smaller torque ripple, the current wave should be a near perfect sine. To do this in the limited space of the rotor is extremely challenging, making also the brushless exciter not an option for a rotating armature.

Mainly because of the lower availability (or the higher maintenance requirements) in aerospace the field windings are placed in the rotor. The trend in aerospace, but also in other industries, is to use permanent magnets in the rotor and thus removing the slip rings problem completely. Because of this, it is safe to say that there are very few (if any at all) reasons for conventional machines to consider a rotating armature.

In the case of a superconducting machine the situation changes, since the superconducting field windings are placed in a cryostat that needs a supply of cryogenic coolant. When placed on the stator, there are no additional added complexities, assuming that the supply of cryocoolant (e.g. the cryocooler) is always stationary. But when the cryostat is placed on the rotor a cryogenic rotating coupling is needed.

The rotating coupling does not only need to provide a leak-free rotational path for the cryogenic fluid to flow from the stator to the rotor and vice versa, it has to be insulated with a vacuum layer to limit the heat intake from the ambient environment.

There are different methods to build these couplings, but an essential component is the rotating seal that either must withstand a high pressure difference or it must provide a low thermal conductivity. An example of an application of such a seal is an electrical machine that requires an airtight seal to operate in a humid environment or one that requires a vacuum airgap to reduce the windage losses [47] [48].

There are a few ways to build a rotary gas seal, but the ferrofluid seal is considered the best in terms of the low leakage and high reliability properties, especially because it allows a vacuum seal [48]. This seal uses a ferrofluid that consists of nanoscale ferromagnetic particles suspended in a fluid. When placed in a strong magnetic field, the liquid will sustain itself against gas pressures.

The basic concept of this seal is illustrated in Figure 5-7. This picture shows the need for an iron flux path around the whole seal that can have a considerable impact on the weight. The ferrofluid can withstand only a certain pressure difference, so in order to create a strong vacuum, several of these stages may be needed as shown in Figure 5-8. In this example every stage can withstand only 0.2 bar of pressure difference, so six stages are needed to create a vacuum.

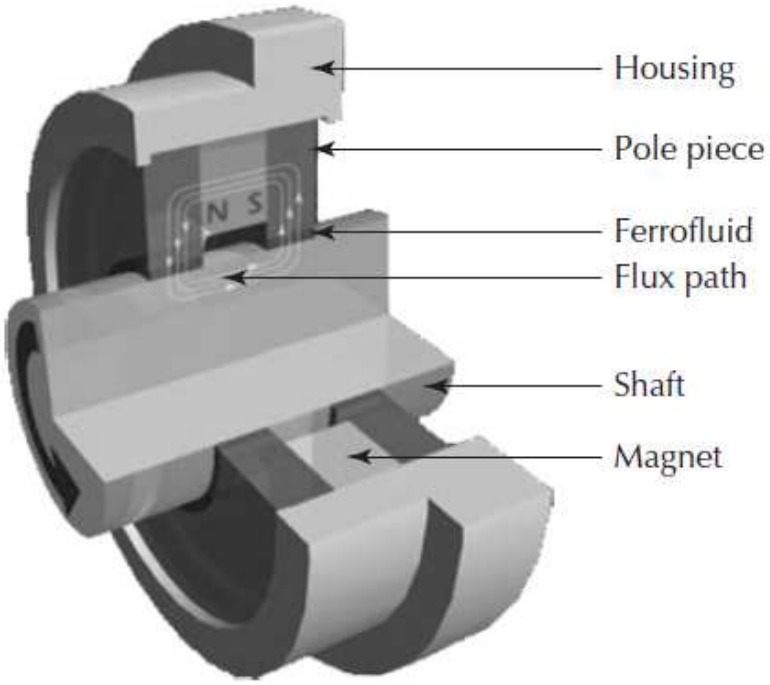

Figure 5-7 Basic concept of a ferrofluid magnetic seal [48].

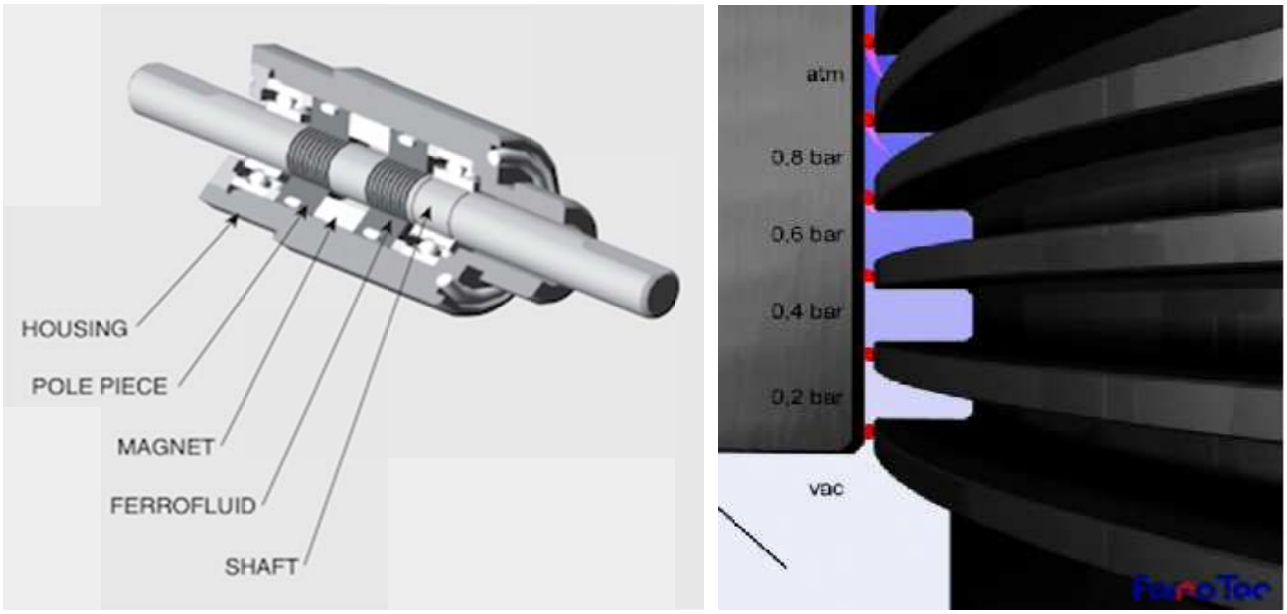

Figure 5-8 Ferrofluid seal for vacuum: left the seal placed in the machine, right a close up of the seal with the pressure differences [49]

Without going too deep into the design of a ferromagnetic seal, from the figures it is clear that to construct such a seal not only a heavy iron flux path is required, also the several stages require a large axial length. Both the weight and the axial length requirements of the propulsion motor are very strict, making the rotary coupling an undesirable component.

For this reason **the rotating armature is chosen**. Although this will require slip rings for the armature, the cryostat will become simpler when placed on the stator. The issues with the slip rings are, due to the long operational experience, expected to be manageable. The result is that the machine complexity is concentrated less in the thermal domain, but more in the electrical domain.

5.6.Machine radial specification

As a starting point, a set of dimensions for the machine are taken as displayed in Table 5-1. These values may change during the designing process.

Parameter	Value
Effective airgap radius (center of eff. airgap)	51.25 cm
Effective airgap	2.5 cm
- Mechanical airgap radial length	0.5 cm
- EM Shield radial length	1 cm
- Airgap cryostat radial length	1 cm
R_rotor	50 cm
R_stator	52.50 cm
R_outer	57.5 cm
R_outer_max	70 cm
R_inner	45 cm
stack length	25 cm

Table 5-1 Pre design machine dimensions

A graphical representation of the radii is shown in Figure 5-9. The airgap is chosen to be 2.5 cm and consists of a mechanical airgap of 0.5 cm, an Electromagnetic (EM) shield of 1 cm and a cryostat wall of 1 cm, see also Figure 5-10. Between R_inner and R_rotor a 5 cm space is allocated for the rotor coils. Likewise between R_stator and R_outer 5 cm is designated for the stator coils. These values are realistic for a starting point and they will be explained throughout the following chapters.

5.7.Conclusion on the machine setup

In this chapter the layout of the design process in the next chapters is set. Also it is chosen to build a partly superconducting synchronous motor. Because of the limited axial space, set as a requirement, the radial machine design was considered. Also it was chosen to place the field windings on the stator and the armature on the rotor in order to exclude a rotating coupling for the cooling. The disadvantage of using slip rings for the armature current is accepted. Finally, the machine radial specification was given to be used as a starting point for the designs in the next chapters.

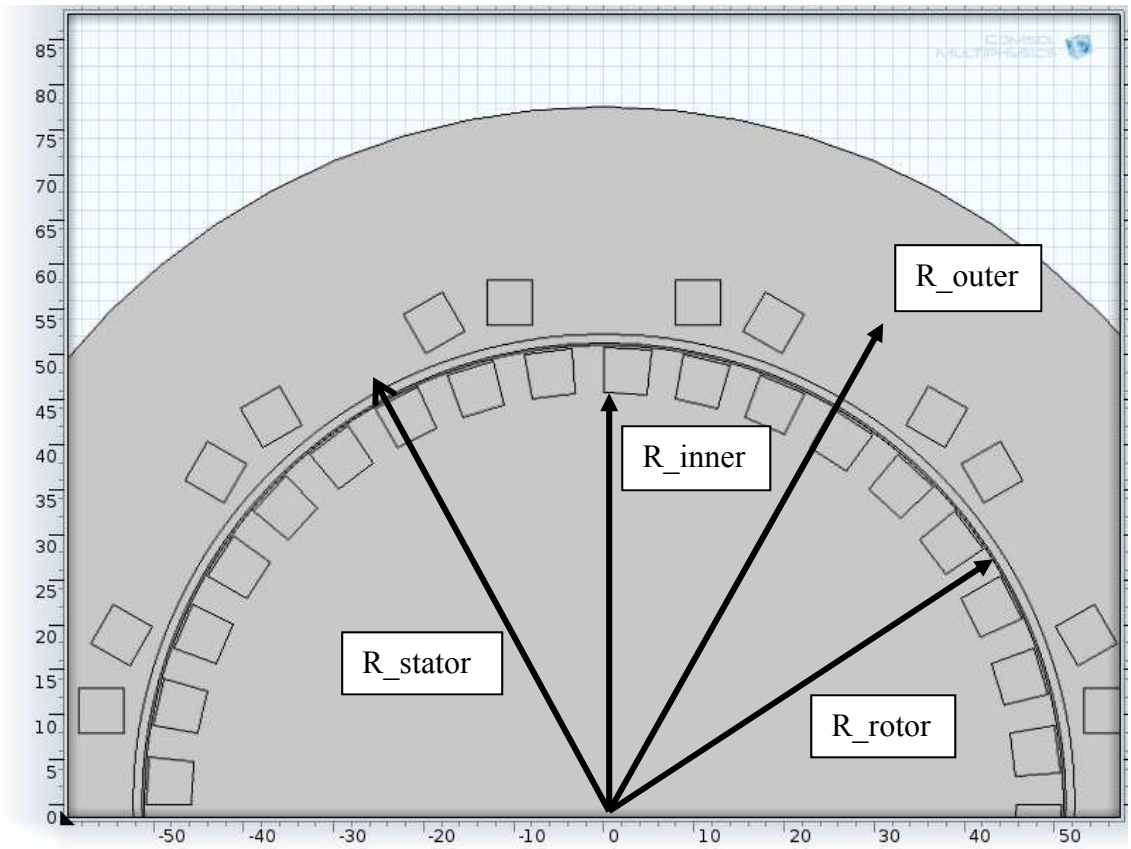

Figure 5-9 Representation of radial dimensions

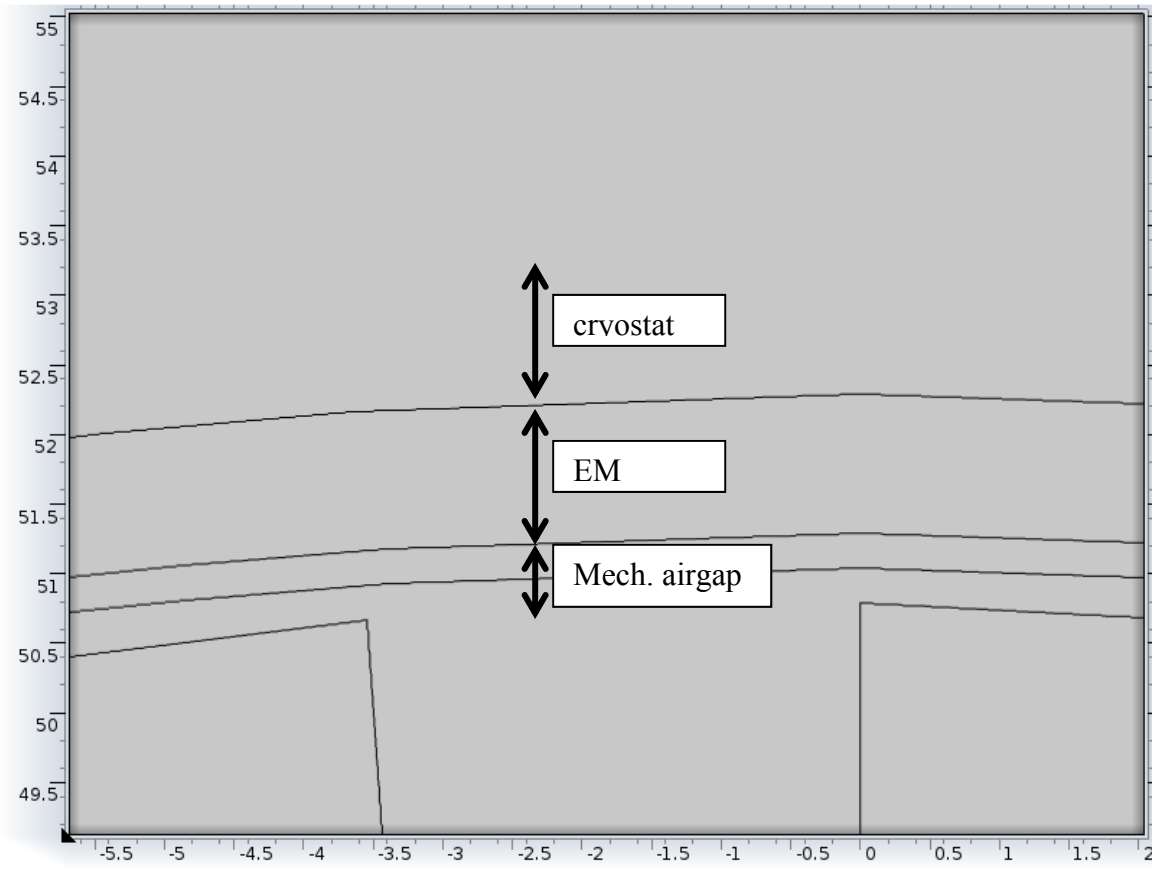

Figure 5-10 Graphical explanation of effective airgap

6. Armature design

In this chapter the armature coils are designed. The aim of this design is to make a choice for the armature winding material, winding distribution and the use of an electromagnetic shield to reduce heating losses in the stator. In order to make these choices, several calculations and simulations are performed. After the correct selections are made, the armature design is considered completed for this chapter. Further analysis like the copper losses is conducted in chapter 9 as part of the full machine analysis.

As described in chapter 5.5, the armature coils are placed in the rotor. These coils are usually made of copper, however aluminium is also considered because of its lower mass density. In Table 6-1 the basic properties of both materials are compared. From the table it is concluded that aluminium is about one third lighter, but it is 60% more resistive than copper. Taking into account the reduced thermal conductivity (60%) aluminium coils will require better cooling performance. However, the cooling of the armature is considered less of an issue compared to the weight improvement and therefore aluminium coils are chosen.

Property	**Copper**	**Aluminium**	**Aluminium norm. to copper**
Electrical resistivity [nΩ/m]	16.7	26.5	1.6
Density [kg/m^3]	8700	2700	0.31
Thermal conductivity [Wm^{-1} K^{-1}]	400	160	0.4

Table 6-1 Comparison copper and aluminium materials

6.1.Possible winding configurations

The armature windings will be designed as a 3-phase system. A higher number of phases may provide certain advantages, but in this thesis they are not considered. The armature coils themselves can be wound in many different ways, but a general distinction is made between the concentrated windings and distributed windings.

In literature the choice of the armature winding configuration for superconducting machines is always the distributed configuration. The reasons are the (significant) lower space harmonics and the fact that “off the shelf” designs are available. These arguments are very decent, especially the lower harmonics would make the distributed winding configuration also for this thesis design an obvious choice.

However, in aerospace the current trend is to choose Fractional Slot Concentrated Windings (FSCW) [50] for the following advantages compared to distributed windings [51]:

- Possible higher torque capabilities
- Smaller and lighter end windings
- Higher winding fill factor
- Less risk of phase-to-phase faults

The major disadvantage is the **considerably more space harmonics**. The advantages of having smaller end windings, which can result in lower weight, and the possible higher power density are the major motivations to consider a FSCW armature configuration. However, the severity of the space harmonics can outweigh the advantages.

Space harmonic content occurs because the windings cannot produce a perfect sinusoidal rotating field in the airgap. In steady state normal operation, the fundamental field rotates in sync with the field windings and therefore create no problems. The harmonics however, are seen as changing fields by the superconductors. As explained in paragraph 3.2.3, changing fields seen by the superconductors can lead to hysteresis losses inside the material. The aim is to limit these heating losses as much as possible.

Next to the space harmonics also time harmonics distort the airgap field. The amount of time harmonics depends on the quality of the power electronics that create the armature AC current. However, the power electronics are not considered, because they are not part of the actual machine design, therefore also the time harmonics are not considered. In this thesis design the armature current is modelled as a perfect sine.

Since the feasibility of this thesis design increases if it more or less follows the current trends, it is worth the effort to perform a more in depth study on the feasibility of a fractional slot concentrated winding configuration for a superconducting machine and to compare it with the distributed version.

In literature, an Electromagnetic (EM) shield is often applied to effectively reduce any harmonics that reach the superconductors. This shield is placed in the airgap, mounted on the field windings (in this case the stator) [14]. This method is also applied in several permanent magnet machines to protect the magnets from overheating and demagnetisation. This shield can (partly) remove the space harmonics and it can increase the feasibility of the FSCW distribution, therefore the EM shield is also designed in this chapter.

6.2.Choice of winding configuration

From literature, it is clear that the distributed configuration is feasible, so the performance of the concentrated design is to be compared to it.

There are many different configurations of concentrated and distributed windings possible, so to make a good comparison a boundary setup is chosen:

- The **full pitch distributed winding** configuration is the “least distributed” design possible. The configuration is illustrated in Figure 6-1 (left). These windings have the smallest possible overlap between phases and have therefore also the smallest end windings for a distributed configuration.

- The **3/2 fractional slot concentrated winding** configuration is the “least concentrated” design possible and is illustrated in Figure 6-1 (right).

The comparison of these two configurations will be used to conclude about the feasibility of using fractional slot concentrated windings. The main comparing criterion is the severity of the space harmonics.

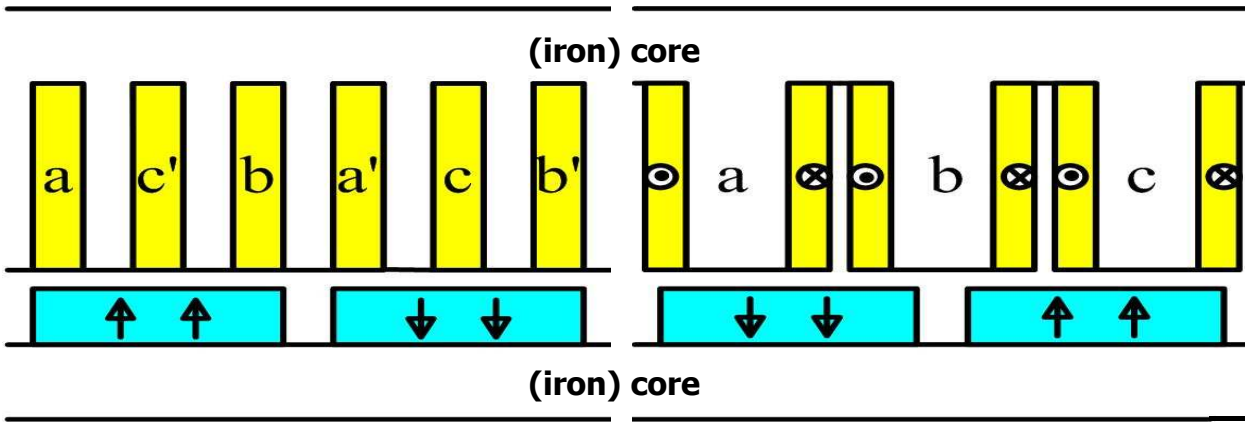

Figure 6-1Winding distributions: Full pitch distributed (left) and 3/2 fractional slot concentrated (right) [52]

6.3.Modelling of space harmonics

The space harmonics can be calculated with analytical models as presented by Polinder et all [52]. However, the validity of these models for this thesis is questionable since the analytical models consider iron core designs. Because this thesis studies an air core design with a large airgap, the attenuation of the harmonics at greater distances from the armature can make a difference. Therefore the harmonic content is also calculated with FEM. The analytical models will be used for an initial verification of the FEM models.

The analytical model to calculate the amplitude of the harmonic content, normalized to the fundamental of the full pitch configuration, is given by [52]:

$$\frac{B_k}{B_1} = \frac{1}{k}\sin\left(\frac{k\pi}{2}\right) \qquad \textbf{(6-1)}$$

The model for the 3/2 concentrated windings is given by [52]:

$$\frac{B_k}{B_1} = \frac{2}{k\sqrt{3}}\sin\left(\frac{k\pi}{3}\right) \qquad \textbf{(6-2)}$$

With the harmonic number $\mathrm{k} = 1,2,4,5,7,8, \ldots$.

For the FEM model, an uniform model is made in Comsol of which the winding configuration can be easily modified. The whole armature winding configuration is built with the following assumptions:

- Full air core inner rotating armature
- 12 pole pairs, resulting in 72 slots
- Slot space is 60% and core space is 40%
- Airgap radius of 50 cm
- Airgap length of 2.5 cm
- Slot depth is 5 cm
- Windings modelled as simple rectangles with an applied current density
- A moderate armature current density of 5 A/mm^2 is used
- A winding fill factor of 0.4 and 0.7 for the distributed and concentrated windings respectively is used
- First no shield is applied
- Single layer slots for distributed windings
- Neglect end winding effects
- Active stack length is 15 cm, the remaining 10 cm is reserved for end windings

With these assumptions a simple model in Comsol is made in Figure 6-2. The harmonic content is calculated at 2.5 cm in the airgap where the field windings are located, since from there the AC field will produce heating losses in the superconductors.

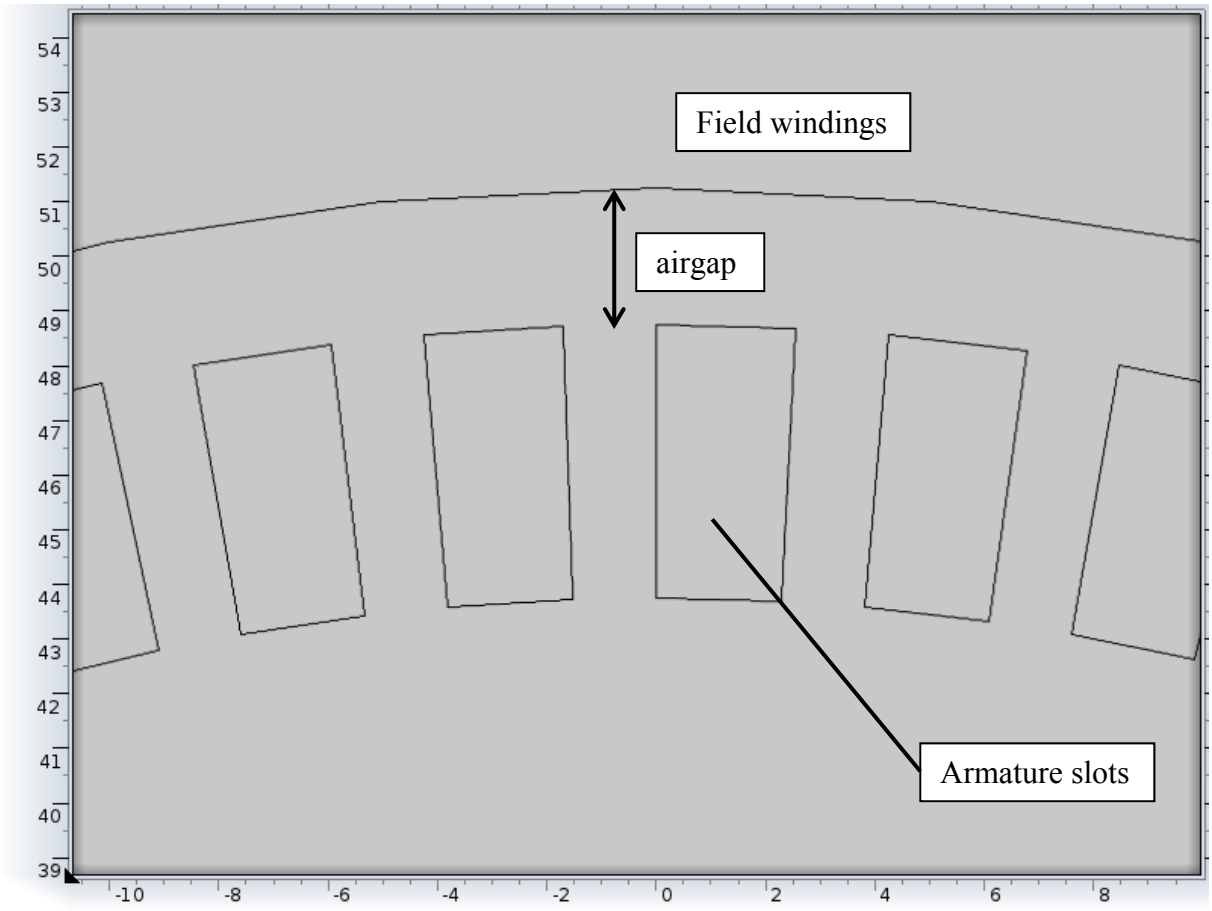

Figure 6-2 FEM model for harmonic analysis

The following balanced armature current densities for the three phases are applied to the whole slot according to the configurations illustrated in Figure 6-1:

$$J_a = FF\sqrt{2}\,J_0\,\cos(\omega t) \qquad \textbf{(6-3)}$$

$$J_b = FF\sqrt{2}\,J_0\cos(\omega t - \frac{2}{3}\pi)$$

$$J_c = FF\sqrt{2}\,J_0\cos(\omega t - \frac{4}{3}\pi)$$

Here **FF** represents the winding fill factor, $\mathbf{J_0}$ the RMS value of the winding current density and **ω** the angular frequency of the phase currents, which is defined as:

$$\omega = 2\pi f_{el} = 2\pi\frac{n}{60}p \qquad \textbf{(6-4)}$$

Here **n** equals the machine rotational speed in RPM and **p** is the number of pole pairs. In this case the rotational frequency is 68.2 Hz or 429 rad/s.

6.3.1. Simulation results and comparison

The FEM model is built in Comsol and with the current densities applied, a steady-state simulation is performed. The resulting magnetic field distribution for both configurations is shown in Figure 6-3.

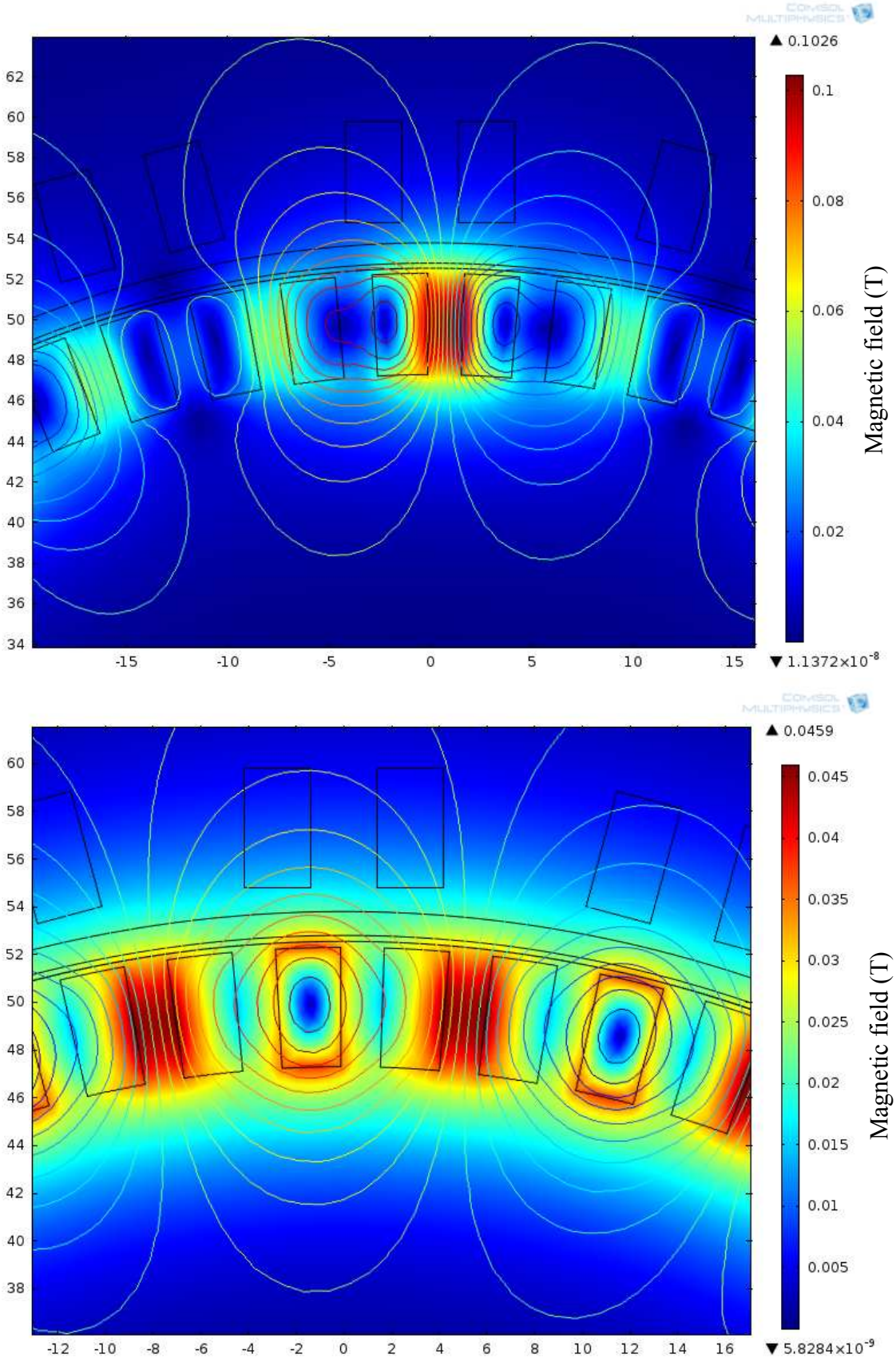

Figure 6-3 Magnetic field distribution for concentrated windings (top) and distributed windings (lower)

From the figures, it is observed that the magnetic fields are not following a certain flux path, as would be the case in an iron core machine, but they are distributed freely in the whole machine.
To perform the harmonic analysis the magnetic field at 2.5 cm from the coils is taken as illustrated in Figure 6-4.

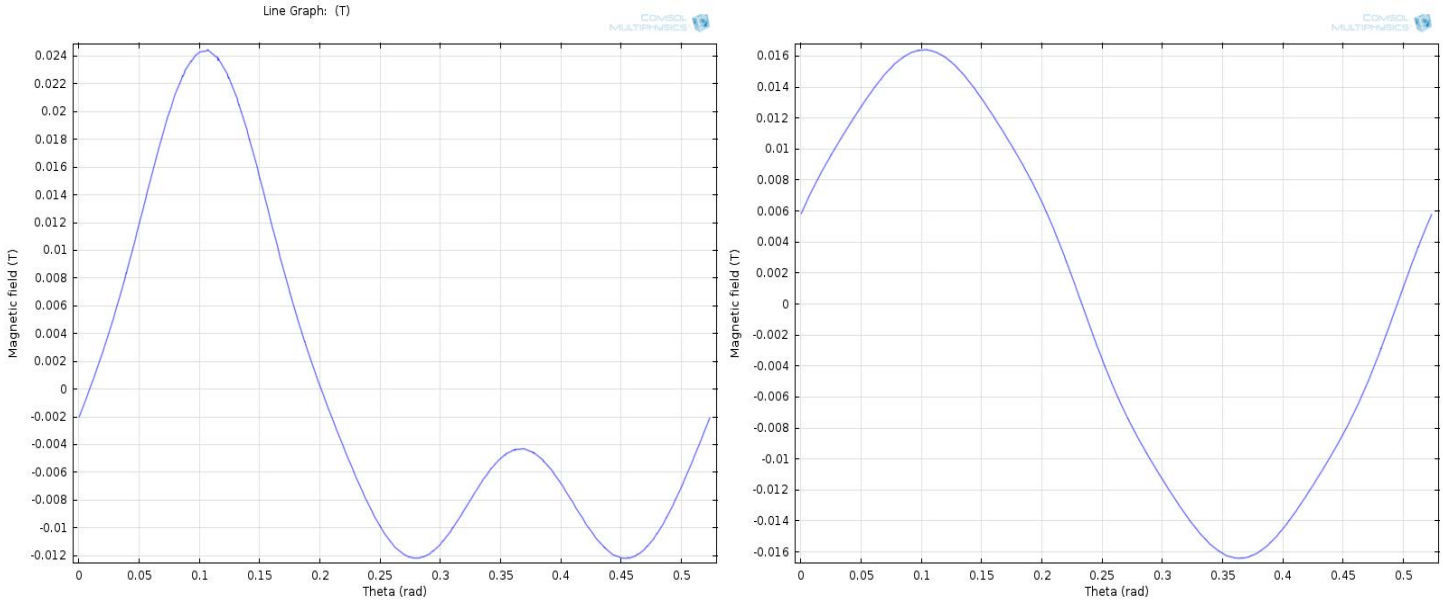

Figure 6-4 Magnetic field at per pole pair 2.5 cm from the coils from Comsol for concentrated windings (left) and distributed windings (right)

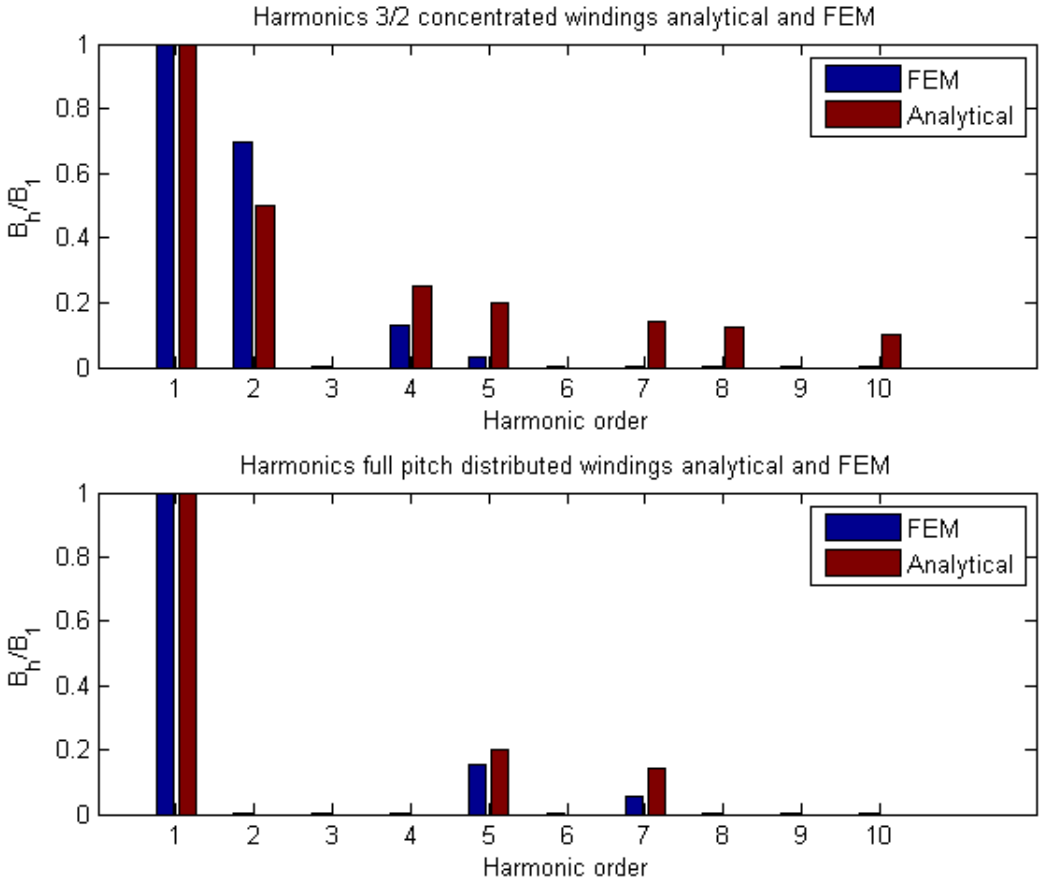

Figure 6-5 Spacial harmonics of concentrated windings (upper) and distributed windings (lower) using analytical and FEM models

From the graphs of Figure 6-4, a Fourier distribution is made using Matlab which represents the space harmonics. The space harmonics calculated with both the analytical model and the FEM model are shown in Figure 6-5. From the results the following can be concluded:

- The results between the analytical and FEM models are only to some degree comparable.
- Harmonics above the 7^{th} order are neglectable according to the FEM results for both winding configurations. This is because higher harmonics attenuate faster across a distance in air than lower harmonics.
- The concentrated configuration has a stronger 2^{nd} harmonic component according to the FEM results compared with the analytical results. This is explained because of the lack of iron cores to "steer" the magnetic field, the field component of the individual phases are less supressed.
- **The space harmonics are high for the concentrated windings**; the second harmonic is more than half the amplitude of the first.
- **The harmonic content is low for the distributed configuration;** the magnetic field is very sinusoidally distributed and it might not need an EM shield at all.

The simulations confirm that the concentrated windings have a greater spacial harmonic content, but this alone is not a good criterion to make a choice. The best measure would be to calculate the heating losses in the HTS windings, but that goes beyond the scope of this thesis. Another method is to analyse the effect of the space harmonics on an EM shield.

6.4.Electromagnetic shield

Now the EM shield is introduced to dampen the space harmonics. The shield is made of a highly conductive material that is placed in the airgap and is mounted on the side of the field windings (in this case the stator). Although Kalsi [14] recommends the use of composite shields in order to withstand fault torques, for a first analysis a solid shield made of aluminium is chosen.

The armature flux that produces the torque will be seen as DC by the shield and will pass through it unhindered. The harmonic content of the flux is seen as AC and will induce eddy currents. These currents produce their own flux that partly counteracts the AC flux that created them. The result is that the harmonic components are damped in the shield at the cost of eddy current heating in the shield. The damping factor of the shield differs per harmonic component and can be described by the following formula:

$$DF_h = \exp\left(-\frac{d}{d_{\Delta,h}}\right) \qquad \textbf{(6-5)}$$

Here d represents the thickness of the shield and d_Δ is the skin depth of a specific harmonic which is given by [52]:

$$d_{\Delta,h} = \sqrt{\frac{2\rho_{shield}}{\mu_{shield}\omega_h}} \qquad \textbf{(6-6)}$$

Here ρ_{shield} is the resistivity of the shield material, μ_{shield} is its magnetic permittivity and ω_h is the angular frequency of a specific harmonic with respect to the field windings (or stator). More useful is to write the skin depth as function of the mechanical frequency and harmonic number k:

$$d_{\Delta,k} = \sqrt{\frac{\rho_{shield}}{\mu_{shield}\pi(k \mp 1)\, f_m\, p}} \qquad \textbf{(6-7)}$$

Here the sign is plus when k is even and it is minus when k is odd. The formula is valid for both winding types, but it is not in general. From the formula can be concluded that the damping is more effective with a thicker shield and a higher relative harmonic frequency. However, a lower number of pole pairs or a lower operating frequency will decrease the damping.

Kalsi [14] suggests that the thickness of the EM shield has to be 3 times the skin depth of the major harmonic component. In that case only 5% of the harmonic's amplitude will pass through the shield. As can be seen in Table 6-2, this would mean that the shield has to be 1.8 cm thick. However, for now the shield thickness is fixed on 1 cm, which means that the shield is less effective, but a larger shield would increase the airgap too much.

Harmonic	Skin depth (cm)	Damping factor (1 cm shield)
2	0.6	0.17
4	0.6	0.17
5	0.4	0.08
7	0.4	0.08
8	0.3	0.05

Table 6-2 Skin depth and damping for different harmonics according to the analytical model

According to the analytical model of the shield the damping factors in Table 6-2 are acquired for both winding configurations. But since this model does not take the aircore and large airgap into account, the effect of the shield is also simulated with FEM.

6.4.1. FEM shield modelling

Since the shielding follows from eddy current induced by time changing fields, a transient simulation is needed. The AC fields induce an electric field in the shield, which results in a current density due to the conductivity of the shield. The current density in turn counteracts the field. In order to simulate this effect, the FEM partial differential equations are therefore extended with the induced current:

$$-\nabla^2 A = \mu(J_{ext} + J_{ind}) \tag{6-8}$$

With the induced current defined according to Faradays Law:

$$J_{ind} = \sigma E_{ind} = -\sigma \frac{\partial A}{\partial t} \tag{6-9}$$

Here **σ** is the electrical conductivity shield of the shield. Substituting into equation (6-8):

$$-\nabla^2 A = \mu J_{ext} - \mu\sigma \frac{\partial A}{\partial t} \tag{6-10}$$

From the differential equations can also be noticed that the induced field counteracts the external field, creating the damping effect. This effect is stronger for a faster changing field.

In Comsol the shield is modelled and meshed as in Figure 6-6. The eddy current effects are very mesh quality sensitive and it was noticed that meshing the shield with at least 6 layers, corresponding with a mesh size of 0.17 cm resulted in no significant calculation errors. This mesh size equals between 1.8-3.5 times the skin depth.

The transient simulation is performed by simulating the rotating the shield at 341 RPM in Comsol, using the build-in moving mesh algorithm. By applying the current densities defined in equation (6-3) and running the simulation for about 0.02 seconds simulation time, the magnetic fields just after the shield were compared.

6.4.2. Simulations results and comparison

The space harmonic contents resulting from the FEM simulations with and without the shield are given in Figure 6-7. For verification of the simulation, also the damping factor is compared with the analytical solution in Table 6-3. Only the concentrated windings are compared, since the amplitude of the harmonics of the distributed windings are in the order of the simulation noise and therefore not reliable.

Both analytical and FEM results are comparable, but the simulation results show a better damping of higher harmonics. This is explained by the lack of an iron core. Without the iron, the magnetic field is freely distributed in the airgap. The result is that harmonics with a larger wavelength, corresponding with a low harmonic number, are stronger at a certain distance from the coils than harmonics with smaller wavelengths.

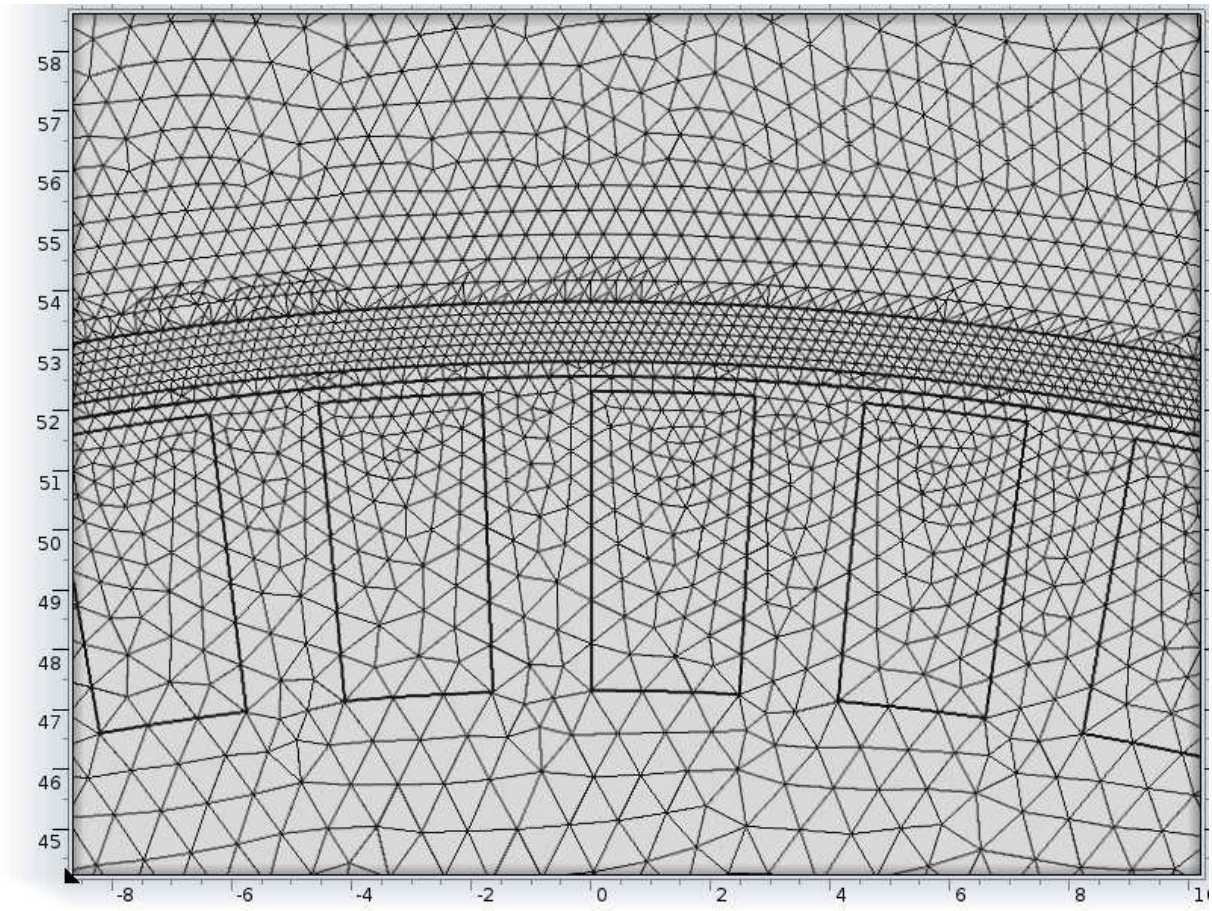

Figure 6-6 Mesh used to calculate the effect of the EM shield in Comsol

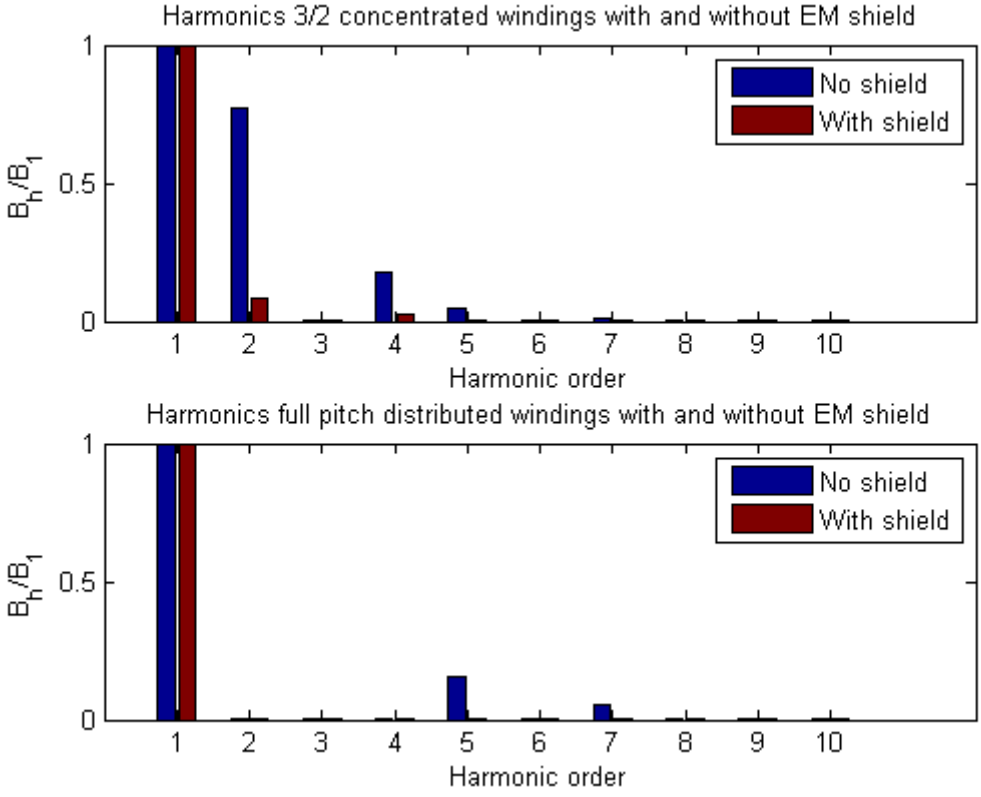

Figure 6-7 Space harmonics FEM results with EM shield and without for both winding configurations

Harmonic	Damping factor analytical	Damping factor FEM
2	0.17	0.11
4	0.17	0.15
5	0.08	0.06
7	0.08	0.06
8	0.05	0.02

Table 6-3 EM shield damping factor for FEM and analytical results for the concentrated configuration

Form the results, it is concluded that the EM shield is very effective for this setup. The harmonics for the concentrated windings are very decent and for the distributed windings they are virtually non-excitant.

It could be said that, with the shield, concentrated windings perform good enough to be applied in a superconducting machine. However, there are two factors that can have a great effect on this decision:

- The eddy current heating losses in the EM shield. The losses cannot be too high and the shield might have to be actively cooled.

- Since the number of poles cannot be defined before the whole machine is designed, the effect of changing the number of pole pairs has to be studied.

Since the FEM model in Comsol has been verified, the two effects are only analysed with FEM. The heating losses in the whole shield are calculated according to:

$$P_{heat} = RI^2 = R\left[\iint_S J_{ind} dS\right]^2 \qquad \textbf{(6-11)}$$

Including equation (6-9), the formula becomes:

$$P_{heat} = L\sigma\left[\iint_S \frac{\partial A}{\partial t} dS\right]^2 \qquad \textbf{(6-12)}$$

With **L** representing the stack length and **S** the surface of the shield as modelled in Figure 6-6.

Using equation (6-12), the heating losses are calculated as function of the number of pole pairs in Comsol and the results are plotted in Figure 6-8. From the results, it is clear that the concentrated windings cause at least an order of magnitude more losses than for the distributed windings. However, it is noted that the losses increase for lower pole pairs. The losses increase from 24 to 120 W for distributed and from 1.1 kW to 2.9 kW for concentrated when comparing 12 pole pairs with 6 respectively.

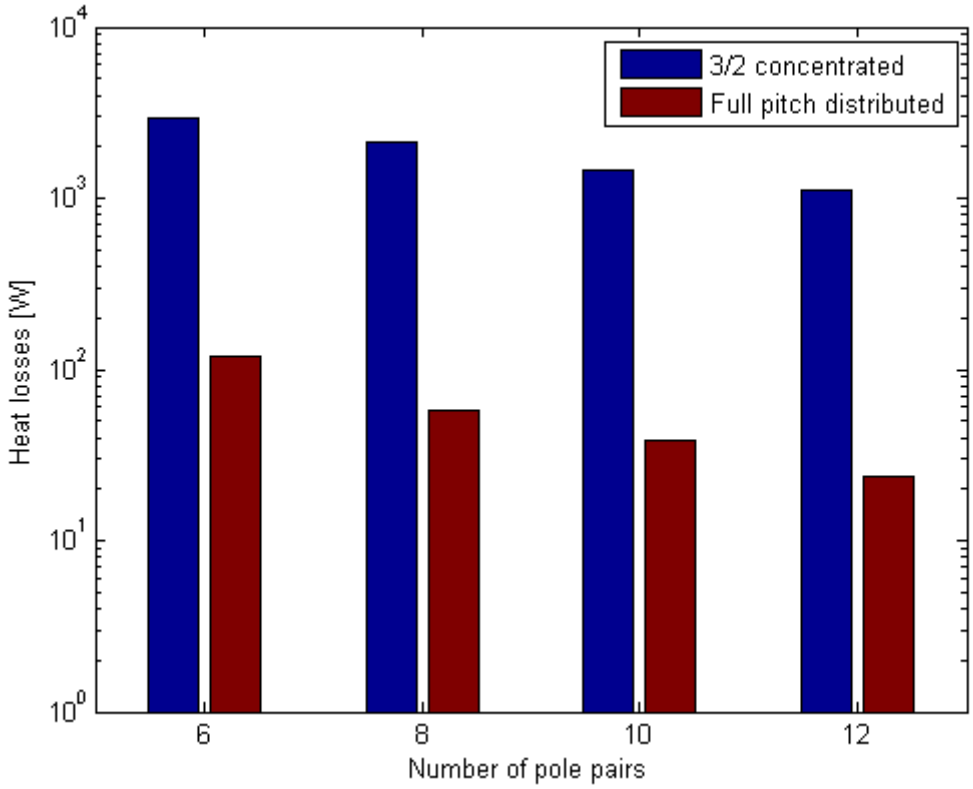

Figure 6-8 Shield heating loss due to eddy currents for both winding distributions

This behaviour results from decreasing the number of pole pairs and thus increasing the size of the winding slots. Because of the bigger slots, the harmonics are stronger at greater distances. This is especially the case for the second harmonic of the concentrated winding configuration, as illustrated in Figure 6-9.

Higher heat losses for the concentrated windings mean that for any given cooling capacity, the distributed configuration can have a much higher current density than for the concentrated configuration. The result is that, when using the cooling capability of the EM shield as a determining factor, using distributed windings has the potential to provide a higher performance than for concentrated windings.

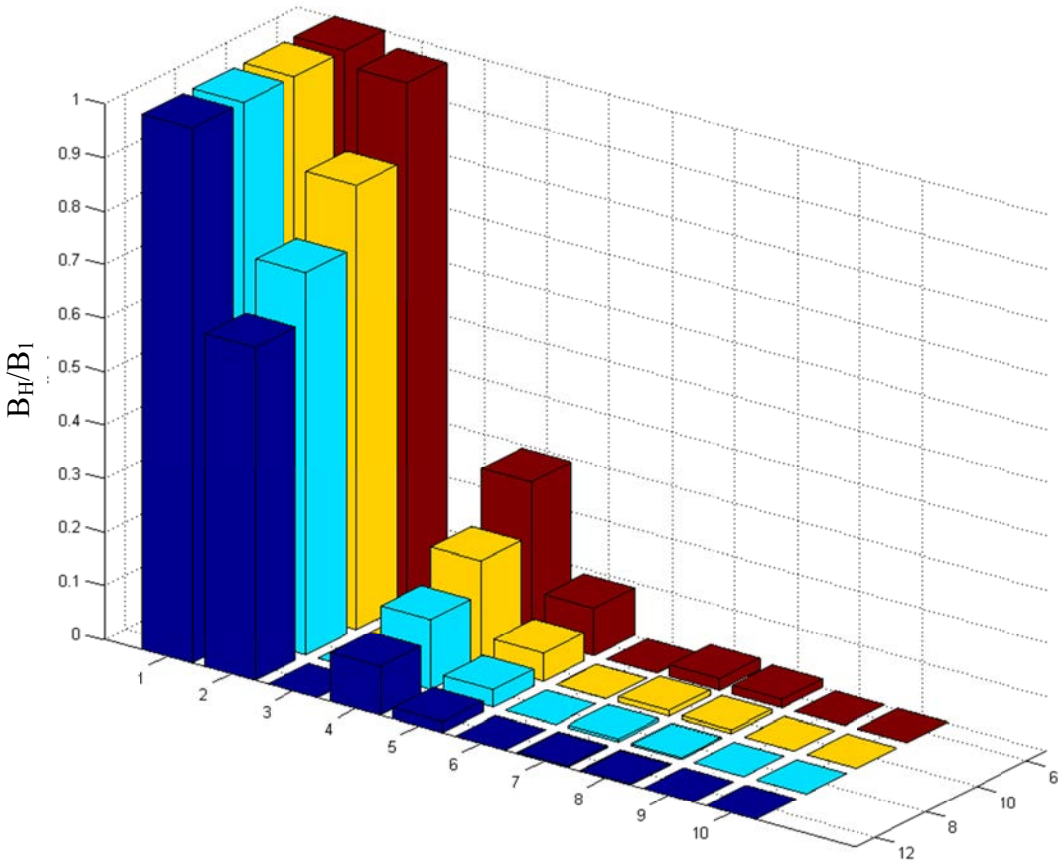

Figure 6-9 Space harmonics for different number of pole pairs for concentrated windings

6.5.Conclusion on armature design

In this chapter the armature was designed. First the winding configuration was chosen by performing a study between the 3/2 fractional concentrated windings and the full pitch distributed windings. The two criteria were the relative amplitudes of the space harmonics with and without the EM shield and the eddy current heating losses taking place in the shield.
Observed was that the space harmonics for the concentrated windings are severe, but acceptable with an EM shield. However, the losses inside the shield are very high, making the configuration less practical. The distributed windings show lower harmonics and virtually none with a shield. The heat losses in the EM shield are at least an order of magnitude higher in the case of concentrated windings compared to distributed windings. This means that, when using the cooling capability of the EM shield as a determining factor, using distributed windings has the potential to provide a higher performance than for concentrated windings.

Concluded is that a distributed winding design is chosen for the thesis design. A full pitch distribution is first considered, because of the small end windings. Because of the natural low space harmonic content and the attenuation in the large airgap, the EM shield may even be discarded. However it must be noted that several factors are discarded, including the time harmonics, dynamic situations and fault situations. It is expected that when including these factors the harmonic losses will increase.

7. Field windings design

In this chapter the field windings are designed. Only the pole pitch parameter is not determined, because it depends on the whole machine analysis and it is therefore calculated in chapter 9. Lacking the pole pitch parameter, the aim of this chapter is to provide the design steps required to design superconducting coils, but the final values like the airgap field are not provided until chapter 9.

The field windings produce a non-changing magnetic field and they are in this case mounted on the stator inside a cryostat. As decided in paragraph 5.3 the field windings will be made with YBCO tapes wound as race track coils.

The following targets are strived for when designing the field coils:

- **Highest possible airgap field**. The field coils are optimized to achieve a highest airgap field, which also results in a higher torque density.
- **The lowest possible weight**. The weight is to be limited as much as possible, therefore no iron is used and the use of aluminium and composites is preferred.
- **Use liquid nitrogen to cool**. This sets the critical current and field curve.

The cryostat itself is considered in chapter 8**.** For the HTS coils design it is assumed that the size of the coils is restricted to leave space for the cryostat:

- Stack/Axial length is 15 cm. The remaining 10 cm is reserved for the cryostat
- In the airgap 1 cm for the cryostat wall is reserved
- 5 cm slot depth. The outer diameter of the field windings becomes 57 cm. The remaining 13 cm is reserved for the mounting of the coils and cryostat.

In the design of the HTS coils the highest priority lies in gaining the highest possible airgap field. The coils are modelled as a simple geometry with a certain applied current density. This current density is linear with the airgap field and it depends on the current rating of the used tape, the winding fill factor and the magnetic field seen by the tape. These 3 factors are combined in the coils mechanical design and the critical current/field optimization. To quantify the coil performance, the effective airgap field and effective stack length are defined.

7.1.Field coils mechanical design

The mechanical design of the coils consists of the dimensioning of the tapes and the support material. The YBCO tape used in this design is the SCS4050 insulated model from Superpower Inc.; see also Figure 7-1 [30]. The 4 mm wide and 0.1 mm thick tape can only bend in one direction with a bending diameter of 11 mm. Because of this bending restriction, using the double pancake race track coil design is the only method to build a wounded coil with HTS tape.

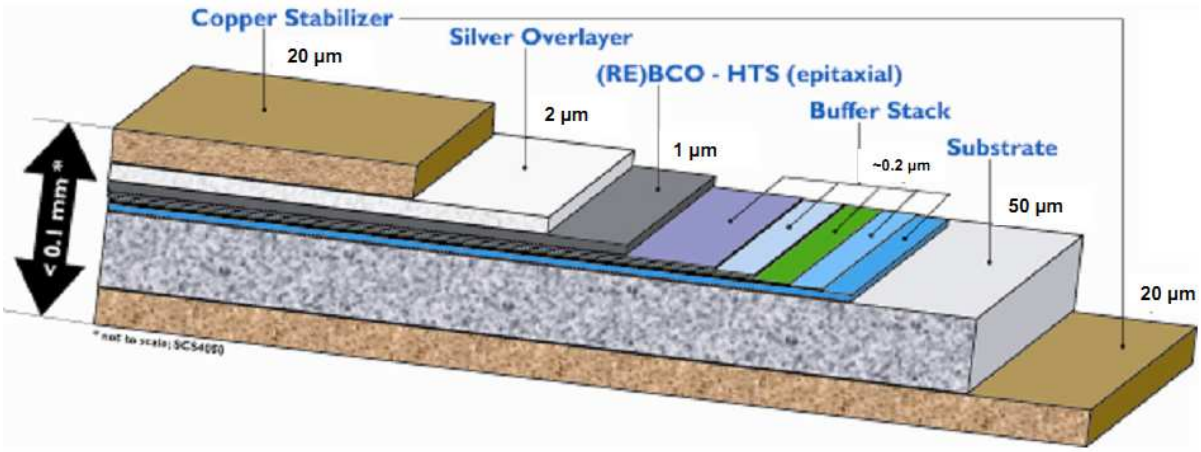

Figure 7-1 HTS tape from Superpower [30]

The double pancakes are made of two coils that are oppositely wound. The first consists of a single tape that is wound from the outside to the inside and the other is wound from the inside to the outside. In this way the coil connections are always on the outside. Since the tapes can only bend in one direction, the pancakes are interconnected with a copper splices. The double pancakes are stacked to acquire the correct height.

The coils cannot be wound with tape only. Since the torque acts directly on the tapes, which are rather brittle, aluminium is added for extra strength. Kalsi [14] gives a good example of how support metal can be added when using BiSCCO tapes at very low temperatures. The example is mostly followed here, but since here YBCO tapes at a higher temperature are considered, the specifications are less harsh. The aim is to use the least amount of support material as possible, since it decreases the winding fill factor that has a direct consequence on the airgap field.

For a single pancake coil the following parts are considered during designing:

- HTS tape
- Aluminium strip wound together with every 3 tapes
- Aluminium metal layer between every pancake
- The pole pitch is yet undefined
- The stack length is 15 cm
- The coil inner bore is 1/3 (=5 cm)of the stack length

Other parts like the mechanical mounting and copper splices for the electrical connections are not designed. Figure 7-2 (left) shows an example of a stacked HTS pancake coil and when zooming in on the black bracket gives Figure 7-2 (right), revealing the arrangement of the HTS tapes (blue) and the aluminium support material (grey). This arrangement of one single section is shown in more detail in Figure 7-3. The chosen dimensions are based on the examples of Kalsi [14].

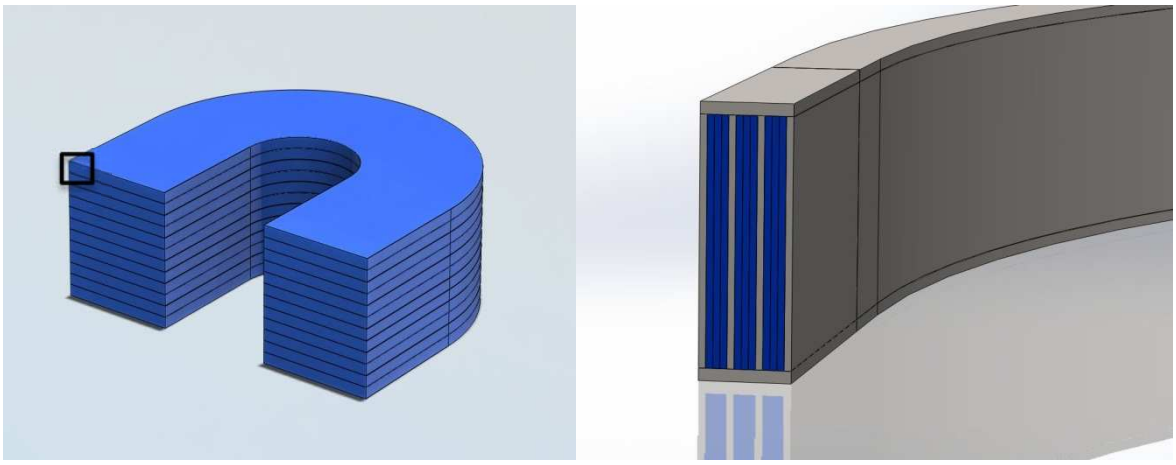

Figure 7-2 Impression of the stacked HTS pancake coils (left) and zoomed in on one pancake revealing the individual blue tapes and grey metal layers (right)

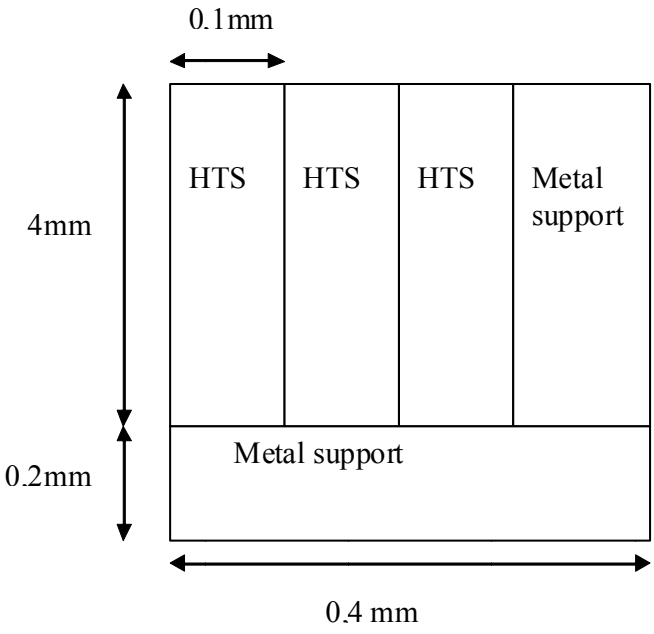

Figure 7-3 Single section of the HTS windings (which is a zoomed-in illustration from Figure 7-2)

With these dimensions the number of turns per coil becomes:

$$\frac{turns}{pancake} = 3 \cdot \frac{total\ winding\ thickness}{3 \cdot t_{HTS\ tape} + t_{support}} \approx 375 \quad \textbf{(7-1)}$$

$$pancakes = \frac{coil\ height}{h_{HTS\ tape} + h_{support}} \approx 12 \quad \textbf{(7-2)}$$

$$turns/coil = 12 \cdot 375 = 4500 \quad \textbf{(7-3)}$$

The function of the support structure is to handle the mechanical stresses resulting from the torque that acts on directly on the windings. The mechanical analysis of these forces are beyond the scope of this thesis, however a simple calculation is performed if the mechanical stresses on the HTS tapes as result of the machine steady-state torque is below the maximum specification.

For simplicity, the forces on the coils are assumed to be equally distributed. This means that the 16.5 kNm torque works at 55cm from the centre of the machine resulting in a force of 30kN. This force is seen by all coils, so by dividing it by the number of pole pairs results in the torque per pole pair. This hoop force creates a hoop stress on every coil:

$$\varepsilon_h = \frac{hoop\ force}{turns\ per\ coil\ x\ support\ metal} \quad \textbf{(7-4)}$$

$$\varepsilon_h = \frac{30\ kN}{4500 \cdot 0.19mm * 4mm} = 8.8\ MPa$$

The value of 8.8 MPa is about a factor of 7 lower than the specification of 550 MPa, meaning that not only is there very limited risk of damage of the windings due to hoop stress, there is a lot of room left for more stresses like those occurring during transients.

With the dimensions of the single section of the coil, the fill factor can be calculated. Assuming that the critical current density of the tapes applies for the whole tape surface (disregarding the fact that only 1% is actually superconducting), the winding fill factor can be calculated as the division of the total tape surface and the total surface including the support material as seen in Figure 7-3:

$$FF_{HTS} = \frac{3 \cdot t_{HTS\ tape} \cdot h_{HTS\ tape}}{\left(3 \cdot t_{HTS\ tape} + t_{support}\right) \cdot \left(h_{HTS\ tape} + h_{support}\right)} \quad \textbf{(7-5)}$$

$$= 0.71$$

With exception of the pole pitch, the coil dimensions and the winding will factor are now defined. The next step is defining the current density and airgap field.

7.2.Current and field calculation

To define the current density and airgap field of the coil, the critical curve of the tapes has to be taken into account. Since the operating temperature is decided to be 65 K, only the current and field are variable. In order to find the critical values, a model in Comsol is made, as illustrated In Figure 7-4 (left) together with the cut line that defines the simple 2D model that is used for the FEM simulation. The resulting simple 2D model is shown in Figure 7-4 (right)

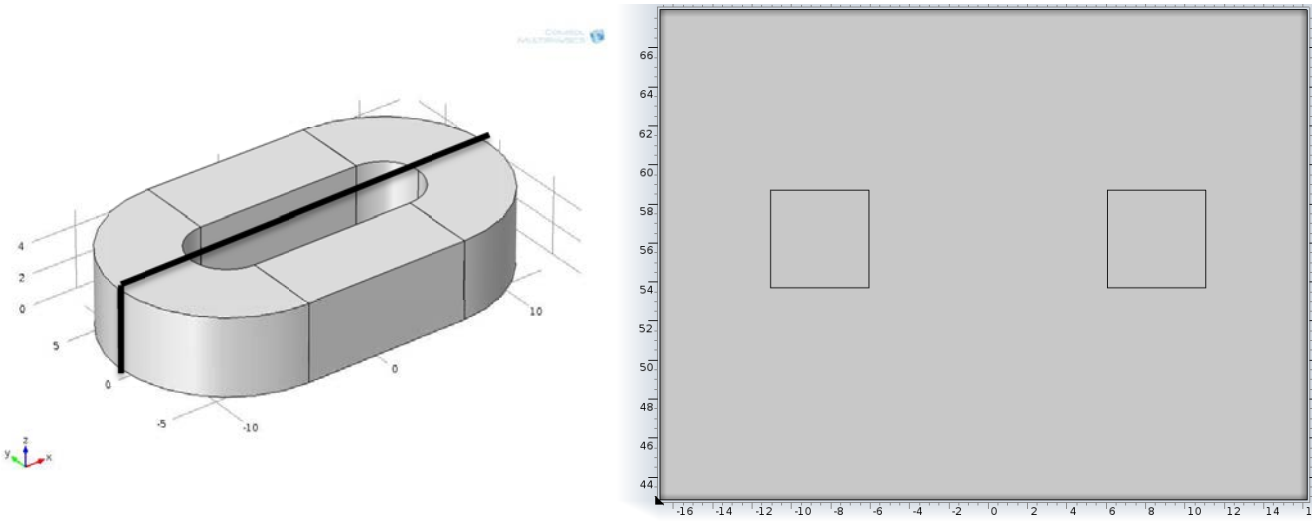

Figure 7-4 The 3D model of the HTS coil with cut line for 2D model (left) and the resulting 2D model (right)

The rectangles in the 2D model represent the HTS windings and for the simulation the current density multiplied with the fill factor (equation (7-5)) is applied on them. The resulting field distribution is displayed in Figure 7-5. In the figure also the observed location of the maximum normal and parallel fields seen by the tapes are illustrated.

To test how the fields and currents relate with respect of the critical values, the coil load line is compared with the critical graphs from Superpower for both maximum fields. The coil load line represents the relation between the current density and the resulting magnetic field at a certain point in the coil.

An illustration of this is found in Figure 7-6. Here the coloured lines represent the critical curve at a specific temperature and the black line is the load line of the coil that depends on the dimensioning of the coil. The intersection of the two lines represents the critical operating point of the respective field direction. The minimum critical current of the two defines the critical current density of the coil. However, this critical current density is not practical, because a small deviation in the current could lead to loss of superconductivity. Therefore, commonly applied in this industry is a safe factor of 0.8 or smaller. This reduces the currents and fields by 20%, but it is a safer operating point.

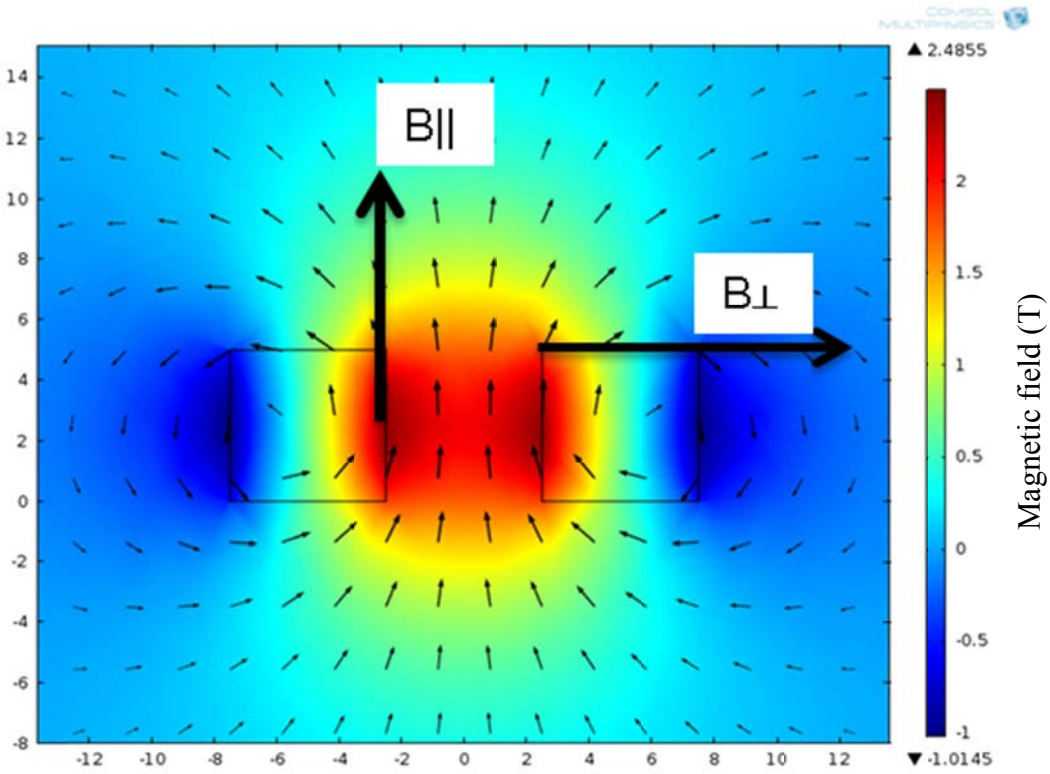

Figure 7-5 Magnetic field distribution at the cross section of a HTS coil. The arrows show the points where the corresponding field is maximum

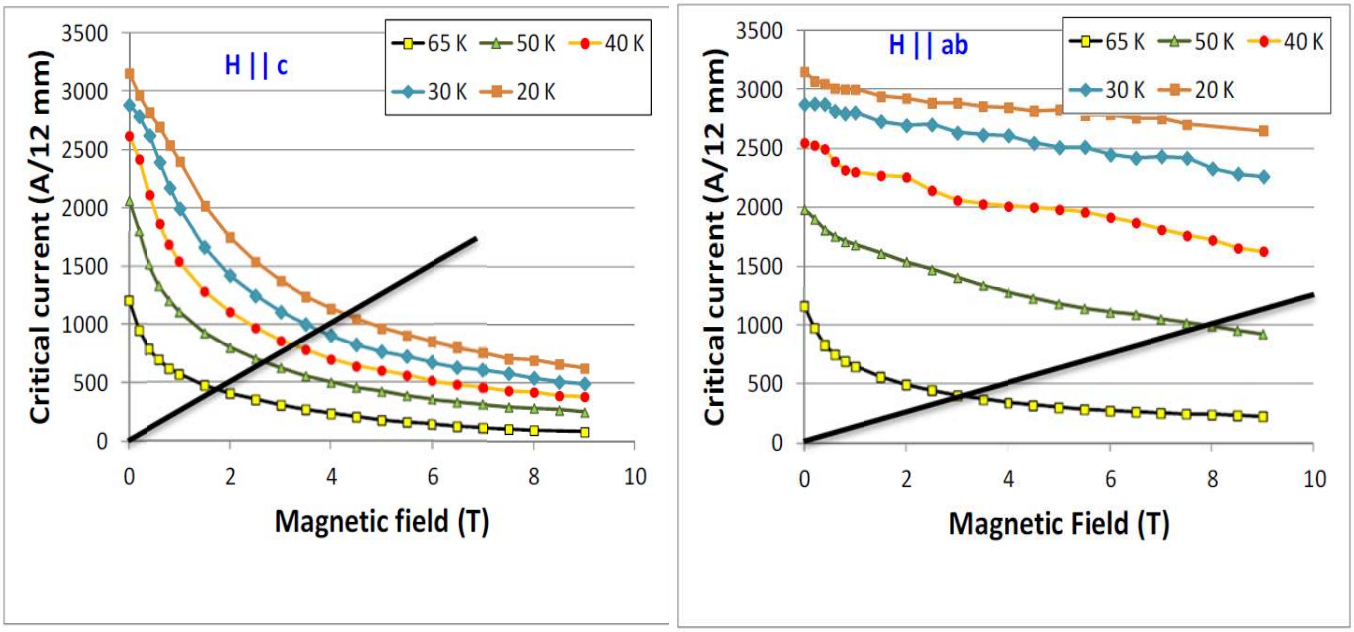

Figure 7-6 Load lines for HTS tape from Superpower (courtesy of Superpower Inc.) together with the coil load lines in the case of the normal field (left) and the perpendicular field (right)

7.3.Effective airgap

In iron core machines the airgap field is usually defined as the field inside the mechanical airgap, since that is also the electrical airgap. However in the case of a full aircore machine the whole machine is essentially the electrical airgap. Just taking the magnetic field in the middle of the mechanical airgap will result in an unrealistic high value because the field decays very fast at greater distances from the HTS coils. For the purpose of illustration, a certain coil configuration is chosen which has a field of 1 Tesla at the face of the coil. When observing the field up to 7.5 cm from the face of the coil, the decreasing field is found as shown in Figure 7-7. The black line depicts the start of the armature coils at 2.5 cm from the HTS coil face.

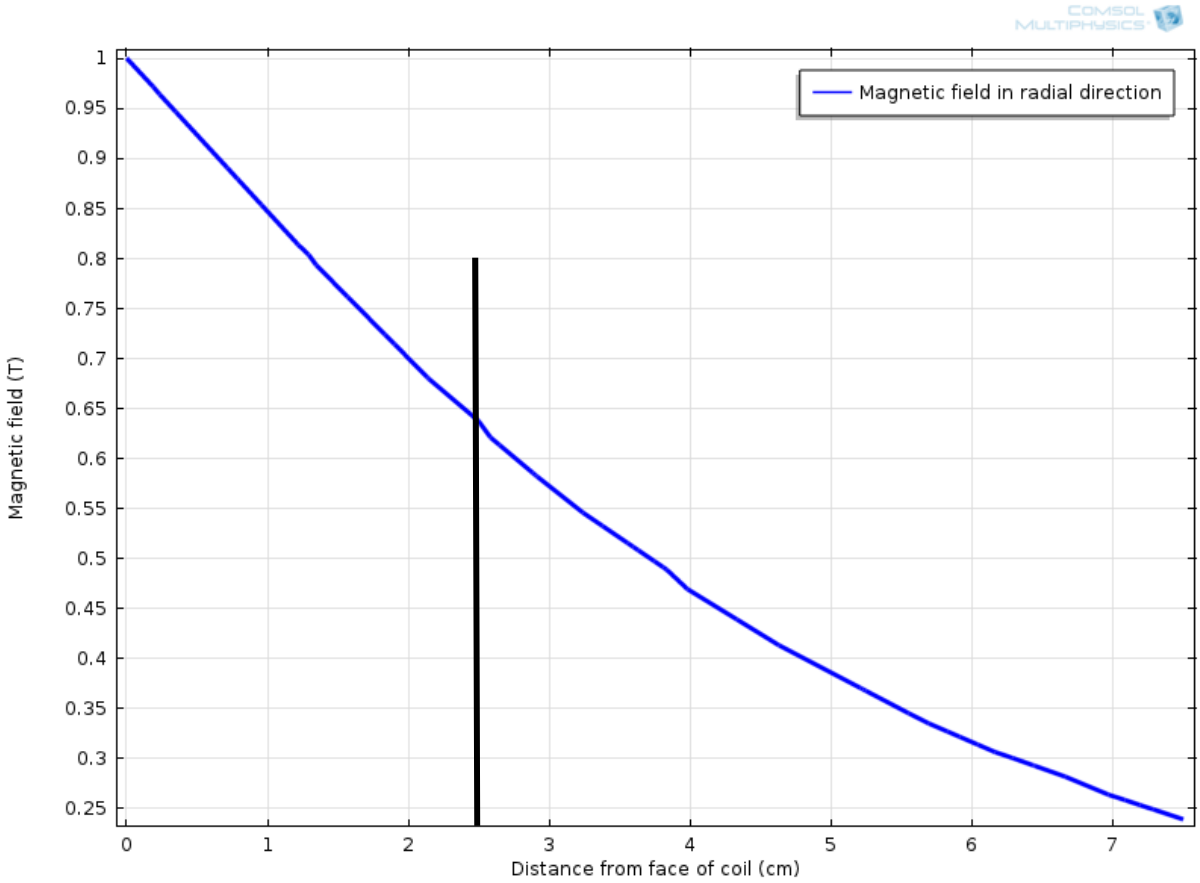

Figure 7-7 Example of magnetic field at distances from face of coil

In order to define an airgap field that is comparable to the definition of those of conventional machines, an effective airgap is introduced. The effective airgap is defined as the average magnetic field seen by the armature coils:

$$B_{eff} = \frac{1}{x_{arm} - x_{gap}} \int_{x_{gap}}^{x_{arm}} B_{fem}(x)dx \qquad \textbf{(7-6)}$$

Here x_{gap} represents the distance from the face of the HTS coils where the armature coils begin, which is equal to the airgap of 2.5 cm. The end of the armature coils is quantized by x_{arm} and B_{fem} is the field distribution retrieved from FEM simulations as shown in Figure 7-7. Using this definition, the effective airgap in the example is 0.41 Tesla, which is significantly lower than the field of 0.8 Tesla in the middle of the airgap or the 1 Tesla at the face of the coil.

7.4.Effective stack length

In conventional iron core machines with a small airgap the end effects are small, meaning that the effective stack length is with a few percent difference equal to the mechanical stack length. In large airgap aircore designs this is no longer the case and end effects can be severe.

To illustrate the end effects a 3D field simulation in Comsol is performed and the field is measured along a surface 3.5 cm above the coil. The model is shown in Figure 7-8. After applying an arbitrary current density in the coil (the result is independent of the current density), the acquired field at the measurement surface is plotted in Figure 7-9.

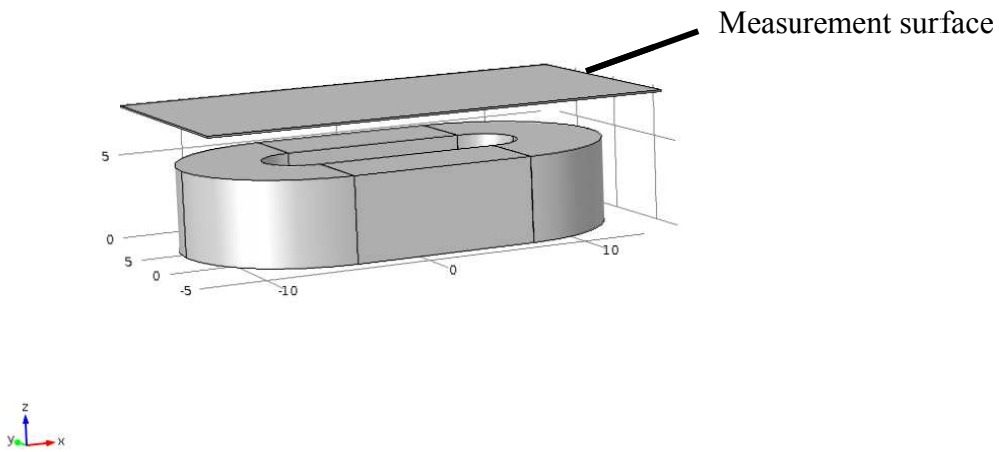

Figure 7-8 FEM model of the HTS coil with measurement surface

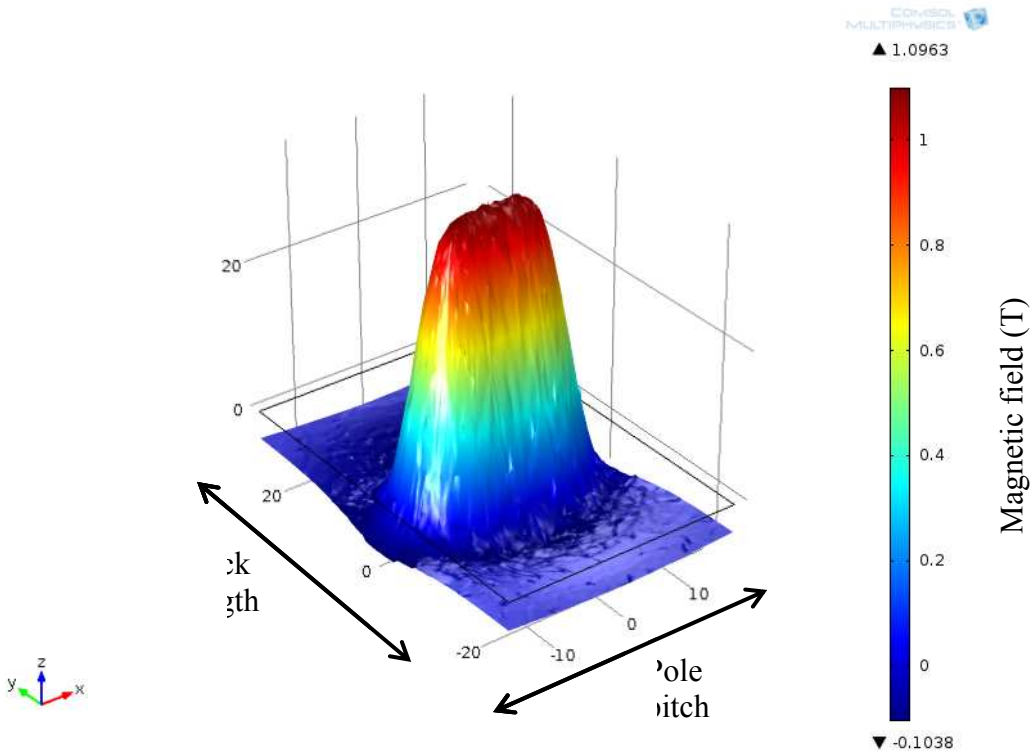

Figure 7-9 Surface magnetic field distribution above the HTS coil

From the figure, it is concluded that the field is cone shaped, so it cannot be assumed that the peak airgap field, which is calculated in a 2D simulation, is seen over the whole stack length. This means that the armature will see a reduced flux. This effect is taken into account by defining the effective stack length.

The effective stack length is defined as the reduced length that sees the peak field constant along the stack of the coil. This length is calculated as follows:

$$L_{eff} = \frac{1}{B_{max}} \int_{L_{stack}} B_{stack}(x)dx \qquad (7\text{-}7)$$

Here B_{max} is the peak field and B_{stack} the field curve along the stack. Applying this formula, the effective stack length is only **about 65%** of the actual length, meaning that the end effects reduce the flux by 35%.

7.5.Conclusion on the field winding design

In this chapter the different steps of the field winding design are described. The construction of the HTS racetrack coil is defined, resulting in the winding fill factor. Also the method of acquiring the critical field and current is given. The effective airgap is defined, which will be used in the next chapters. In addition the effective stack length is calculated, which resulted to be only 65% of the mechanical stack length. With this information the pole pitch will be determined in chapter 9, after which the design of the field windings is finalized.

8. Cryostat design

In this chapter a first design of the cryostat is performed. Of this design, the heating occurring in the cold part is calculated. The method of removing these heat losses is also included. The aim of this chapter is to give a conclusion on the feasibility of the cryostat design and its heat losses.

In order to keep the superconductors at a temperature of 65 K, they are placed in a stationary cryostat. The function of the cryostat is to keep the HTS coils at the low temperature by shielding them from external the heat sources. The cryostat design is divided by the structural design, the calculation of the heat losses and the analysis on how to cool the cold mass.

8.1.Structure of the cryostat

In this paragraph, the mechanical design of the cryostat is performed. Any cryostat structure consists of the basic components illustrated in Figure 8-1. For the design, the most important components that are the vacuum isolation wall and the cold mass mounting. The current leads are not considered a structural problem and they are therefore designed paragraph 8.2.

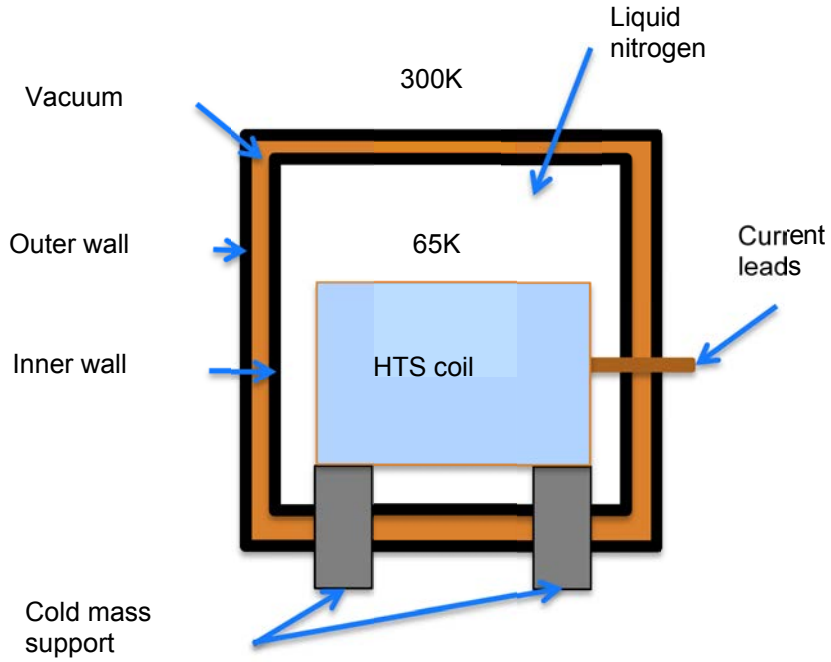

Figure 8-1 Basic schematic illustration of any cryostat

8.1.1. Vacuum isolation

As shown in Figure 8-1, the vacuum isolation wall consists of an inner and outer wall with in between a vacuum in order to reduce the heat leak as a result of thermal conduction. Since this isolation wall contributes to the airgap, the total wall thickness in the airgap is chosen to be not more than 1 cm.

Based on the example of Mijatovic [27] the inner and outer walls are chosen to consist of aluminium with a thickness of 0.3 cm. The main purpose of these walls is to provide mechanical strength and support of the vacuum. The remaining 0.4 cm is reserved for the vacuum space and for the extra isolation to reduce thermal radiation into the cold mass.

Because of the large temperature difference between the warm and the cold wall, thermal radiation can be significant. Therefore, common in the industry, a Multi-Layer Isolation (MLI) is applied. By using several layers of reflective material inside the vacuum space between the walls, a large portion of the radiation is reflected. An example of this MLI is given in Figure 8-2. The actual design of this isolation layer and the resulting heating is performed in the paragraph 8.2.

Figure 8-2 Example of MLI material (courtesy of RUAG [53])

8.1.2. Cold mass support

The HTS coils (cold mass) in the cryostat have to be supported and mounted to the outer frame of the machine. Because of the limited available axial space of the design, the mounting structure is designed to use the radial space as much as possible.

In designing the mechanical support structure, several assumptions are made with respect to the mechanical material strengths, since the mechanical stress analysis of materials is beyond the scope of this thesis. It should be noted that in order to provide a complete design of the cold mass support, also the mechanical analysis should be performed.

The first mounting component is the aluminium ring on which the superconducting coils are mounted, see Figure 8-3. This ring extends 3 cm radially for mechanical strength and it acts as a mounting point for the several rods that connect the cold mass to the warm outer structure of the motor. These rods are an essential part of the cryostat design, since they have to be thermally isolating. Not only do they see a large thermal difference, they also have to be rigid enough to endure the large torque of the motor. The combination of strength and insolating means that most materials like metals are not suitable. As it is common in literature, it is chosen to use Glass Fibre Reinforced Plastic (GFRP) instead.

The thermal conduction losses through the rods are reduced by limiting the contact surface and by increasing the distance between the inner and outer vacuum wall. The rods are chosen to be 4 cm in diameter and they span the distance of 5 cm between the inner and outer vacuum wall, see Figure 8-3. For this design it is chosen to use 10 of these rods, however a full mechanical analysis is required to select a good number of rods.

For now it is considered that the cold mass is only supported by these rods. This will be not enough in a practical design when considering bending of the rods due to forces like gravity, which may damage the vacuum walls in the airgap. Therefore smaller mounting parts should be added, but in this study they are not considered for simplification.

Now that the basic structure of the cryostat is defined, the heating losses are calculated in the next section.

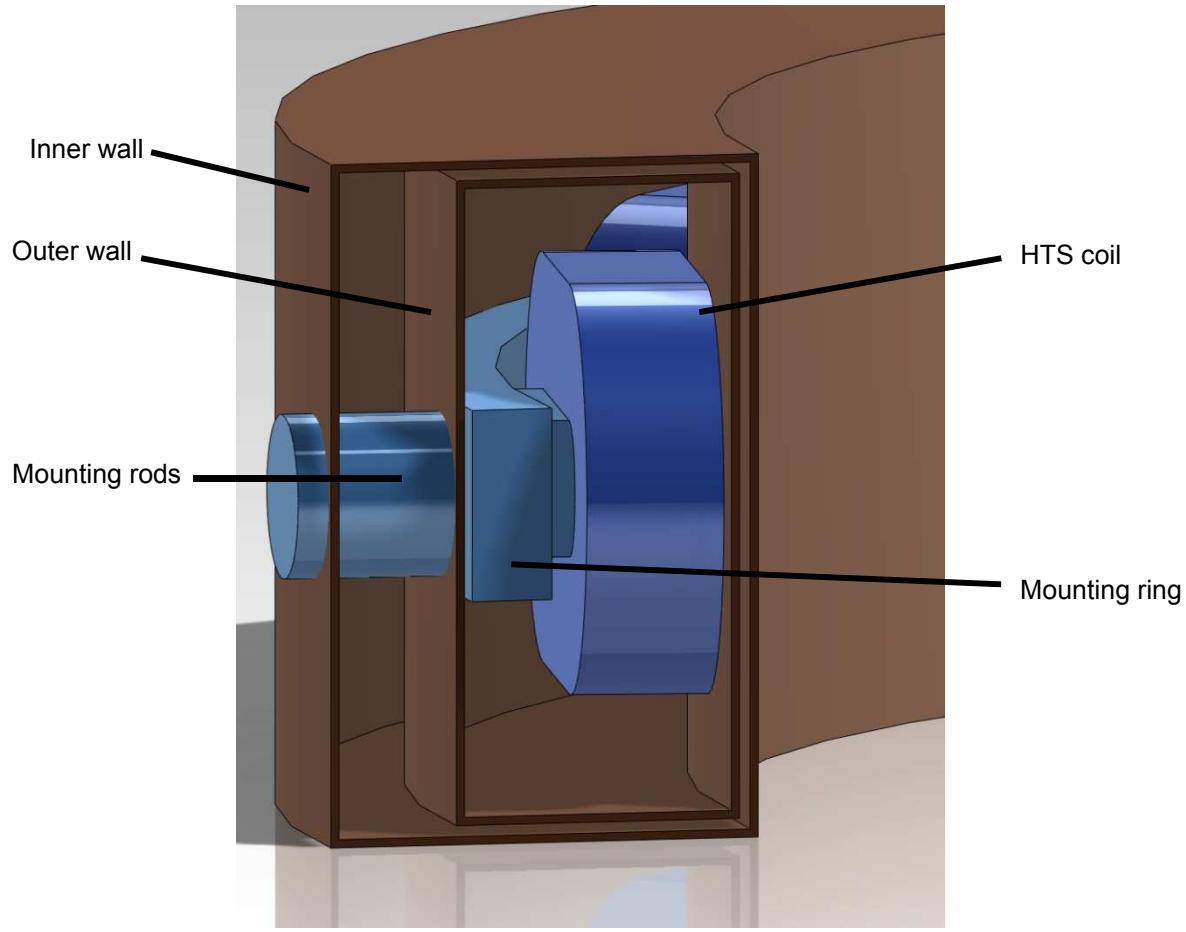

Figure 8-3 Cryostat design

8.2.Heat sources in the cryostat

In this section the major heat losses in the cryostat are calculated. The following heat sources are considered:

- Electrical conduction losses
- Current leads
- Thermal conduction
- Thermal radiation

For the calculation of the heat losses only the steady state operation is assumed.

8.2.1. Electrical conduction

Although the superconductor has no electrical resistance when it is operated within its superconducting state, the transition between the superconductor state and normal state is gradual. This effect results in a voltage across the HTS tape that in combination with the high current leads to conduction losses.

The (empirical) formula for the generated voltage is:

$$E_e = E_0 \left(\frac{I}{I_c}\right)^n \qquad \textbf{(8-1)}$$

Here $\mathbf{E_e}$ is the voltage per meter, $\mathbf{E_0}$ is the electric field criterion of1 $\mu V/cm$, $\mathbf{I}$ is the operating current, $\mathbf{I_c}$ is the critical current and $\mathbf{n}$ defines how steep the transition between the superconducting and normal state occurs. In this design it is chosen for the operating current to be 80% of the operating critical current. The n-value for the used tape is about 30 [54]. The calculated voltage is:

$$E_e = 10^{-4} \cdot (0.8)^{30} = 1.24 \cdot 10^{-7} V/m \qquad \textbf{(8-2)}$$

The total wire length per coil was calculated as 400m and by using 12 coils the conduction losses are calculated:

$$\begin{aligned} P_c &= E_e \cdot I \cdot wire\ length \\ &= 1.24 \cdot 10^{-7} \cdot 0.8 \cdot 150 \cdot 400 \cdot 12 = 70mW \end{aligned} \qquad \textbf{(8-3)}$$

The conduction losses are considerably low compared to other losses. The reason for this is the high n-value of the tapes and the rather low amount of tape that is used.

8.2.2. Current leads

The current leads are one of the major heat sources of the cryostat. They form a bridge for the current from the warm to the cold part and are made from resistive material like copper or brass [14]. These leads do not only produce resistive losses, but they also form a thermal conductive path from ambient to the cryostat.

According to Kalsi [14], there are several types of current leads, but here the conduction cooled lead is used. This type is introduces more heat losses, but it is much less complex and it performs well enough at liquid nitrogen temperatures. The current leads consist of a pair of metal rods that see both a large thermal difference and they conduct the large current of the superconductors. The thermal conduction from the warm to the cold part through the current leads is given by [17]:

$$Q = \frac{\rho L I^2}{A} + \frac{KA\Delta T}{L} \tag{8-4}$$

Where $\mathbf{I}$ is the current in the lead, $\mathbf{L}$ is the length of the lead $\boldsymbol{\rho}$ is the average resistivity of the material, $\mathbf{A}$ is the area of the cross section of the material, $\mathbf{K}$ is the average thermal conductivity of the lead material and $\Delta\mathbf{T}$ is the temperature difference between the warm and the cold part of the cryostat. For this calculation the average value of the temperature dependent parameters is used. Although the temperature differences are rather big, for a first order calculation these assumptions are valid.

Rearranging equation (8-4) results to [14]:

$$Q = \left(\sqrt{\frac{\rho L I^2}{A}} - \sqrt{\frac{KA\Delta T}{L}}\right)^2 + 2I\sqrt{\rho K \Delta T} \tag{8-5}$$

The heat intake can be minimized by balancing out the thermal conduction and the resistive heating losses. In equation (8-5) this can be achieved by setting the first term to zero. This results in the following ratio:

$$\frac{L}{A} = \frac{1}{I}\sqrt{\frac{K}{\rho}\Delta T} \tag{8-6}$$

Using this ratio of the current lead length and cross sectional area, the minimum heat intake from the leads is given as:

$$Q = 2I\sqrt{\rho K \Delta T} \tag{8-7}$$

The heat intake from the current leads can be reduced by using a lead material with a very low $\rho \cdot \mathrm{K}$ value. Also a high K/ρ is needed for a smaller wire diameter. In literature, different materials are considered like copper and brass and for a few materials the losses are calculated in Table 8-1 considering $\Delta\mathrm{T} = 300 - 65 = 235\ \mathrm{K}$ and $\mathrm{I} = 60\ \mathrm{A}$.

Material	ρ [$\mu\Omega m$]	K [W/m/K]	$\rho \cdot K$ [$\mu\Omega W/K$]	L/A [m^{-1}]
platinum	0.011	70	0.77	20381
aluminium	0.027	250	6.75	24585
copper	0.017	400	6.8	39191
brass	0.04	109	4.36	13337
constantan	0.05	20	1.0	5110

Table 8-1 Properties of materials considered for current leads

The use of copper or aluminium seems a logical choice, but due to their high thermal conductivity the $\rho \cdot K$ factor is much larger than that of brass or constantan. Using constantan results in the lowest losses (except for platinum).

When using constantan and considering a lead length of 5 cm (the maximum distance between the inner and outer vacuum wall) and the corresponding wire cross section of $0.1\ cm^2$, the total losses in the cryostat from the current leads become:

$$Q = 2 \cdot 2 \cdot 60\sqrt{10^{-6} \cdot 235} = 3.7\ W \qquad \textbf{(8-8)}$$

Using more complex current leads, like the vapour cooled current leads [14], could decrease the heat losses more and could be considered in future work.

8.2.3. Thermal conduction

Thermal conduction losses through the cold mass support structure are one of the major heat sources in the cryostat. Thermal conduction by the vacuum layer between the warm and cold part is neglectable, but the mounting structure of the cold parts are providing a thermal conductive path.

The heat conduction through a solid is given by:

$$Q_{conduction} = \frac{A}{L} K \Delta T \qquad \textbf{(8-9)}$$

Here **A** is the cross area of the solid, **L** is the length of the solid between the inner and outer wall and K is the average thermal conductivity of the used material. Assuming 10 solid round glass fibre reinforced plastic (GFRP) mounting rods of 4 cm in diameter, the losses become:

$$Q_{conduction} = 10\frac{0.25\pi 0.04\text{^}2}{0.05} 0.66 \cdot (300 - 65) = 39W \qquad \textbf{(8-10)}$$

It is important to notice that this value may change after the mechanical analysis of the whole machine, since the number of rods and the rod dimensions can change to meet the mechanical specifications. Also the conduction through the extra structures to support the inner wall of the cryostat is not included, but it is assumed that they can be optimized for neglectable conduction losses.

8.2.4. Thermal radiation

From the warm outer wall to the cold inner wall of the cryostat, heat is radiated which could be a significant heat source. The thermal radiation of a body of surface **A** at a temperature **T** is:

$$Q_{radiation}[W] = \varepsilon \cdot \sigma \cdot A \cdot T^4 \qquad \textbf{(8-11)}$$

Where **σ** is the Stefan-Boltzmann constant and **ε** is the combined steady state emissivity of the inner and outer wall materials. Because the cryostat inner and outer wall dimensions are much larger than the distance in between, they can be modelled as two parallel plates. When taking the outer wall area **A** and the emissivities $\boldsymbol{\varepsilon_1}$and $\boldsymbol{\varepsilon_2}$ for the both wall materials, the equation becomes then [55]:

$$Q_{radiation}[W] = \sigma \cdot A \cdot (T_1^4 - T_2^4) \cdot \frac{\varepsilon_1 \varepsilon_2}{\varepsilon_1 + \varepsilon_2 - \varepsilon_1 \varepsilon_2} \qquad \textbf{(8-12)}$$

Both walls are made of aluminium with an emissivity of 0.04-0.15, depending on surface roughness [55]. Here a value of 0.04 is used. The transferred radiation heat from the outer wall with a surface of $3.1\mathrm{m}^2$ becomes:

$$Q_{radiation}[W] = 5.67 \cdot 10^{-8} \cdot (300^4 - 65^4) \cdot \frac{0.04^2}{0.04 + 0.04 - 0.04^2} = 9.35W \qquad \textbf{(8-13)}$$

A heat loss of 9.35 W is considerable for a cryostat and therefore it is lowered by adding a multi-layer insulation (MLI) in the vacuum part. The MLI is wrapped on the cold wall to reduce radiation and it is made from many layers of aluminium with thermal isolation in between [53]. N layers of MLI reduce the losses to about 1/(N+1) of the radiation and an optimum is achieved with 30 layers per cm [56]. In the 0.4 cm gap, 12 layers are placed and the final radiation is then decreased by a factor of 13, resulting in a heat loss of only **0.7 W**.

The final heat losses are summarized in Table 8-2. It can clearly be seen that the conduction losses are the main heat source in the cryostat. It must be emphasised that since only the steady state operation is considered, the acquired heating and cooling values are minimum. Operation during start-up and during faults is much more demanding for the cooling system and therefore they should be considered for future work.

Heat source	**Losses [W]**
Electrical conduction	0.07
Thermal conduction	**39**
Thermal radiation	0.7
Current leads	3.7
Total	43.07

Table 8-2 Heat sources in the cryostat

8.3.Cooling of the cryostat

Now that the heat losses are calculated, it is analysed in this section on how feasible these losses can be removed from the cryostat. The thermal energy is removed with liquid nitrogen and only the steady state situation is considered. First it is assumed that the liquid nitrogen is precooled available in tanks. Secondly, also the possibility of using a cryocooler is considered.

When using precooled liquid nitrogen stored in tanks, it is important to know how much nitrogen is needed during operation per unit of time. This calculation is not straight forward, since the efficiency of cooling with a liquid flow depends on many variables, like the cooling surface. Since the actual

cooling system is not designed here, in order to make a simple calculation, it is assumed that the system is capable of extracting enough heat from the cold mass to increase the temperature of the liquid nitrogen by a few degrees.

The temperature of the nitrogen that enters the cryostat is assumed to be 65K. The temperature rise is limited for better performance of the HTS coils. This means that the nitrogen will not boil off and will leave the cryostat in its liquid state. For a first order calculation of the amount of liquid nitrogen needed per second, a perfect heat transfer from the coils to the liquid is assumed. Assuming a constant specific heat capacity of nitrogen, the flow of litres nitrogen per second needed to remove a heat load of **P** Watt, while allowing a certain $\Delta\mathbf{T}$, is:

$$F = \frac{P}{\rho \cdot C \cdot \Delta T} \; [litre/s] \qquad \textbf{(8-14)}$$

Here **ρ** represents the density of 0.81 [kg/litre] and **C** the thermal capacity of 2042 [J/kg/K] of liquid nitrogen. When allowing a **temperature increase of 2 degrees**, the amount of liquid nitrogen needed is **0.78 L/min.** This means that for one hour of flight **at least 47 litres or 38 kg** of nitrogen is required. This value is the **minimum** flow needed to remove the steady state heat from the cold mass, without considering the efficiency of the cooling system. It is expected that in practice the required flow is higher.

Instead of using liquid nitrogen stored in tanks, the use of a cryocooler to cool the nitrogen in a closed loop flow is also considered. As explained in chapter 3.5.2, the cryocooler made by Lockheed Martin [35], can remove 20 Watt at 70 K and it is expected to provide at least 15 Watt at 65 K. A minimum of three of these coolers would be sufficient. More realistic would be to use at least five coolers to incorporate some form of redundancy and safety. The total cooler weight would become 35 kg.

From these calculations it can be carefully concluded that the use of cryocoolers is preferred over the use of nitrogen tanks, because it will result in a much lighter cooling system. Also the cryocoolers can work (practically) indefinitely, which make them much more reliable. A disadvantage of these cryocoolers is their low efficiency, resulting in 600 W of power per device. The cryocoolers would then in total consume 3 kW of power, which is 0.5 percent of the motor power target.

8.4.Conclusion on the cryostat design

In this chapter a first design of the cryostat was performed. The most important structures were designed including the vacuum walls and the cold mass support. By comparing with example cryostat designs found in literature [27], a realistic design was made. Yet, for the design the mechanical stresses are not calculated, so the design and some heat losses would change if a full mechanical analysis would be performed.

The major heat sources in the cryostat are calculated with the result of 43 W of heat losses with the conduction losses of the cold mass mounting being the major source. To remove these losses with liquid nitrogen stored in tanks, at least 38 kg of nitrogen per hour is needed. Cooling with cryocoolers is preferred since it can operate much longer than one hour at the same weight.

It is concluded that the cryostat design is feasible and the heat losses can be removed by using the Lockheed Martin cryocooler that is optimized for aerospace.

9. Total machine analysis

The aim of this chapter is to combine the results of the previous chapters and to perform the necessary full-machine calculations to give a final statement on the feasibility of the superconducting propulsion motor for the hybrid helicopter concept. Also the final parameters including the torque, weight and efficiency of the total machine are calculated.

9.1.Complete machine model

In this chapter the complete machine is considered, including the armature and the excitation coils. For the electromagnetic simulations a 2D model in Comsol is used, as illustrated in Figure 9-1. As was concluded in chapter 6, the machine is designed with the full pitch distributed winding configuration. The superconducting racetrack field coils are placed on the outer part and the distributed windings are placed on the rotor. The current distributions in the windings are defined in chapter 6 and chapter 7 for the armature currents and the field currents respectively.

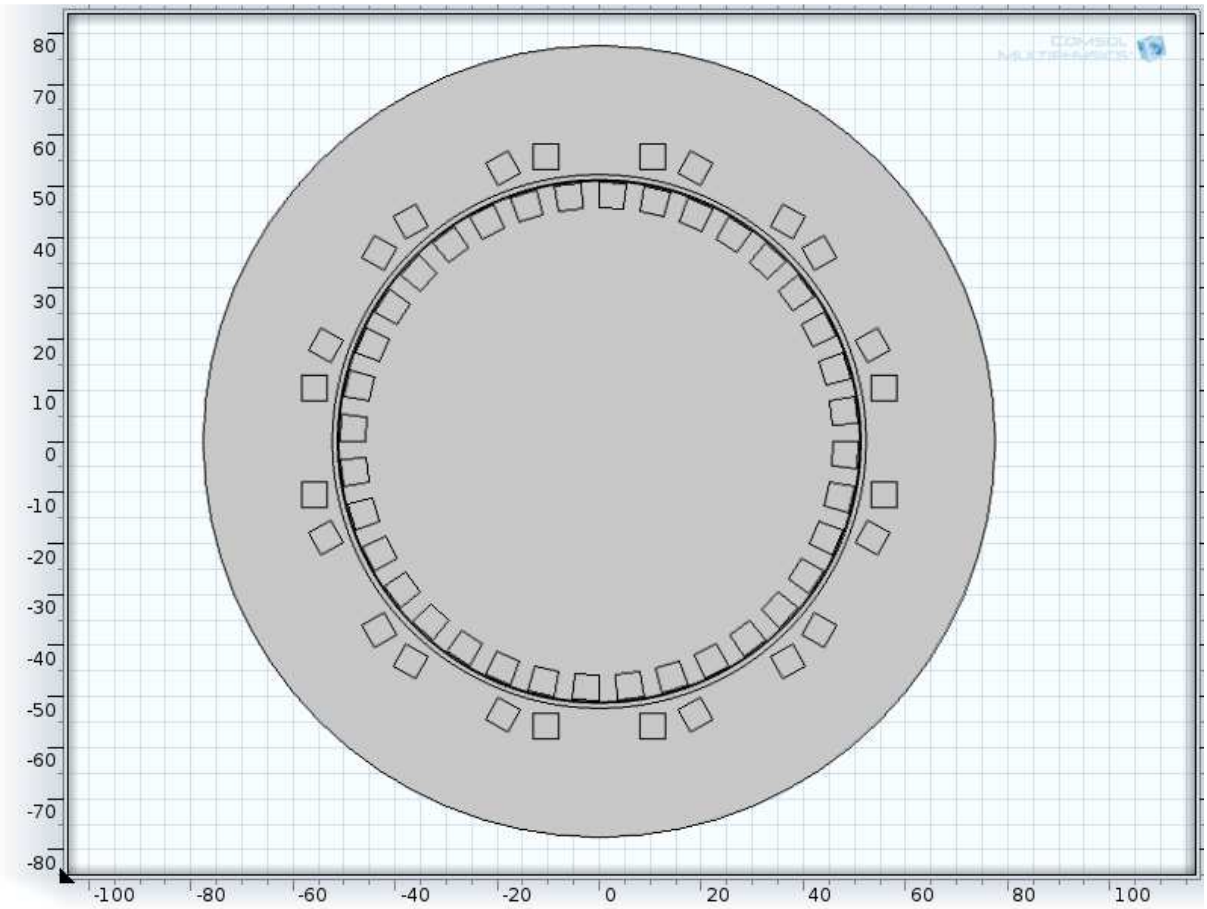

Figure 9-1 2D model in Comsol of the whole machine

9.2.Machine electromagnetic torque

In this section not only is the torque calculated by sweeping it as function of the machine pole pitch, also the optimum pole pitch is calculated. The optimum is chosen at the maximum torque configuration. For the torque calculations the Finite Element Method (FEM) is used in Comsol.

9.2.1. Torque calculation method

In FEM there are different ways to calculate the torque. The build-in method of Comsol uses the Maxwell Stress Tensor (MST) method, which is defined as [57]:

$$T_{MST} = l_{eff}\, r \int_L H_{tan,arm} B_{norm,field}\, dl \qquad \textbf{(9-1)}$$

Here, $\mathbf{H_{tan,arm}}$ is the tangential magnetic field strength produced by the armature coils in the middle of the airgap, $B_{norm,field}$ is the normal magnetic field density produced by the field coils in the middle of the airgap, **r** is the airgap radius, **L** is the airgap circumferential length and $\mathbf{l_{eff}}$ is the effective stack length.

Although the MST is very fast and easy to use in Comsol, it is very sensitive to the mesh quality and mesh symmetry, which can cause inaccurate results. By using a symmetrical model and a high quality mesh the risk of wrong results is reduced, but for comparison the torque was also calculated with the Lorentz force method, which is implemented for a 2D model as:

$$T_L = \sum_{n=1}^{3} l_{eff}\, J_{n,ph} \iint_S B_A\, r\, dA \qquad \textbf{(9-2)}$$

Here $\mathbf{J_{n,ph}}$ represents the phase current density, $\mathbf{l_{eff}}$ the effective stack length, $\mathbf{r}$ the local machine radius and $\mathbf{B_A}$ the local field from the excitation coils seen by the armature windings.

In addition to the Lorentz method, the toque is also calculated by the change in electromagnetic co-energy [57]:

$$T = \left.\frac{\partial W'(I,\theta)}{\partial \theta}\right|_{I=constant} \qquad \textbf{(9-3)}$$

With **W** representing the magnetic energy in the whole machine and $\boldsymbol{\theta}$ representing the rotor angle. By performing two simulations with a small change in the rotor angle, while keeping the currents constant, the torque is calculated.

With the torque calculation defined, the torque is calculated using a static simulation. Since the maximum torque is here of interest, the machine is positioned in the maximum torque or maximum load angle position.

9.2.2. Determination of the maximum torque

In this section the maximum torque is calculated using Comsol simulations. The major parameter that has influence on the maximum torque is the machine pole pitch or the number of pole pairs. When changing the number of pole pairs also the following parameters are directly influenced:

- **Airgap radius**. When the number of pole pairs changes, the HTS coils (outer coils) become bigger or smaller. Because they are racetrack coils, they do not bend along the curve of the airgap. The result is that the outer radius of the HTS field windings increases when the number of pole pairs increases. To counteract this, the airgap radius is decreased so that the outer radius of the HTS coils remains 60 cm.

- **Airgap field**, when the coils become larger, the magnetic field can penetrate deeper trough the airgap into the armature resulting in a higher effective airgap field.

- **Critical current and field**. Because of the HTS coils changing in size, the magnitude of the maximum field at a constant field current inside the coil will change as well. The reason this occurs is that when the inner bore of the coil becomes smaller, the magnetic field becomes more concentrated and a larger field is seen by the superconductors. The result is that for every pole pair number, the critical current density and magnetic field have to be recalculated.

In the search of the maximum torque, the following parameters are kept constant:

- **Coils slot depth**, the slots are kept at 5 cm
- **The armature current density**, which is kept at 5 A/mm^2 with a fill factor of 0.4
- **The armature winding configuration**, which is kept at the full pitch distributed configuration
- **The effective stack length,** which is assumed not to be substantially influenced by the change in field coil size

Incorporating all the parameters, which are not independent, becomes too computationally intensive and can only be considered when using a optimizing algorithm.

Using the 2D model as described in section 9.2, the maximum torque is simulated as function of the number of pole pairs. With every parameter change, the 2D model is rebuild and the airgap radius is recalculated. The critical values are recalculated using the critical curve in Matlab, see Figure 9-3. The steps required to recalculate the machine torque are scripted in Matlab. A graphical flow diagram of the programming is shown in Figure 9-2.

The resulting pole pair vs. torque diagram is shown in Figure 9-4. From this result the following can be concluded:

- The resulting critical current density in the HTS windings is **144 A/mm^2** and the critical field inside the coil is **2.3 T**, incorporating the 0.8 safe factor
- The critical current in a single HTS tape is **58 Amps**
- The resulting effective airgap field **is 0.8 T**
- The maximum torque is 5kNm, without including the safe factor and **4.4 kNm**, when including the safe factor of 0.8
- The **optimum number of pole pairs is 6**, corresponding with a pole pitch of $\pi/6$

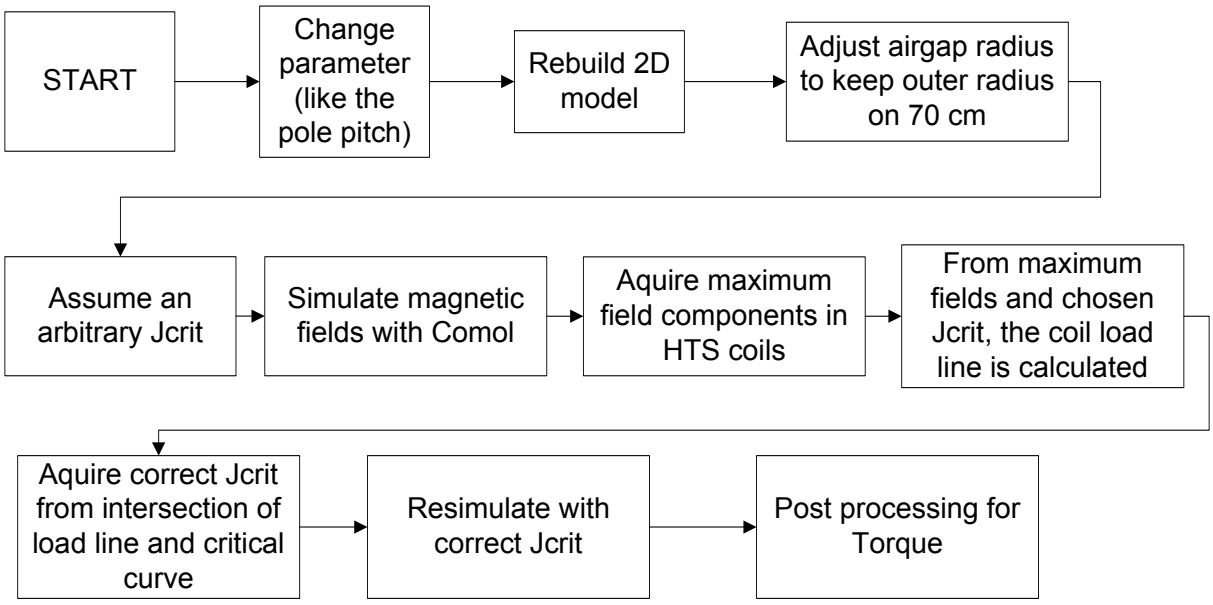

Figure 9-2 Code diagram for calculating the torque

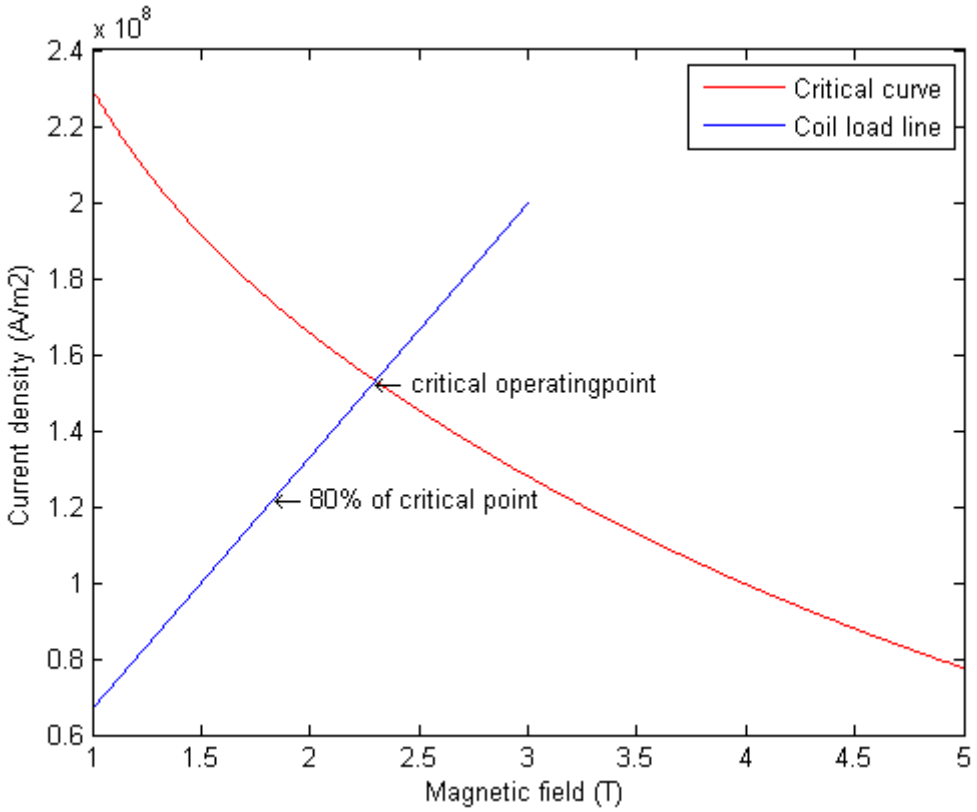

Figure 9-3 HTS coil operating point determination

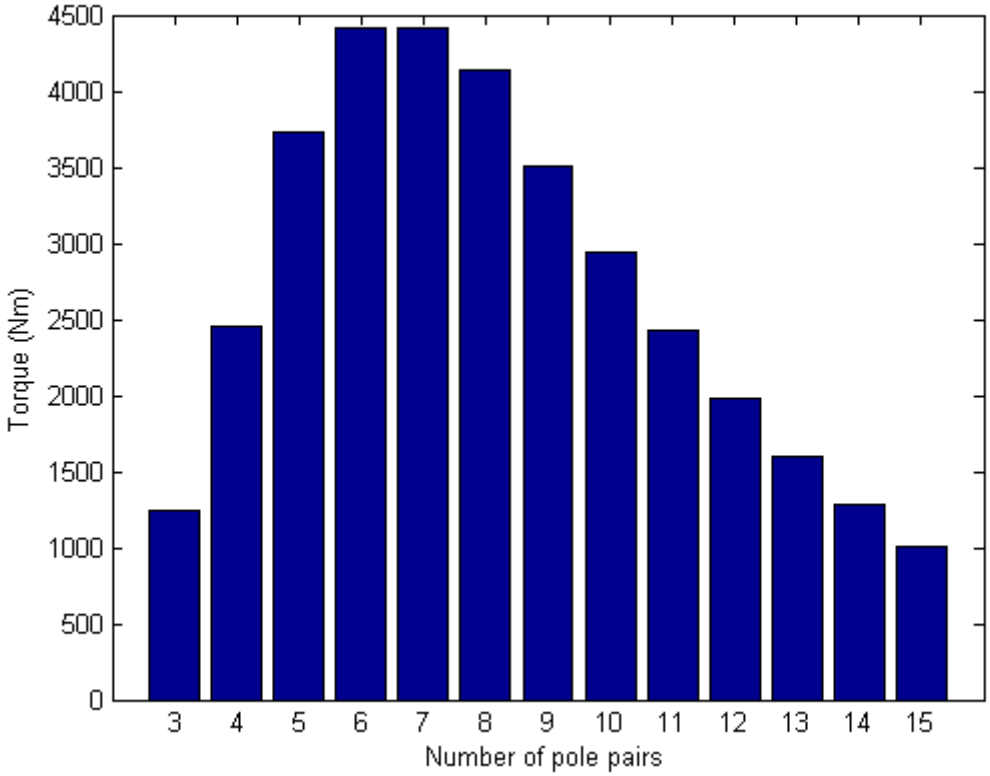

Figure 9-4 Torque as function of the number of pole pairs

The clear optimum at 6 pole pairs is explained as follows:

- When the number of pole pairs is lower than six, the field coils are very large. Not only does the airgap radius (and thus the active surface) decrease in order to keep the outer diameter at 60 cm, also the coils become too big compared to the size of the machine. This means that the excitation flux becomes less effectively linked with the armature coils. For illustration of this effect, the 2D model of the machine with 3 pole pairs is shown in Figure 9-5 (left).

- When the number of pole pairs is higher than six, the field coils become smaller. The machine looks more like a conventional low speed machine with many slots and poles, see Figure 9-5 (right) for an example of a 9 pole pair machine. However, due to the lack of iron to force the flux path and the large airgap, the flux links more effective with the other field coils than with the armature coils. The flux leakage becomes dominant and the torque decreases.

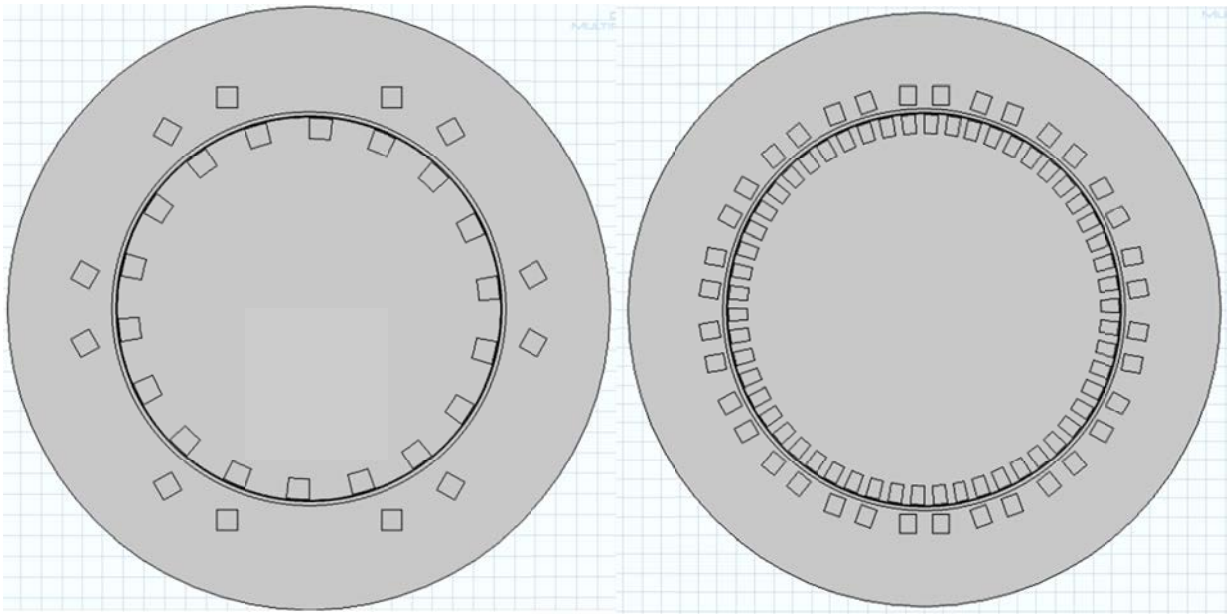

Figure 9-5 2D model in Comsol of 3 pole pairs (left) and 9 pole pairs (right)

9.3.Total machine weight estimation

Now that the complete machine is designed, the total machine weight can be estimated. To do this, a 3D model of the designed parts is made in Solid Works.

The following components are made in Solid Works:

- EM shield
- HTS support structure
- HTS coils
- Cryostat walls
- Armature coils
- Armature support

The combined construction of the whole machine is illustrated in Figure 9-6. The end windings are modelled as single layer windings.

The main construction material is chosen to be Glass Fibre Reinforced Plastic (GFRP). This composite material is very strong, lightweight, thermal and electrical isolating. Because of the electrical isolating properties, it endures no eddy current losses, making it the perfect material for the armature support.

The cryostat support rods are also made of GFRP, because of their thermal insulating property. The material of the support structure of the superconducting coils is chosen to be aluminium, because this metal can conduct heat very good so that cooling close to the support is less of an issue. The HTS coils themselves are made of aluminium metal support and YBCO tape, consisting mostly of steel and copper.

Using the volumes made in Solid Works and the material densities, the weight of the components is calculated with the results shown in Table 9-1.

The total weight of the machine with these components is found to be: **351 kg.** This weight could be lowered by performing a 3D mechanical simulation to see where material can be removed. Also, the weight can be reduced by considering more composite materials. However, these methods are beyond the scope of this thesis.

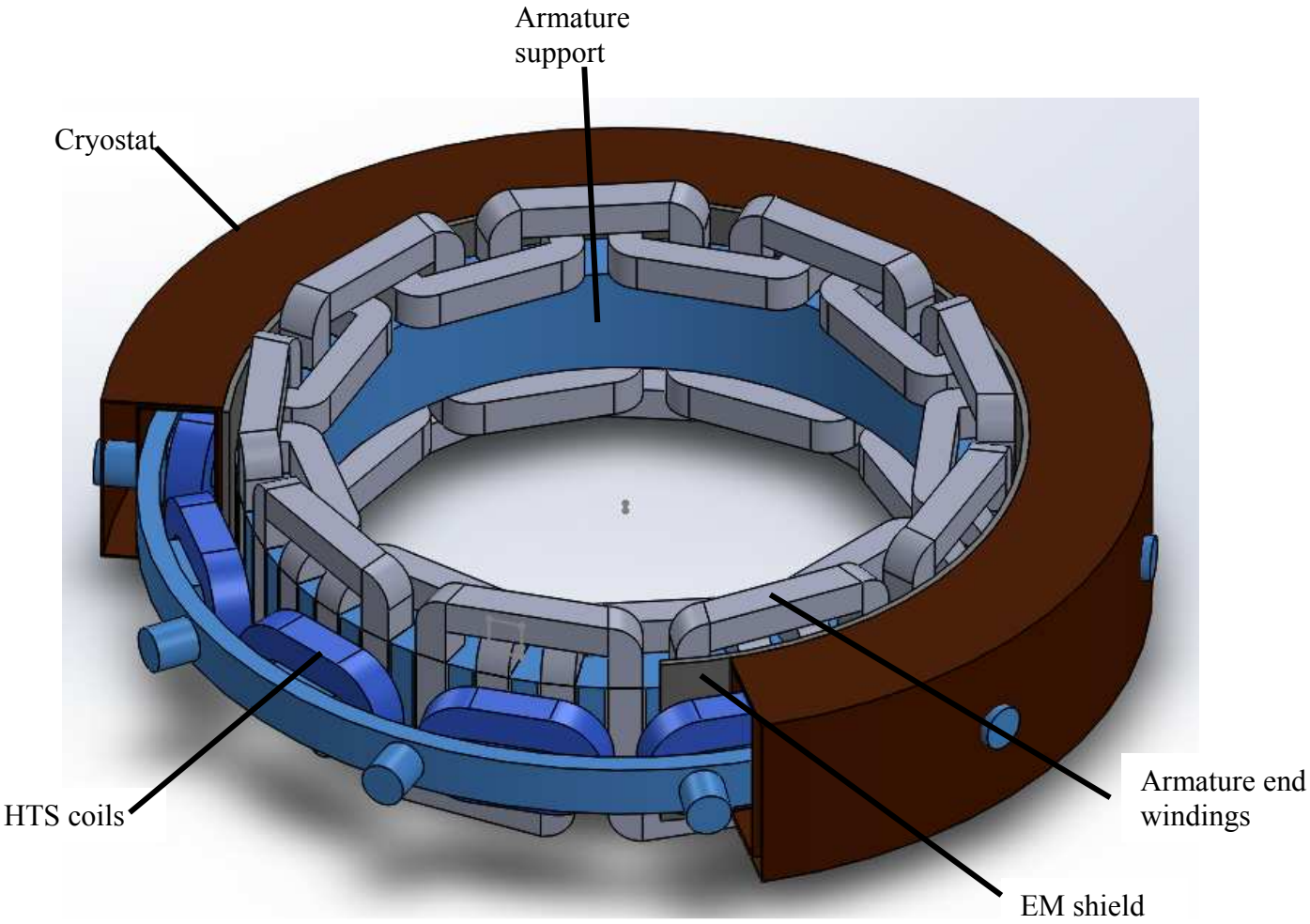

Figure 9-6 Solidworks model of the complete machine

Component	Material	Density {kg/m^3]	Weight [kg]
EM shield	Aluminium	2700	16.1
HTS support structure	Aluminium	2700	30.2
Cryostat support rods	Glass fibre reinforced plastics	2000	6.6
HTS coils	YBCO + support	7100	113.3
Cryostat walls	Glass fibre reinforced plastics	2000	23.2
Armature coils	Aluminium	2700	114.4
Armature support	Glass fibre reinforced plastics	2000	47.1
Total machine			**350.9**

Table 9-1 Mass of different components

9.4.Machine efficiency

In this section the machine electrical efficiency is calculated. Included in this calculation are the resistive losses and the cryostat cooling power, however the power required to cool down the armature coils and EM shield are not considered in this thesis. In Table 9-2 the different loss sources are represented. The calculated machine torque is 4.4 kNm, which corresponds with a power of 157 kW. The resulting electrical efficiency of the motor is **95%.**

Loss source	P [kW]
Armature Resistive losses	4.8
Cryostat cooling	3
EM shield induced losses	0.1
Total	**7.9**

Table 9-2 Loss contributions

9.5.Final machine parameters

In this section the machine parameters are discussed and compared to the target specifications. The target values are compared with the acquired values in Table 9-3. From the table it can be concluded that the resulting values are only between 10-30% of the target values.

Property	Target value	Acquired value
Nominal power (kW)	590	157
Nominal torque (kNm)	16.5	4.4
Power-to-Weight Ratio (kW/kg)	4 - 5	0.4
Torque-to-Weight Ratio (Nm/kg)	110 - 130	13
Torque Volumetric Density (kNm/m^3)	43 - 51	11
Expected weight (kg)	150	351

Table 9-3 Technical specification comparison

From these results and estimations, it is concluded that the superconducting electrical propulsion motor may not be feasible. The most important targets, namely the design nominal power and the torque density, are 27% and 12% of the target values respectively. The very low attained specifications can be explained as following:

- **Operating temperature of superconductors**. The use of liquid nitrogen limits the temperature of the superconductors at 65 Kelvin or higher. The resulting critical current of 60 A is too low in order to achieve airgap fields more than 0.8 T, while lower temperature machines have reported airgap fields of more than 2 T.

- **No iron use**. By disregarding any iron, the machine weight was kept as low as possible. However, with the lack of iron no flux path could be designed. This results in a lot of leakage flux, which decreases the airgap field. The weight decrease is partly counteracted by the higher amount of conductor material needed for the aircore design. Especially the high amount of HTS material has a large impact on the weight.

- **Large airgap**. The airgap length of 2.5 cm is 5% of the airgap radius and 17% of the active axial length. The large airgap, which is unavoidable to any superconducting design, makes it more advantageous to design larger machines.

It is not expected that further optimizing the design will yield significant better results, since these issues will remain. Therefore only (significant) changes in the machine specifications can improve the design enough. The most obvious change would be to use a lower operating temperature.

9.6.Conclusion on the complete machine

In this chapter the final properties of the whole machine are calculated by combining the results from the previous chapters. The most important calculated properties are the torque, which resulted in 4.4 kNm and the total weight, which was estimated at 351 kg. These results and also their derivatives, like the power density, are only 10-30% of the target values. From these results it was concluded that a superconducting electrical propulsion motor is not feasible with current technology and specifications.

10. Conclusion and recommendations

10.1. Conclusion

The goal of this thesis was to perform a first technical feasibility study on an electrical main propulsion motor using superconducting technology for the hybrid helicopter concept. In order to give an answer to that question such a machine was designed.

The need for more environmental friendly aircraft has resulted in the aerospace industry to consider a hybrid helicopter concept. Such a helicopter would combine the high efficiency of diesel engines and electrical motors and batteries. The feasibility of such a concept is mostly determined by the feasibility of its main electrical propulsion motor.

The specifications of such a motor are very challenging, especially the target torque of 16.5 kNm with a total weight of only 150 kg. One of the few possible electrical machine types that may be able to meet these specifications is a superconducting motor. Therefore in this thesis the feasibility of such a superconducting machine design was researched.

The first design challenge was to decide which superconducting technology had to be used. In order to make an informed choice, different superconductors were analysed for their performance, resulting in YBCO technology being chosen for its electrical performance and high operating temperature. It is concluded that the technology can be used as either tapes or bulks to make coils. It is also noted that superconductors suffer from AC heat losses and that therefore only DC applications are considered. After studying the cooling system, the choice is made to use liquid nitrogen at 65 Kelvin.

The second design choice was on the machine topology. Since there are different ways to build a superconducting machine, all with their advantages and disadvantages. The concept of a fully superconducting machine, where both the stator and the rotor are superconducting, performs in theory the best, however due to problems with AC losses it is not considered. From the other machine topologies only the bulk flux concentrating and the synchronous machines are both found practical, high performing and also considered for aerospace applications in literature.

In order to determine which of the two topologies performs better, Finite Element Method (FEM) simulations using Comsol and Matlab were used. The result was that the synchronous machine performs much better than the bulk flux concentrating topology in terms of torque capability at the same weight and volume.

The third major design choice was made on how the machine is to be structured. Because of the limited axial space available, a radial design was opted. It was chosen to place the field windings on the stator and the armature on the rotor in order to not use a rotating coupling for the cooling. In this way, the added weight and volume of the coupling is avoided. The disadvantage of using slip rings for the armature current is considered less of an issue.

After the machine structure was defined the actual design of the machine was started with the armature coils. First the winding configuration was chosen by performing a study between fractional pitch concentrated windings and full pitch distributed windings. The two criteria were the relative amplitudes of the space harmonics with and without the EM shield and the eddy current heating losses taking place in the shield.

Observed was that the space harmonics for the concentrated windings are too severe, but they are acceptable with an EM shield. However, the losses inside the shield are very high, making the configuration less performing for a given cooling capability. The distributed windings show acceptable harmonics and virtually none with a shield. Decided is that a full pitch distributed winding design is chosen for the thesis design.

The next design part is the superconducting field coils. The field windings were designed as stacked double pancake racetrack coils with YBCO tapes. Also the cryostat that houses the superconducting coils was designed. By comparing with example cryostat designs found in literature [27], a realistic design was made. Yet, no mechanical analysis was performed, since that goes beyond the scope of this thesis

The major heat sources in the cryostat are calculated with the result of 47 W of heat losses. To remove these losses with liquid nitrogen stored in tanks, at least 38 kg of nitrogen per hour is needed. Cooling with the Lockheed Martin cryocooler or a similar cryocooler is preferred, since it can operate much longer than one hour at about the same weight.

After the design of the whole machine, the final properties were calculated. The most important calculated properties are the torque, which resulted in 4.4 kNm and the total weight, which was estimated at 351 kg. These results and also their derivatives, like the power density, are only 10-30% of the target values and the estimated weight is more than double of the target specification.

From these results it is concluded that after a first study it is estimated that a superconducting electrical propulsion motor may not be feasible with current technology and specifications.

10.2. Recommendations

This thesis concludes that the superconducting electrical propulsion motor may not be feasible with current technology and specifications. Yet it is expected that the machine performance can be improved with future work.

The most important recommendation for future work is to consider liquid hydrogen instead of liquid nitrogen for cooling. This would bring the operating temperature down from 65K to about 20K. When not including any other design changes, operating at 20 K compared to 65 K, may result in **a torque and power increase of 3-4 times.**. This increase will bring the machine specifications much closer to their target values. However, components like the cryostat and cryocooler will have to be redesigned for this lower temperature.

Using hydrogen is not an unrealistic choice for aerospace, since hydrogen is also considered to replace kerosene for aircraft in the (near) future. It is expected that using liquid hydrogen can improve the machine performance enough to meet the target specifications, but an in-depth research is required before any conclusions can be made.

For the design in this thesis certain variables have been chosen, like the slot depth, however they have not been optimized for weight or torque. Also some parameter dependences, like the dependence of the effective stack length and pole pitch, have not been researched. Better performance is expected if a full machine optimization is performed including most machine parameters. Therefore this optimization is considered important for future work on this type of electrical machine.

Also it is believed that the estimated weight of the machine can be lowered with at least a few dozen kg by removing material and by replacing the HTS support structure material with carbon fibre composites. Therefore it is important that in future work a thorough mechanical analysis of the structures is performed.

Several design issues are mentioned, but not fully analysed. Examples are the cooling system inside the cryostat, the cooling system of the armature coils and EM shield, any induced AC losses in the HTS coils and armature current time harmonics. Including these issues will improve the reliability of the feasibility study and are therefore important recommendations.

The machine was studied only in steady state operation. Dynamic situations like start-up, load change or fault situations are not analysed. These situations can result in higher heating losses and more mechanical stresses. It is recommended that these situations are analysed for a more complete feasibility study.

Bibliography

[1] "European Commission environmental goals for 2020," European Commission, 2011. [Online]. Available: http://ec.europa.eu/energy/energy2020/energy2020_en.htm. [Accessed 24 7 2012].

[2] Cleansky, "The Clean Sky JTI (Joint Technology Initiative)," 2012. [Online]. Available: http://cleansky.eu . [Accessed 25 7 2012].

[3] C. D. Sanabria-Walter, "HIGH TORQUE PERMANENT MAGNET MACHINES FOR AEROSPACE PROPULSION," EADS Internal Report, 2011.

[4] "Institut für Flugzeugbau," [Online]. Available: www.ifb.uni-stuttgart.de.

[5] Pc-aero, "Pc-aero," 2012. [Online]. Available: http://www.pc-aero.de/. [Accessed 22 8 2012].

[6] Sikorsky, "Project Firefly:Sikorsky unveils electric helicopter technology demonstrator," 2010. [Online]. Available: http://www.gizmag.com/sikorsky-project-firefly/15993/. [Accessed 6 12 2011].

[7] Rolls-Royce, The Jet Engine, vol. 5th edition, Rolls-Royce plc Technical Publications Department,, 2005.

[8] "Diesel Engines," 2012. [Online]. Available: www.dg.history.vt.edu/ch5/ices.html. [Accessed 21 8 2012].

[9] EADS, "ELECTRIC-POWERED SYSTEMS," 2011. [Online]. Available: http://www.eads.com/eads/int/en/our-innovation/our-technologies/Eco-efficiency/Electric-powered-systems.html. [Accessed 7 12 2011].

[10] "Ecomotors," 2012. [Online]. Available: www.ecomotors.com. [Accessed 22 8 2012].

[11] Flightglobal, "EADS unveils hybrid eco-helicopter," 2010. [Online]. Available: http://www.flightglobal.com/news/articles/ila-eads-unveils-hybrid-eco-helicopter-concept-342861. [Accessed 6 12 2011].

[12] S. R. Durkee and A. Muetze, "Conceptual design of an electric helicopter powertrain.," in *5th IET International Conference on Power Electronics, Machines and Drives (PEMD 2010)*, Brighton, UK, 2010.

[13] H. Onnes, "Investigations into the properties of substances at low temperatures, which have led, amongst other things, to the preparation of liquid helium.," *Nobel Lecture.,* 1913.

[14] S. S. Kalsi, Applications of High Temperature Superconductors to Electric Power Equipment., John Wiley & Sons. IEEE Press., 2011.

[15] J. Bednorz and K. Muller, "Possible high Tc superconductivity in the Ba-La-Cu-O system.," *Zeitschrift fur Physik B Condensed Matter,* 1986.

[16] "Superconductivity," Wikipedia, [Online]. Available: http://en.wikipedia.org/wiki/Superconductivity. [Accessed 9 6 2012].

[17] Y. Iwasa, Case Studies in Superconducting Magnets: Design and Operational Issues, Springer US, 2009.

[18] M. Dhallé, Interviewee, *Private conversation.* [Interview]. 10 11 2011.

[19] "Diamagnetism," Wikipedia, [Online]. Available: http://en.wikipedia.org/wiki/Diamagnetism. [Accessed 2 8 2012].

[20] K. Matsumoto and P. Mele, "Artificial pinning center technology to enhance vortex pinning in YBCO coated conductors.," in *IOP Publishing.*, 2009.

[21] M. Sjöström, Hysteresis Modelling of High Temperature Superconductors, PhD Thesis ed., ÉCOLE POLYTECHNIQUE FÉDÉRALE DE LAUSANNE, 2001.

[22] K. Vinod, R. Kumar and U. Syamaprasad, "Prospects for MgB2 superconductors for magnet application.," 2006.

[23] "HoffmanLab," 2010. [Online]. Available: http://hoffman.physics.harvard.edu/materials/Cuprates.php. [Accessed 13 9 2010].

[24] S. Electric, 2012. [Online]. Available: http://global-sei.com/super/hts_e/spec.html and http://global-sei.com/super/magnet_coil_e/ index.html. [Accessed 23 10 2011].

[25] B. Goddard, J. Lukasik and K. Sykulski, "ALTENATIVE DESIGNS OF A SUPERCONDUCTING SYNCHRONOUS GENERATOR: THE SOUTHAMPTON APPROACH," *IEEE,* 2008.

[26] J. Schrieffer and J. Brooks, Handbook of high-temperature superconductivity: theory and experiment., Springer Verlag., 2007.

[27] N. Mijatovic, "Superconducting Wind Turbine Generators," Center for Electric Technologies, Technical university of Denmark., 2012.

[28] J. F. Gieras, "Advancements in Electric Machines.," *Springer Link,* 2008.

[29] D. Larbalestier, A. Gurevich, D. M. Feldmann and A. Polyanskii, "High-Tc superconducting materials for electric power applications," Applied Superconductivity Center, Department of Materials Science and Engineering, Department of Physics, University of Wisconsin, Wisconsin, 2001.

[30] SuperPower, "SuperPower," 2012. [Online]. Available: http://www.superpower-inc.com/content/products. [Accessed 23 10 2011].

[31] Bruker, "Bruker Energy & Supercon Technologies," 2012. [Online]. Available: http://www.bruker-est.com/hts-coils.html. [Accessed 4 9 2012].

[32] THEVA, "THEVA Dünnschichttechnik GmbH," 2012. [Online]. Available: http://www.theva.com/prod. [Accessed 19 10 2012].

[33] R. Radebaugh, "Cryocooler: The state of the art and recent developments.," National Institute of Standards and Technology, Boulder..

[34] t. H. Brake and G. Wieferinck, "Low-power cryocooler survey. University of Twente," *Elsevier Science cryogenics.,* 2002.

[35] J. R. Olson, P. Champagne, E. Roth and T. Nast, "VERY HIGH CAPACITY AEROSPACE CRYOCOOLER," in *AIP Conference Proceedings*, Palo Alto CA, USA, 2012.

[36] H. e. a. Park, "Analysis of Temperature Dependent Quench Characteristics of the YBCO Coated Conductor.," *IEEE TRANSACTIONS ON APPLIED SUPERCONDUCTIVITY, VOL. 20, NO. 3, JUNE 2010.,* 2010.

[37] G. Klaus, M. Wilke, J.Frauenhofer, W. Nick and H. Neumüller, "Design Challenges and Benefits of HTS Synchronous Machines," *IEEE,* 2007.

[38] P. J. Masson, P. Tixador and C. Luongo, "Safety Torque Generation in HTS Propulsion Motor for General Aviation Aircraft," *IEEE TRANSACTIONS ON APPLIED SUPERCONDUCTIVITY,* vol. 17, no. 2, 2007.

[39] C. Oberhauser and H. R. Kinner, "SOME CONSIDERATIONS IN THE DESIGN OF A SUPERCONDUCTING ALTERNATOR," Cambridge, 1967.

[40] "Advanced Magnet Lab," 2012. [Online]. Available: http://www.magnetlab.com/technology/double-helix/. [Accessed 19 12 2012].

[41] H. Neumueller, W. Nick and B. Wacker, "Advances in and prospects for development of

high-temperature superconductor rotating machines at Siemens," *IOPscience,* 2006.

[42] R. Fair, C. Lewis, J. Eugene and M. Ingles, "Development of an HTS Hydroelectric Power Generator for the Hirschaid Power Station," *IOPscience,* 2010.

[43] H. Ohsaki, Y. Terao and M. Sekino, "Wind Turbine Generators using Superconducting Coils and Bulks," *Journal of Physics: Conference,* 2010.

[44] P. Masson and C. Luongo, "High Power Density Superconducting Motor for All-Electric Aircraft Propulsion," *IEEE TRANSACTIONS ON APPLIED SUPERCONDUCTIVITY,* vol. 15, no. 2, 2005.

[45] C. Luongo, P. Masson and T. Nam, "Next Generation More-Electric Aircraft: A Potential Application for HTS Superconductors," *IEEE TRANSACTIONS ON APPLIED SUPERCONDUCTIVITY,* vol. 19, no. 3, 2009.

[46] A. Parviainen, DESIGN OF AXIAL-FLUX PERMANENT-MAGNET LOW-SPEED MACHINES AND PERFORMANCE COMPARISON BETWEEN RADIAL-FLUX AND AXIAL-FLUX MACHINES, Lappeenranta, Finland: Lappeenranta University of Technology, 2005.

[47] K. Sivasubramaniam, T. Zhang and M. Lokhandwalla, "Development of a High Speed HTS Generator for Airborne Applications," *IEEE TRANSACTIONS ON APPLIED SUPERCONDUCTIVITY,* vol. 19, no. 3, 2009.

[48] R. Flitney, Seals and Sealing Handbook (Fifth Edition), Elsevier, 2007.

[49] "FerroTec," 2012. [Online]. Available: http://seals.ferrotec.com. [Accessed 20 11 2012].

[50] E. Tsampouris, M. Beniakar and A. Kladas, "Geometry Optimization of PMSMs Comparing Full and Fractional Pitch Winding Configurations for Aerospace Actuation Applications," *IEEE TRANSACTIONS ON MAGNETICS,* vol. 48, no. 2, pp. 943-946, 2012.

[51] A. EL-Refaie, "Fractional-Slot Concentrated-Windings Synchronous Permanent Magnet Machines: Opportunities and Challenges," *IEEE TRANSACTIONS ON INDUSTRIAL ELECTRONICS,* vol. 57, no. 1, pp. 107-121, 2010.

[52] H. Polinder, M. Hoeijmakers and M. Scuotto, "Eddy-Current Losses in the Solid Back-Iron of PM Machines for different Concentrated Fractional Pitch Windings," *Electric Machines & Drives Conference,* vol. 1, pp. 652-657 , 2007.

[53] "RUAG," 2012. [Online]. Available: http://www.ruag.com/space/Products . [Accessed 19 9 2012].

[54] J. Hernandez-Llambes and D. Hazelton, "ADVANTAGES OF SECOND-GENERATION HIGH TEMPERATURE SUPERCONDUCTORS FOR PULSED POWER APPLICATIONS," Superpower inc., 2009.

[55] G. Ventura and L. Risegari, The Art of Cryogenics: Low-Temperature Experimental Techniques., Elsevier, 2008.

[56] T. Flynn, Cryogenic engineering., Marcel Dekker New York. , 1997.

[57] J. Pyrhönen, DESIGN OF ROTATING ELECTRICAL MACHINES, John Wiley & Sons Ltd, 2008.

[58] R. Weinstein, A. Gandini and R. Sawh, "Higher Jc Obtained by Reduction of Pinning Potential," *IEEE TRANSACTIONS ON APPLIED SUPERCONDUCTIVITY,* vol. VOL. 19, no. ISSUE 3, pp. 3231-3234, 2009.

[59] "Coalition of commercial application of superconductors (CCAS)," [Online]. Available: http://www.ccas-web.org/superconductivity/. [Accessed 29 8 2012].

[60] L. Kovalev, K. Ilushin and V. Penkin, "Hysteresis and reluctance electric machines with

bulk HTS elements," *IOPscience,* 2000.

[61] M. Tomita and M. Murakami, "High-temperature superconductor bulk magnets that can trap magnetic fields of over 17 tesla at 29 K.," *Nature,* vol. 421, pp. 517-520, 2003.

[62] Z. Deng, M. Miki and K. Tsuzuki, "Pulsed Field Magnetization Properties of Bulk RE-Ba-Cu-O as Pole-Field Magnets for HTS Rotating Machines," *IEEE TRANSACTIONS ON APPLIED SUPERCONDUCTIVITY,* vol. Vol 21, no. 3, 2010.

[63] H. Matsuzaki, Y. Kimura and I. Ohtani, "Mechanical design of a synchronous rotating machines with Gd-Ba-Cu-O HTS bulk pole-field magnets operated by a pulsed-field magnetization with armature copper coils," *IOPscience,* vol. Journal of Physics: Conference Series 43, pp. 776-779, 2006.

[64] W. Xian, Y. Yan and W. Yuan, "Pulsed Field Magnetization of a High Temperature Superconducting Motor," *IEEE TRANSACTIONS ON APPLIED SUPERCONDUCTIVITY,* vol. 21, no. 3, pp. 1171-1174, 2011.

[65] infrared-thermography, 2012. [Online]. Available: http://www.infrared--hermography.com/material.htm. [Accessed 19 9 2012].